Post-Tectonic Landscape Evolution of Sedimentary Basins in Southeastern Arizona and Northern Chile

by

Matthew Cross Jungers

A Dissertation Presented in Partial Fulfillment
of the Requirements for the Degree
Doctor of Philosophy

Approved July 2014 by the
Graduate Supervisory Committee:

Arjun Heimsath, Chair
Kelin Whipple
Ramon Arrowsmith
Enrique Vivoni
Duane DeVecchio

ARIZONA STATE UNIVERSITY

August 2014

ABSTRACT

Sedimentary basins are defined by extensional tectonics. Rugged mountain ranges stand in stark relief adjacent to muted structural basins filled with sediment. In simplest terms, this topography is the result of ranges uplifted along normal faults, and this uplift drives erosion within upland drainages, shedding sediment into subsiding basins. In southeastern Arizona's Basin and Range province extensional tectonics waned at approximately 3-5 Myr, and the region's structural basins began transitioning from internal to external drainage, forming the modern Gila River fluvial network. In the Atacama Desert of northern Chile, some basins of the Central Depression remain internally drained while others have integrated to the Pacific Ocean. In northern Chile, rates of landscape evolution are some of the slowest on Earth due to the region's hyperarid climate. While the magnitude of upland erosion driven by extensional tectonics is largely recorded in the stratigraphy of the structural basins, the landscape's response to post-tectonic forcings is unknown.

I employ the full suite of modern geomorphic tools provided by terrestrial cosmogenic nuclides – surface exposure dating, conventional burial dating, isochron burial dating, quantifying millennial-scale upland erosion rates using detrital TCN, quantifying paleo-erosion rates using multiple TCN such as $^{21}Ne/^{10}Be$ and $^{26}Al/^{10}Be$, and assessing sediment recycling and complex exposure using multiple TCN – to quantify the rates of landscape evolution in southeastern Arizona and northern Chile during the Late Cenozoic. In Arizona, I also use modern remnants of the pre-incision landscape and digital terrain analyses to reconstruct the landscape, allowing the quantification of incision and erosion rates that supplement detrital TCN-derived erosion rates. A new chronology for key basin high stand remnants (Frye Mesa) and a flight of Gila River terraces in Safford basin provides

a record of incision rates from the Pliocene through the Quaternary, and I assess how significantly regional incision is driving erosion rates. Paired nuclide analyses in the Atacama Desert of northern Chile reveal complex exposure histories resulting from several rounds of transport and burial by fluvial systems. These results support a growing understanding that geomorphic processes in the Atacama Desert are more active than previously thought despite the region's hyperarid climate.

DEDICATION

To Jeff Kellogg

A man who understood rivers better than anybody…

ACKNOWLEDGMENTS

I could not have gotten to the starting line of this project without the guidance of my past mentors and friends David Dethier and Paul Bierman. They both played huge roles in helping me become the scientist that I am today, and they have never stopped encouraging me and offering advice.

I am very happy that I can add Arjun Heimsath to that list of scientific mentors and friends that pushed me professionally and offered support at the right times. Each meeting with Arjun during my first year at Arizona State University, he encouraged me to think bigger and find something that truly inspired me. That is a lesson I will never forget. Then there was that time that he said I just had to check out these incredible surfaces near Safford, AZ…

The rest of my committee has also helped along the way. Kelin Whipple always manages to ask the next hard question. Ramon Arrowsmith took me on a whirlwind tour of the greater Salt River basin in the summer of 2009, and really got me started thinking about 'life after faulting' in Arizona. Enrique Vivoni always had great insight and a kind word during the hard times when the elevators seemed like the only thing working properly in ISTB4. Phil Christensen remains as an honorary committee member and always helped me keep my dissertation in perspective. Duane DeVecchio was quick to step in and offer his eye to this project, and his enthusiasm and engaging questions were invigorating at the end.

Ronald Amundson believed in me enough to bring me along to Chile in 2009 and subsequent field seasons. I do not know whether I am more inspired by Ron's sharp intelligence or his remarkable humility and kindness. I truly value my collaborations with Ron.

I got into this whole mess with Wendy Bohon and Matt Rossi, and we're getting out of it at just about the same time. I couldn't have asked for a better cadre. Roman DiBiase and Byron Adams provided an incredibly high standard to strive for from day one, and I'm lucky to call them colleagues and friends. The same goes for the rest of the broader Whipsath crew, with special appreciation for Erin DiMaggio, Marina Foster, Andy Darling, and Scott Robinson.

I would still be stuck in some inefficient loop without Allen McNamara's guidance in Numerical Methods. One of the best courses I have ever had the pleasure to take.

Conversations and help in the field from Arizona Geological Survey geologists Phil Pearthree, Joe Cook, Ann Youberg, and Mike Conway were revitalizing and helped reassure me that all this hard work was worth it. Arizona is a special place, and southeastern Arizona is the crown jewel in my humble opinion.

Greg Balco and Dave Shuster were great hosts during my time at the Berkeley Geochronology Center, and they remain great collaborators.

I would like to thank the fraction of my friends and family who realize that getting a PhD is quite different from 'still being in college'.

Kolee has been my best and most reliable field assistant from my earliest trips to Safford, Sonoita, Winkelman, Klondyke, etc. She was always game to get out for the weekend and camp while I tried to get my head around this project, and she developed a keen eye for quartz. I love you more than anything, Kolee. Thank you for your unflagging support.

TABLE OF CONTENTS

CHAPTER Page

CHAPTER Page

CHAPTER Page

LIST OF TABLES

Table Page

LIST OF FIGURES

Figure Page

Figure Page

PREFACE

'All our results in geology are tainted by the tacit assumption of simplicity that does not exist.'

- Grove Karl Gilbert -

(as quoted by William Morris Davis and Baylor Brooks in 'The Galiuro Mountains, Arizona', *American Journal of Science*, 1930)

CHAPTER 1

Introduction

1.0 Motivation

Topography is the expression of surface processes driven by the external forcing of tectonics and climate, and the uplift of mountain ranges along convergent tectonic boundaries generates the most significant regions of continental relief on Earth. The degree to which feedbacks between climate and tectonics dampen or enhance this relief development has been, and remains, a fundamental question for modern geomorphology (e.g., Molnar and England, 1990; Whipple and Meade, 2006). The impact of uplift on the rates of landscape evolution may be isolated by quantifying rates of surface processes across a range of uplift rates, holding lithology and climate generally constant (e.g., DiBiase et al., 2010). This approach has shown that in a tectonically active landscape, upland erosion rates are primarily a function of uplift rate and the ability of fluvial systems to incise and 'keep up' with this uplift. It has recently been shown that, in these rapidly eroding landscapes, sediment generation on hillslopes, previously thought to threshold at some upper limit of soil production, is indeed keeping pace with incision rates on the order of 1 mm/yr (Heimsath et al., 2012; Larsen et al., 2014). Current and future studies of landscape evolution in actively uplifting areas are incredibly important in continuing to refine our understanding of how close to steady-state, or an equilibrium between uplift rate and erosion rate, natural landscapes are capable of achieving. However, when active uplift ceases, and orogens begin to decay, how do our lessons from active landscapes translate? Can we apply the same rules and tools to interrogate landscapes that are evolving primarily in response to climate

(changing over timescales ranging from millennia to millions of years) or their own internal dynamics?

Previous studies of decaying landscapes have reported some of the slowest erosion rates on Earth (e.g., Bierman and Caffee, 2001) on the order of 0.001 mm/yr (1 m/Myr), reinforcing the ability of active tectonics to generate truly fast rates of landscape evolution. Slow rates in Namibia such as those cited above (Bierman and Caffee, 2001) are also a function of potentially inefficient fluvial processes in an arid climate, but other work in wetter, but still tectonically quiescent, regions finds upland erosion rates on the order of 10 m/Myr – e.g., rates ranging from 20-30 m/Myr in the southern Appalachian Mountains, a range that's been decaying in the absence of tectonics for hundreds of millions of years (Matmon et al., 2003). My work in southeastern Arizona and northern Chile is motivated by this previous work in both tectonically active and tectonically quiescent landscapes. A primary goal of my work is quantifying how the high-relief ranges of Arizona's Basin and Range are evolving in the absence of tectonics over the last few million years, and I evaluate the rates of landscape evolution in a hyperarid region, northern Chile's Atacama Desert.

Southeastern Arizona's Basin and Range physiographic province is an ideal setting to investigate questions of post-tectonic landscape evolution. It is a region defined by two stages of extensional tectonics: (1) mid-Tertiary low-angle extension and metamorphic core complex exhumation (Spencer and Reynolds, 1989) and (2) high-angle normal faulting associated with the Basin and Range Disturbance at 8-12 Myr (Scarborough and Peirce, 1979). The modern landscape of high-relief ranges and intervening basins is most significantly a result of the latter episode of extension. However, regional tectonics have been inactive for approximately 3-5 Myr (Smith, 1994), and previously internally drained structural basins have integrated into the modern Gila River system (Figure 1). Fortuitously,

in many basins of the region, remnants of each structural basin's pre-incision high stand record the geometry of the paleo-landscape and preserve the stratigraphy of each basin's final stages of post-tectonic filling (Menges and McFadden, 1981; Morrison, 1985; Menges and Pearthree, 1989). Previous studies identified the importance of these high stand deposits, and were able to define rough age constraints for some of the surfaces based on magnetostratigraphy of underlying fill and soil development on the surfaces themselves (~1-2 Myr for the Martinez Surface of Sonoita Creek basin; Menges and McFadden, 1981). However, this landscape had not been revisited and reinvestigated with some of the more recently available tools for process geomorphology - namely higher resolution topographic data, software capable of digital terrain analyses, and a suite of terrestrial cosmogenic nuclide (TCN) applications.

The Atacama Desert is one of the driest places on Earth, and for this reason it is an ideal place to investigate how rates of landscape evolution may slow under hyperarid conditions. Previous work employing TCN abundances in rock and sediment in the Atacama Desert have identified some of the slowest erosion rates on Earth, leading to the preservation of very old landforms (e.g., Nishiizumi et al., 2005). However, recent work has shown that hillslope and fluvial processes in the Atacama Desert may be more active than previously assumed (e.g., Placzek et al., 2010). We use paired ^{10}Be and ^{21}Ne abundances to determine whether sediment is undergoing simple exposure and erosion or more complex exposure histories. When quantifying exposure ages or erosion rates with a stable nuclide such as ^{21}Ne, accounting for inherited TCN abundances developed across multiple rounds of exposure is crucial. Active erosion-deposition cycles in the Atacama Desert are ongoing under the modern hyperarid climate, and these processes should be accounted for when sampling for TCN studies in this region of northern Chile.

A summary of the following chapters is presented below. Since chapters 2-5 are written as individual manuscripts for submission to peer-reviewed journals, there is some necessary redundancy in background material between chapters.

2.0 Chapter Outline

Chapter 2 uses two TCN, ^{21}Ne and ^{10}Be to investigate the stability of a chronosequence of landforms in the Atacama Desert of northern Chile. We measure concentration depth profiles in landforms – a modern channel, an adjacent low terrace, and a nearby alluvial fan – to assess whether each component of the landscape is stable, and, if stable, the timing of abandonment. We find that the modern channel is actively aggrading at a rate of 2 m/Myr over a timescale of 200-300 kyr. Before abandonment, the adjacent low terrace was developed during a similar, earlier period of channel aggradation also on the timescale of hundreds of thousands of years at a rate of 2 m/Myr. The alluvial fan, previously thought to be a relict landform abandoned at 2 Myr, has an apparent exposure age of ~300 kyr based on a concentration depth profile of ^{10}Be. Soil development within the fan's soil suggests an age much older than mid-Pleistocene, but the TCN abundances do not allow for more than approximately 1 million years of stability with some reworking of the surface. This study not only underscores the ongoing importance of active erosion-deposition cycles in the hyperarid Atacama Desert, but also provides over half of the published TCN depth profiles available for the Atacama Desert. We strongly encourage any future applications of TCN in the Atacama to carefully account for inherited TCN abundances in alluvial deposits and for the possibility of complex exposure due to multiple rounds of erosion-transport-deposition-reworking.

Chapter 3 builds off of Chapter 2, and highlights even more clearly the necessity for multiple nuclide approaches to TCN studies in the Atacama Desert. We provide additional examples of how site-specific inheritance compares to surface concentrations, and the potential implications for surface exposure dating. Nearly all our samples have undergone complex exposure histories, requiring more careful treatment in any interpretation of how TCN abundances in sediment relate to surface processes. Indeed, with the exception of the sites treated with detail in Chapter 2, interpretations of our other data are confounded by TCN ratios that defy simple explanation. The simplest and most reasonable explanation is that sediment within the Central Depression of northern Chile experiences multiple rounds of exposure and re-exposure to TCN production, and measured abundances of TCN do not reflect rates of landscape evolution. Stable TCN such as ^{21}Ne are especially prone to cumulative buildup of TCN in sediment through time, and a radionuclide such as ^{10}Be should always be measured in concert with stable TCN. Inferences of surface exposure ages in the Atacama Desert based on one TCN alone with no accounting for inherited TCN abundances should be considered only with great caution.

Chapter 4 reconstructs the pre-incision topography of Aravaipa Creek basin in southeastern AZ, and uses digital terrain analyses in conjunction with TCN burial dates to quantify rates of incision and erosion associated with the drainage integration of the Gila River system. I identify components of the modern landscape that preserve the geometry of Aravaipa Creek basin's high stand prior to drainage integration with the Lower San Pedro basin downstream. I then interpolate these components to reconstruct the paleo-landscape. By subtracting a digital elevation model (DEM) of the modern landscape from the reconstructed DEM, I quantify where incision was highest, and what volume of material has been eroded from the system post-integration. ^{26}Al/^{10}Be burial dates of latest stage basin fill

provide a maximum age constraint for the timing of incision and allow the translation of incision and erosion magnitudes from the landscape reconstruction into rates of landscape evolution driven by drainage integration.

Chapter 5 takes an integrated approach of modern topographic analyses and TCN-derived rates of modern and paleo-erosion rates plus burial dates to investigate the post-tectonic landscape evolution of a paired basin and range in southeastern Arizona. The Pinaleno Mountains and Safford basin comprise one of the highest relief landscapes in Arizona providing a modern orographic gradient in climate established by uplift during earlier extensional tectonics. We use detrital TCN to investigate patterns of upland erosion rates across the relief structure of the Pinaleno Mountains, and we then compare those rates to paleo-erosion rates derived from TCN burial dates of late stage basin fill in Safford basin (Frye Mesa). Burial dates from Frye Mesa also constrain the timing of latest stage basin fill in Safford basin (~2 Myr), and subsequent incision by the Gila River network. TCN burial dates of Gila River terraces along the northeast margin of Safford basin constrain the timing of when the Gila River established itself in Safford basin, and how quickly it has incised from ~3 Myr to the present. We then can consider how regional incision rates may be driving modern millennial-scale upland erosion rates.

Chapter 6 is a synthesis of Chapters 2-5, and it offers recommendations for further work in southeastern Arizona and northern Chile.

Chapter 2 was published in 2013 in *Earth and Planetary Science Letters* and should be cited:

Jungers, M. C., Heimsath, A. M., Amundson, R., Balco, G., Shuster, D., & Chong, G. (2013). Active erosion–deposition cycles in the hyperarid Atacama Desert of Northern Chile. *Earth and Planetary Science Letters*, *371*, 125-133.

Chapter 3 is a manuscript in preparation for *Quaternary Geochronology*.

Chapter 4 is a manuscript in preparation for *Earth Surface Processes and Landforms*.

Chapter 5 is a manuscript in preparation for *Geological Society of America Bulletin*.

References

Bierman, P. R., & Caffee, M. (2001). Slow rates of rock surface erosion and sediment production across the Namib Desert and escarpment, southern Africa.*American Journal of Science*, *301*(4-5), 326-358.

DiBiase, R. A., Whipple, K. X., Heimsath, A. M., & Ouimet, W. B. (2010). Landscape form and millennial erosion rates in the San Gabriel Mountains, CA.*Earth and Planetary Science Letters*, *289*(1), 134-144.

Heimsath, A. M., DiBiase, R. A., & Whipple, K. X. (2012). Soil production limits and the transition to bedrock-dominated landscapes. *Nature Geoscience*, *5*(3), 210-214.

Larsen, I. J., Almond, P. C., Eger, A., Stone, J. O., Montgomery, D. R., & Malcolm, B. (2014). Rapid soil production and weathering in the Southern Alps, New Zealand. *Science*, *343*(6171), 637-640.

Matmon, A., Bierman, P. R., Larsen, J., Southworth, S., Pavich, M., & Caffee, M. (2003). Temporally and spatially uniform rates of erosion in the southern Appalachian Great Smoky Mountains. *Geology*, *31*(2), 155-158.

Menges, C. M., & McFadden, L. D. (1981). Evidence for a latest Miocene to Pliocene transition from Basin-Range tectonic to post-tectonic landscape evolution in southeastern Arizona: Arizona Geological Society Digest 13. *Soc. Digest*, *13*, 151-160.

Menges, C. M., & Pearthree, P. A. (1989). Late Cenozoic tectonism in Arizona and its impact on regional landscape evolution. *Geologic evolution of Arizona: Arizona Geological Society Digest*, *17*, 649-680.

Molnar, P., & England, P. (1990). Late Cenozoic uplift of mountain ranges and global climate change: chicken or egg?. *Nature*, *346*(6279), 29-34.

Morrison, R. B. (1985). Pliocene/Quaternary geology, geomorphology, and tectonics of Arizona. *Geological Society of America Special Papers*, *203*, 123-146.

Scarborough, R. B., & Peirce, H. W. (1978, November). Late Cenozoic basins of Arizona. In *Land of Cochise, Southeastern Arizona, New Mexico Geological Society Twenty-Ninth Field Conference Guidebook, ed. JF Callender, JC Wilt, and RE Clemons* (pp. 253-259).

Spencer, J. E., & Reynolds, S. J. (1989). Middle Tertiary tectonics of Arizona and adjacent areas. *Geologic evolution of Arizona: Arizona Geological Society Digest*, *17*, 539-574.

Smith, G. A. (1994). Climatic influences on continental deposition during late-stage filling of an extensional basin, southeastern Arizona. *Geological Society of America Bulletin*, *106*(9), 1212-1228.

Whipple, K. X., & Meade, B. J. (2006). Orogen response to changes in climatic and tectonic forcing. *Earth and Planetary Science Letters*, *243*(1), 218-228.

Figure Caption

Figure 1.1. Final stages of the Basin and Range disturbance. (A) Structural basins were filled with sediment, and most basins were still internally drained. (B) Following the cessation of extensional tectonics in the region, basins continued to fill with sediment and faults were buried. Basins began to integrate with the mainstem Gila River via a combination of basin spillover and headward drainage capture. (C)Following integration with an adjacent basin, sedimentary fill was incised as its basin adjusted to a new, lower baselevel. (D) As a new, through-flowing drainage network was established, integrated basins graded to the Gila River. The shift to an oscillating climate in the Quaternary may be preserved in flights of terraces that record alternating periods of floodplain stability followed by rapid incision. Figure adapted from Menges and Pearthree, 1989.

Figure

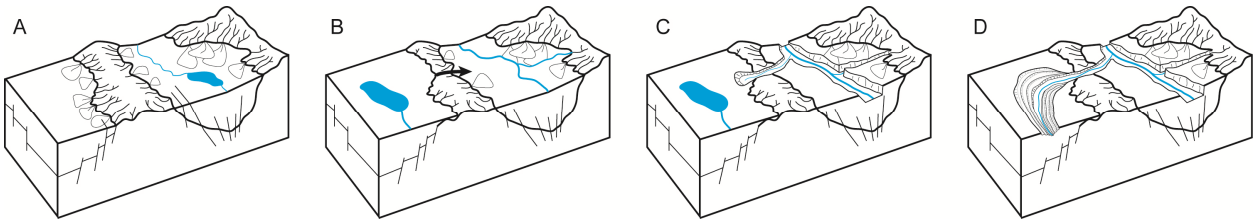

Figure 1.1

CHAPTER 2

Active Erosion-Deposition Cycles in the Hyperarid Atacama Desert of Northern Chile

Matthew C. Jungers*
School of Earth and Space Exploration, Arizona State University, ISTB4, Room 795, 781 E. Terrace Road Tempe, AZ 85287 (matthew.jungers@asu.edu)
*Corresponding author

Arjun M. Heimsath
School of Earth and Space Exploration, Arizona State University, ISTB4, Room 795, 781 E. Terrace Road Tempe, AZ 85287 (arjun.heimsath@asu.edu)

Ronald Amundson
Department of Environmental Science, Policy and Management, 137 Mulford Hall, University of California, Berkeley, CA 94720 (earthy@berkeley.edu)

Greg Balco
Berkeley Geochronology Center, 2455 Ridge Road, Berkeley, CA 94709

David Shuster[1,2]
1. Department of Earth and Planetary Science, 479 McCone Hall, University of California, Berkeley, CA 94720 (dshuster@berkeley.edu)
2. Berkeley Geochronology Center, 2455 Ridge Road, Berkeley, CA 94709

Guillermo Chong
Departamento de Ciencias Geológicas, Universidad Católica del Norte, Antofagasta, Chile (Gchong@ucn.cl)

Accepted to Earth and Planetary Science Letters
April 2013

Keywords: Atacama; Cosmogenic Nuclides; Hyperarid; Surface Processes; Fluvial Processes; Geomorphology; Landscape Evolution; ^{10}Be; ^{21}Ne

Abstract

There is significant debate over the rates and types of fluvial activity at the Plio-Pleistocene boundary in the hyperarid Atacama Desert of Chile. To quantify fluvial processes and help resolve this debate, we measure terrestrial cosmogenic nuclide (TCN) (^{10}Be and ^{21}Ne) concentration depth profiles in three settings representing a chronosequence: (1) a late Pliocene alluvial fan representative of major regional deposits, (2) a modern, active channel and (3) an adjacent low terrace inset into the Pliocene alluvium. Late Pliocene deposits that are widely preserved in the region contain TCN profiles consistent with relatively rapid stripping of upland sediment at the Plio-Pleistocene boundary. Deposits inset into these Late Pliocene features record cut and fill cycles that rework sediment throughout the Quaternary. The TCN profile in the modern channel is best explained by sediment aggradation at 2.1 m Myr^{-1} during the last 250,000 years. Similarly, the adjacent low terrace sediments contain TCN concentration profiles consistent with aggradation of 2.0 m Myr^{-1} over a period of 250,000-750,000 years prior to the last 250,000 years of stability. In summary, depth profiles of two TCNs provide constraints on the rates of sediment deposition, sources of sediment and transport history, as well as the subsequent exposure conditions of the sediment following deposition. Our results are consistent with early Quaternary initiation of hyperaridity for the region. During the Quaternary, winter precipitation events experienced at our sites' latitude (24°S) drive active erosion-deposition cycles. The northward migration of the subtropical front during Quaternary glacial cycles may have enhanced precipitation at 24°S, leading to more active fluvial processes during cooler periods.

1.0 Introduction

Alluvial landforms of the Atacama Desert of Chile are widely dominated by pre-Pleistocene deposits, and the hyperarid region is remarkable for the modest to negligible Quaternary modification of the landscape (e.g., Dunai et al., 2005). Landscape reconstructions indicate that prominent Miocene and Pliocene alluvial deposits represent large regional erosion/depositional events, whereas Quaternary processes have locally incised into or lap over these regional fluvial deposits (Amundson et al., 2012). Additionally, bedrock hillslopes are covered with dust and salt, and are in large part isolated from present drainage networks. As a result, Quaternary channels are typically left to rework sediment eroded from adjacent Pliocene and Miocene deposits rather than sediment produced from bedrock or saprolite in an actively eroding upland. Constraints on the magnitudes, frequencies and rates of fluvial processes are sparse.

The proposed change in magnitude and nature of the post-Pliocene, Quaternary sedimentary processes in the Atacama Desert should be recorded in terrestrial cosmogenic nuclide (TCN) surface concentrations, as well as in the TCN depth profiles observed in fluvial deposits. Prior work in the Atacama Desert focused on the exposure ages of surface clasts (Dunai et al., 2005; Nishiizumi et al. 2005; Ewing et al., 2006; Gonzalez et al., 2006; Carrizo et al., 2008; Evenstar et al., 2009; Placzek et al., 2010). We show, however, that depth profiles of TCNs, particularly ^{10}Be and ^{21}Ne, provide additional and novel insights into the transport and deposition history of sampled sediment.

To further quantify rates of fluvial processes in the Atacama Desert, we present a dataset of in-situ produced cosmogenic ^{10}Be and ^{21}Ne concentration depth profiles in alluvial sediments from the central Atacama Desert that include the regional late Pliocene deposits and younger, localized Quaternary fluvial features inset into this regional landform. To

interpret these data, we (1) compare surface concentrations of cosmogenic nuclides to depth profiles, (2) investigate the complexity of sediment exposure histories, and (3) use cosmogenic nuclides to quantify Quaternary deposition in active channels.

1.1 Setting

The Atacama Desert spans approximately 8-10 degrees of latitude within the structurally defined Central Depression of Northern Chile. Three factors are commonly cited as the cause for the region's extreme lack of precipitation: (1) the rain shadow of the Andes to the east, blocking moisture from the Atlantic Ocean; (2) the region's position within the subtropical high-pressure belt; and (3) the upwelling of cold water to the west related to the Pacific Ocean's Humboldt current (e.g., Houston, 2006). Additionally, the Coastal Cordillera between the Central Depression and the Pacific Ocean minimizes the amount of moisture that can reach the Atacama. A north-south gradient in mean annual precipitation sets the boundaries of ecosystems. The hyperarid north (19°-23°S) is largely abiotic, and increasing fog and precipitation from 26°-29°S enables vegetation to begin taking hold near the southern extent of the desert (Navarro-González et al., 2003; Rundel et al., 1991; Owen et al., 2010).

Our study is focused within the hyperarid central Atacama Desert, between 21°-24°S (Figure 1), an area that now experiences minimal winter rainfall (< 3 mm yr^{-1}) sourced from the Pacific Ocean. Specifically, we centered our study around 24°S latitude, near a boundary between moisture effects from two wind belts, the southern westerlies and the tropical easterlies (Maldonado et al., 2005). North of 24°S, most of the moisture carried by the tropical easterlies is excluded from the northern Atacama Desert by the rain shadow of the Andes. During the summer, however, convective precipitation related to the South

American Summer Monsoon can deliver moisture to the eastern edge of the northern Atacama Desert (Zhou and Lau, 1998; Ammann et al., 2001; Placzek et al., 2010). South of 24°S, precipitation thus increases with latitude and is delivered primarily in the form of winter precipitation from Pacific fronts and cutoff lows (Vuille and Ammann, 1997; Latorre et al., 2006; Placzek et al., 2010). The rare precipitation events that have delivered the minimal rainfall recorded near 24°S are most likely attributed to the interception of these cold air masses by increasingly high topography to the east of the Central Depression (Vuille and Ammann, 1997; Placzek et al., 2010). Any past shift in the boundary between these two moisture regimes would be significant to processes active across our study sites since they are near the modern boundary. Independent studies of the late Quaternary paleoclimate of northern Chile suggest that the northernmost boundary of Pacific-derived moisture has shifted toward the equator during recent glacial periods (Lamy et al., 1998; Lamy et al., 2000; Stuut and Lamy, 2004; Maldonado et al., 2005; Heusser et al., 2006). It is therefore possible that the magnitude of precipitation fluctuated to levels higher than the present for hyperarid sites located from 22-24°S, including our study area.

The pace of hillslope and fluvial processes in the Atacama Desert is widely thought to be slower than most places on Earth. However, a growing regional catalog of erosion rates and exposure ages derived from TCN concentrations in bedrock, boulders, and sediment reveals active processes, likely of varying magnitude and duration, from the Miocene to the present (Dunai et al., 2005; Nishiizumi et al., 2005; Kober et al., 2009; Evenstar et al., 2009; Owen et al., 2010; Placzek et al., 2010; Amundson et al., 2012). Such studies also reveal that results from opposite ends of the cosmogenic nuclide-derived surface process rate spectrum mirror the modern day gradient of an increasingly hyperarid climate from 24°S northward. Dunai et al. (2005) reported a wide range of exposure ages, from 4-37

million years, for surficial cobbles on an alluvial fan remnant in the northern Atacama Desert. The preservation of such relict landforms requires negligible erosion from their deposition to the present. Such low erosion rates are consistent with the extremely low probability of precipitation within the northern Atacama Desert, as predicted by the modern climate gradient. In contrast, Placzek et al. (2010) collected samples along a transect from the Andes, across the Central Depression, to the Coastal Cordillera, roughly parallel to ~24° S and reported minimum exposure age-maximum erosion rate pairs derived from ^{10}Be, ^{26}Al, and ^{21}Ne concentrations that suggested active surface processes throughout the Pleistocene. Placzek et al. interpret low cosmogenic nuclide concentrations in fluvial sediment to mean: (1) sediment is not simply being derived from nearby, long-exposed boulders, and (2) surface processes must be active in the Pleistocene. Cyclical shifts of wetter conditions during the Quaternary may have driven the surface processes inferred by Placzek et al.

1.2 Study Approach

Our goal is to quantify rates of Pliocene and Quaternary surface processes in the Atacama Desert. To do so, we sampled a TCN depth profile from a regionally extensive Plio-Pleistocene fill that was the focus of previous cosmogenic nuclide surface exposure studies (Ewing et al., 2006) and other isotopic studies investigating pedogenic processes (Ewing et al., 2007; 2008). We chose two additional sites to explore the nature of inset Quaternary features: (1) the modern channel of an active wash system; (2) an adjacent terrace of the same system. These three field sites represent a chronosequence of the regional fluvial systems that span what is hypothesized to be a major climate and hydrological change in the late Pliocene (Wara et al., 2005).

Questions addressed by our data include: (1) how active are modern alluvial channels in the present hyperarid climate, (2) when did the fluvial network last incise into its alluvial bed, abandoning its lowest terraces, and (3) are the broad alluvial fans widely observed throughout the Central Depression still active, or are they stable, relict landforms related to a past climate?

2.0 Methods

2.1 Determining Sediment Deposition Rates with TCN Depth Profiles

The rate and duration of sediment deposition, bioturbation, and erosion control the concentrations of cosmogenic nuclides as a function of depth within the upper few meters of an alluvial deposit (e.g., Lal and Arnold, 1985; Phillips et al., 1998; Granger and Riebe, 2007). Most commonly, TCN concentration depth profiles are used to infer the duration that a deposition surface has been stable. The determination of a surface exposure age for a fluvial terrace must account for 'inherited' TCN concentrations in sediment produced during exposure upstream from the terrace (Anderson et al., 1996):

$$N(z,t) = N_0 e^{-\lambda t} + \frac{P_0 e^{\frac{-\rho z}{\Lambda}}}{\lambda + \frac{\rho \varepsilon}{\Lambda}}\left(1 - e^{-\left(\lambda + \frac{\rho \varepsilon}{\Lambda}\right)t}\right), \qquad (1)$$

where N is cosmogenic nuclide concentration [atoms g^{-1}], t is time [yr], N_0 is the inherited concentration of the cosmogenic nuclide [atoms g^{-1}], ε is erosion rate[cm yr^{-1}] (assumed to be zero for our purposes), λ is the decay constant for a radionuclide [yr^{-1}], z is depth below the deposit surface [cm], P_0 is the cosmogenic nuclide production rate at the surface [atoms g^{-1} yr^{-1}], Λ is the attenuation length for cosmogenic nuclide production [g cm^{-2}], and ϱ is sediment density [g cm^{-3}].

In a few cases, profiles of TCNs with depth have not shown the expected relationship of an exponential decline with depth that is diagnostic of an attenuation profile produced during a period of stability. Rather, these profiles reflect an increase in TCN concentrations with depth (Clapp et al., 2001; Nichols et al., 2002). In such a case, the TCN concentration depth profiles can be used to infer steady-state deposition rates for the sediment by fitting the data to analytical models that quantify the TCN concentration as a function of depth and sediment deposition rate. The difference in form between a TCN concentration depth profile that is a function of deposition rate (equation 2 below) vs. a function of exposure time and erosion rate (equation 1) is clearly observable (Figure 2).

Lal and Arnold (1985) first defined the steady-state solution for TCN concentrations in accumulating sediment as a function of depth and sedimentation rate:

$$N(z,D) = N_i e^{\frac{-\lambda z}{D}} + \frac{P_0}{\frac{D\rho}{\Lambda} - \lambda}\left(e^{\frac{-\lambda z}{D}} - e^{\frac{-\rho z}{\Lambda}}\right), \qquad (2)$$

where D is deposition rate [cm yr^{-1}], N_i is the cosmogenic nuclide concentration of sediment being deposited at the surface [atoms g^{-1}], and all other variables are as defined for equation 1. Note that this formulation of Lal and Arnold's solution accounts for decay of radionuclides unlike several later formulations (e.g., Phillips et al., 1998; Clapp et al., 2001; Nichols et al., 2002). Versions of equation 2 that do not account for decay are best suited for settings where erosion-deposition cycles are much shorter than the half-life of any cosmogenic radionuclide of interest. If sediment deposition rates are on the order of 1 m Myr^{-1} or slower, as in the Atacama Desert, then radionuclide decay must be accounted for (Lal and Arnold, 1985).

Clapp et al. (2001) and Nichols et al. (2002) both reported sediment deposition rates from alluvial deposits in semi-arid landscapes of the American Southwest. Clapp et al. fitted their data to a deposition rate of 280 m Myr^{-1} which implies that the 350 cm deep exposure of sediment that they sampled was deposited over approximately 12,500 years. This inferred period of deposition is much shorter than the half-life of ^{10}Be (their nuclide of interest), so decay of ^{10}Be was not an issue. Nichols et al. reported slightly slower deposition rates of 17 and 38 m Myr^{-1}, but these rates still suggested an erosion-deposition cycle shorter than the half-lives of their two target nuclides, ^{26}Al and ^{10}Be.

2.2 Sample Collection and Processing

At each site, we collected sediment at regular intervals from the land surface to depths of 75 - 200 cm. The maximum sampled depth was set by either sedimentary deposit boundaries, or by practical constraints on digging. Samples were first sieved to extract the 250-1000 μm fraction, and pebbles larger than 1000 μm were then crushed and sieved to bulk up the total amount of sample in the 250-1000 μm range since samples were not quartz-rich. We then isolated quartz via cleaning in aqua regia and subsequent etching in HF and HNO_3. We extracted ^{10}Be through column chromatography, and $^{10}Be/^{9}Be$ ratios were measured via accelerator mass spectrometry at the Purdue Rare Isotope Measurement Laboratory at Purdue University. Table 2.1 shows complete results.

We measured cosmogenic ^{21}Ne at the Berkeley Geochronology Center by encapsulating 150 mg aliquots (of the same purified quartz analyzed for ^{10}Be) in a Ta packet, heating them under vacuum using a 150 W diode laser, purifying the released gas by reaction with hot and/or cold getters and cryoseparation of Ne from other noble gases, and analyzing the resulting Ne in a MAP-215-50 mass spectrometer. Balco and Shuster (2009) describe

analytical details. Ne isotope ratios in all steps were indistinguishable from a two-component mixture of atmospheric and cosmogenic neon, so we computed cosmogenic Ne concentrations on this basis. Analyses of the CRONUS-A quartz standard during the period of these measurements yielded a cosmogenic ^{21}Ne concentration of 338.9 ± 3.8 x 10^6 atoms g^{-1}.

2.3 Modeling Approach

We fit equation 2 to our observed TCN concentrations by determining the values of the free parameters N_i and D that minimized the chi-squared misfit between modeled values and our data:

$$M = \sum_{j=1}^{n} \left[\frac{N(z_j, D) - N_j}{\sigma_j} \right]^2 , \qquad (3)$$

where $N(z_j,D)$ is the modeled cosmogenic nuclide concentration at depth z_j and a given deposition rate, N_j is the measured cosmogenic nuclide concentration at depth z_j, σ_j is the one standard error analytical uncertainty at depth z_j, and n is the number of samples in our profile. We utilize the 'fmincon' function of the MATLAB Optimization Toolbox to identify a minimum in an objective function for fitting modeled deposition profiles to our data (see Supplementary Material for example M-files).

3.0 Results and Discussion

3.1 Late Pliocene Fan ('Yungay')

To place the data from our younger field sites in a regional context, we first report the TCN profile from an alluvial fan that is part of a prominent regional depositional blanket

into which Quaternary features are incised and deposited (Figure 1). The Yungay site is on the distal end of alluvial fans derived from adjacent uplands and small mountains. Amundson et al. (2012) noted that these fans fill in, and thus postdate, early Pliocene or Miocene stream channels. In addition, the source areas of the fans (the surrounding uplands) are now encased in salt and dust, and are largely inactive as a sediment source. Based on these relations, Amundson et al. (2012) interpret the fan aprons around the uplands to be the result of regional response to the onset of hyperarid conditions, and the fans are composed of the sediment stripped from surrounding uplands as vegetation declined or disappeared during this regional aridification. Evidence supporting this hypothesis is that the surrounding uplands have little saprolite, and largely consist of salt fractured fresh igneous rock covered with sulfate/chloride/nitrate salts and silicate dust.

The age of the alluvial aprons are constrained at ~ 2.1 to 2.2 Myr by K-Ar or Ar-Ar dating of ash embedded within the upper meter of sediment in a deposit near our site (Ewing et al., 2006), and by ^{10}Be concentrations of surface boulders/clasts (Ewing et al., 2006; Amundson et al., 2012). At the ash site, ^{10}Be concentrations ranged from 6.27 x 10^6 to 1.13 x 10^7 atoms g^{-1}, yielding minimum apparent exposure ages from 0.988 to 2.42 Myr – ages consistent with the nearby ash dates. The range of apparent boulder ages is most likely a function of differences in boulders' exposure histories both prior to and after deposition. Such scatter in exposure ages combined with observations that the salt-laden soils have undergone at least partial surficial alteration by past climatic oscillations (Ewing et al., 2006), motivates the use of a TCN concentration depth profile through the soils and sediments to better constrain the age of the apron.

The depth profile of ^{10}Be at Yungay decreases exponentially with depth from 0.5 m to 2 m, with the surface having the lowest ^{10}Be concentration (Figure 3). This pattern is

suggestive of an attenuation profile that is truncated near the surface by an "active transport layer" as described by Nichols et al. (2002) for biotically and hydrologically active sites in the southwest United States. There is no evidence for biotic processes impacting the Yungay soil throughout its history, nor is there evidence of re-activation of distributary channels. However, the upper few tens of centimeters appear to be composed of more recent dust and sulfate salt overlain upon a dense sulfate horizon that may have been truncated, or at least modified, by more pluvial intervals (Quade et al., 2008). At Yungay, these intervals must not have been so humid or prolonged as to remove the salts in the profile.

We model the evolution of ^{10}Be and ^{21}Ne concentrations in sediment undergoing either simple exposure or steady erosion (Figure 4). If sediment is buried and shielded from further TCN production, the continued radioactive decay of ^{10}Be moves the sediment's TCN signature from the steady state erosion island (Lal, 1991) into the 'complex exposure' field. ^{10}Be/^{21}Ne ratios for sediment in the Yungay profile plot within the steady state erosion island, suggesting rapid erosion of the sediment from the uplands and deposition in the Yungay fan complex. This is consistent with the hypothesis of Amundson et al. (2012) of a relatively rapid geomorphic response to a profound climate change near 2.2 to 2.0 Myr, one that is contemporaneous with the onset of the Pacific ENSO cycle (Wara et al. 2005).

It is important to note that, considered without the underlying profile, our surface sample's ^{10}Be concentration of 6.98 $\pm$ 0.241 x 10^6 atoms g^{-1} would suggest a minimum exposure age of ~1.4 Myr. This age agrees with previously reported exposure ages of 0.92 - 2.1 Myr inferred from surface samples at the same site (Amundson et al., 2012). Fitting the truncated attenuation profile with equation 1 (using exposure time and inheritance as free parameters and assuming no erosion) suggests, however, an apparent exposure age of approximately 300,000 years and an inheritance of 8.4 x 10^6 atoms g^{-1} (Figure 3). We take this

300,000 years an extreme minimum for the timing of this fan surface's abandonment, with a maximum age of ~2 Myr for the deposit inferred from the ash dated in a loosely correlative fan deposit 16 km to the southwest (Ewing et al., 2006). This difference between the fan's maximum and minimum age estimates is expected. Surface exposure dates derived from TCN concentrations in alluvial deposits provide minimum estimates for a surface's age by definition (Gosse and Phillips, 2001), and even slow erosion of the surface will have a large effect on a deposit's apparent exposure age. A study investigating young displacement on the Atacama Fault System reported a similar result in dating alluvial fans 15-20 km to the northwest of our site (Gonzalez et al., 2006). Gonzalez et al. measured ^{21}Ne quartz clasts from the surfaces of abandoned alluvial fans, and they correct for ^{21}Ne inheritance by subtracting TCN abundances measured in modern channel sand collected from each fan's source catchment from surface clasts' ^{21}Ne concentration. Apparent exposure ages derived from corrected ^{21}Ne concentrations ranged from 350,000-550,000 years, in contrast to maximum ages of 3-5 Myr for the bajada derived from ashes 1-3 m below the fan's surfaces. Our data and that of Gonzalez et al. suggest that an effort should be made to constrain deposits' TCN inheritance when determining surface exposure ages in the Atacama Desert.

3.2 Modern Channel ('Floating Man')

We selected a wash system incised into the regional alluvial deposits (Figure 1) to determine both the long term stability of these systems and to better understand their sediment sourcing and cycling. We begin by examining the active wash (named 'Floating Man' in the field).

In the modern channel, ^{10}Be and ^{21}Ne concentrations increase as a function of depth into the channel's alluvial bed (Figure 5). This pattern is the reverse of an attenuation profile

that develops in a stable soil (see Yungay above), and is consistent with TCN concentrations that develop in alluvium aggrading at a relatively constant rate. Surface concentrations are lowest and should be a function of either the upland erosion rates (Brown et al., 1996; Bierman and Steig, 1996; Granger et al., 1996) or the exposure history of the sediment being sourced by the fluvial system. Progressively deeper samples accumulate TCNs at lower and lower production rates until they are completely shielded by burial from further nuclide production. We fit the ^{10}Be and ^{21}Ne profiles to solutions for equation 2 to identify the best-fit values for ^{10}Be and ^{21}Ne at the surface and a best-fit deposition rate. The data are best described by inherited ^{10}Be and ^{21}Ne concentrations of $3.72 \pm 0.076 \times 10^6$ atoms g^{-1} and $59.3 \pm 1.90 \times 10^6$ atoms g^{-1}, respectively, and a deposition rate of 2.1 ± 1.0 m Myr^{-1}. We fit only the upper three samples for each nuclide at this site because the ^{10}Be/^{21}Ne ratio for the deepest sample is significantly different than the overlying samples' ^{10}Be/^{21}Ne ratios (Figure 4), suggesting a different sediment source. A variation in sediment source, and associated cosmogenic nuclide concentrations, would violate the assumption of a consistent input concentration at the profile's surface which equation 2 requires. Our model suggests that the upper 50 cm of sediment accumulated over approximately 250,000 years. Since it is possible that this deposition profile continues below our deepest sample, 250,000 years is a minimum estimate for the duration of the current aggradation within the wash. We note that including the ^{10}Be concentrations at 75 cm does not significantly affect the best-fit deposition rate for this site. If the deepest sample is included in the deposition model, then this profile reflects 375,000 years of deposition.

The ^{10}Be/^{21}Ne ratios for samples in the modern channel require intermittent burial and shielding of the sediment during its transport through the fluvial system (Figure 4). This complex exposure history for sediment in the modern channel is indicative of two important

features for this Quaternary fluvial system: (1) Sediment is being sourced from older alluvial deposits that have undergone at least one episode of exposure and burial. This scenario is consistent with our observations that hillslopes provide little sediment and the modern washes largely tap and rework older alluvial fan deposits. (2) The cut-fill nature of this system reflects cycles of sediment transport (exposure), deposition (shielding), and remobilization (re-exposure) in the drainage network during the Quaternary.

3.3 Stream Terrace ('Dancing Bag')

Adjacent to the active wash is a small terrace remnant inset into the regional, Pliocene alluvium (Figure 1). We examined an exposure of this terrace created by the present wash. The profile revealed ~ 50 cm of relatively unweathered alluvium over a salt-cemented hardpan. The field interpretation of this stratigraphy is that the incising stream truncated the well-developed soil (Ewing et al., 2006) in the alluvial fan down to a restrictive layer and left an overlying cap of more recent sediment. The adjacent wash was at some point able to breach the salt-cemented layer, incise, and is now aggrading (as discussed in the previous section).

Unlike the other two sites, the ^{10}Be concentrations in the terrace are constant as a function of depth. A constant relationship between cosmogenic nuclide and depth is not uncommon in a well-mixed upland soil (Jungers et al., 2009), but it is unusual and unexpected in a physically stable surface such as an abandoned fluvial fill terrace in an abiotic environment. Previous work suggests two possible scenarios for the development of a depth-invariant cosmogenic nuclide profile:

1) Mixing of sediment by biota (gophers, ants, worms, trees, etc.) produces a constant relationship between cosmogenic nuclide concentrations and depth (Perg et al., 2001; Granger and Riebe, 2007; Jungers et al., 2009) because the timescale of mixing is significantly shorter than the time needed to develop the cosmogenic nuclide attenuation profile of Figure 2.

2) Cosmogenic nuclide concentrations in well-mixed fluvial sediment deposited very recently and rapidly will be depth-invariant since the sediment would represent an averaged sample of sediment from the eroding uplands (Anderson et al., 1996). Such a deposit must be younger than approximately 100,000 years (at this site's latitude and elevation) to have not developed a cosmogenic nuclide attenuation profile.

The setting of our stream terrace site seems to preclude both of these possibilities. First, there are no biota, a requirement of scenario 1. Second, the roughly constant cosmogenic nuclide concentration profile with depth at this terrace is similar to the concentrations observed in the modern channel, which could only be possible under scenario 2 if the terrace was deposited effectively 'yesterday'.

We approach the interpretation of this somewhat unusual TCN depth profile by leveraging our knowledge of when the modern channel incised below the terrace's surface. We have determined that the cosmogenic nuclide profile in the modern channel is best explained by a steady-state deposition rate of 2.1 m Myr^{-1}, and this requires that the channel incised below this terrace site and has subsequently been aggrading for at least 250,000 years. Using this known minimum estimate for the duration of stability for the sampled terrace, we solve equation 1 for N_0, which provides an initial condition for each of our sampled depths.

Note that $N(z,t)$ is the observed concentration for each depth in our profile. We find that the initial condition for this terrace's sediment was a steady-state deposition profile similar in form to the profile observed in the modern, aggrading channel (Figure 6). The best-fit deposition rate for the terrace's initial condition is approximately 2 m Myr^{-1}, a rate in agreement with the modern rate of 2.1 m Myr^{-1}. Thus, we infer that (1) deposition rate for this fluvial system during its previous aggradation cycle was nearly the same as the modern rate, (2) the 150 cm thick package of sediment preserved in this terrace was deposited over a period of 750,000 years, and (3) during the past ~ 250,000 years of stability, the cosmogenic nuclide concentration depth profile has transitioned from a steady-state deposition profile toward an attenuation profile, leading to a roughly depth-invariant isotopic profile. It is also possible that the terrace deposit is composed of more than one depositional unit. If deposition in the terrace was limited to the sediment above the stratigraphic discontinuity at 50 cm (the salt-cemented layer), then the inferred duration of deposition for terrace sediment is only 250,000 years prior to terrace abandonment. A process model summarizes the relationship between deposition and erosion cycles and ^{10}Be concentrations for both the low terrace and modern channel sites (Figure 7).

Further information about this profile and its sediment can be interpreted from the ^{10}Be/^{21}Ne ratios. The ^{10} Be/^{21}Ne ratios, like that of the channel, suggest complex exposure histories that would be expected from repeated reworking of sediment as it moves through this alluvial system from source to sink (Figure 4).

4.0 Conclusions

We use ^{10}Be and ^{21}Ne concentration depth profiles in a chronosequence of alluvial features in the Atacama Desert to quantify changes in the rates of surface processes and the

sources of sediment from the late Pliocene to the present. A TCN profile from a ~2 Myr alluvial fan is consistent with the rapid erosion and deposition of sediment from upland rock and saprolite exposed in the local watershed in response to the onset of hyperaridity at the Plio-Pleistocene boundary. Occasional moisture and aeolian processes reworked the upper centimeters of the fan since the Pliocene.

In contrast to the Plio-Pleistocene fans, Quaternary washes and terraces have sediment with complex exposure histories, suggestive of a reworking of soils from the ancient alluvial fans rather than a tapping of upland bedrock. A TCN profile in a modern channel reveals active fluvial aggradation of 2.1 m Myr^{-1}. On a small fluvial terrace above the modern channel that is partially incised into the adjacent ancient fans, we interpret the ^{10}Be profile to represent ~250,000-375,000 years of exposure history. Prior to terrace abandonment, the fluvial system aggraded 2 m Myr^{-1} for ~250,000 – 750,000 years before abandonment.

In summary, while fluvial activity has continued in this region of the Atacama Desert throughout the Quaternary, the nature of these processes and their rates appear to have undergone a fundamental change at approximately the Plio-Pleistocene boundary. Pre-Quaternary erosion and sedimentation linked upland bedrock and hillslopes to fluvial systems, potentially culminating in a stripping of hillslope sediment and the deposition of widespread fan complexes near the end of the Pliocene. The large alluvial deposits created in the Tertiary have largely been preserved and have experienced a nearly uninterrupted duration of soil formation via salt accumulation. In contrast, Quaternary processes have been remarkably slow and of a different nature. The Quaternary fluvial systems appear to source sediment from the ancient fans, and impact only a small fraction of the total watershed of which they are a part. The TCN concentrations within a typical Quaternary

system indicate oscillations between incision and aggradation, and these processes are ongoing under the present, hyperarid climate. The most recent erosion-deposition cycle for our study area began between 250,000 and 400,00 years ago, and we note that this is coincident with the especially cold stadials associated with MIS 10 and MIS 12 at 340,000 and 420,000 years ago, respectively (Bard and Rickaby, 2009). If the subtropical front was pushed farther north than normal during these cooler periods, then it is possible that the associated increased moisture, and likely precipitation, at 24°S could have initiated the most recent incision event for this study's fluvial system.

Acknowledgements

This work was supported by an American Chemical Society Petroleum Research Fund grant to AMH. We are grateful for the constructive reviews offered by two anonymous reviewers.

References

Ammann, C., Jenny, B., Kammer, K., Messerli, B., 2001. Late Quaternary Glacier response to humidity changes in the arid Andes of Chile (18-29 degrees S). Palaeogeography Palaeoclimatology Palaeoecology 172, 313-326.

Amundson, R., Dietrich, W., Bellugi, D., Ewing, S., Nishiizumi, K., Chong, G., Owen, J., Finkel, R., Heimsath, A., Stewart, B., 2012. Geomorphologic evidence for the late Pliocene onset of hyperaridity in the Atacama Desert. Geological Society of America Bulletin 124, 1048-1070.

Anderson, R.S., Repka, J.L., Dick, G.S., 1996. Explicit treatment of inheritance in dating depositional surfaces using in situ Be-10 and Al-26. Geology 24, 47-51.

Balco, G., Shuster, D.L., 2009. Production rate of cosmogenic Ne-21 in quartz estimated from Be-10, Al-26, and Ne-21 concentrations in slowly eroding Antarctic bedrock surfaces. Earth and Planetary Science Letters 281, 48-58.

Bard, E., Rickaby, R.E.M., 2009. Migration of the subtropical front as a modulator of glacial climate. Nature 460, 380-U393.

Bull, W.B., 2009. Geomorphic Responses to Climatic Change. The Blackburn Press, New Jersey.

Carrizo, D., Gonzalez, G., Dunai, T., 2008. Neogene constriction in the northern Chilean Coastal Cordillera: Neotectonics and surface dating using cosmogenic Ne-21. Revista Geologica De Chile 35, 1-38.

Clapp, E.M., Bierman, P.R., Nichols, K.K., Pavich, M., Caffee, M., 2001. Rates of sediment supply to arroyos from upland erosion determined using in situ produced cosmogenic Be-10 and Al-26. Quaternary Research 55, 235-245.

Dunai, T.J., Lopez, G.A.G., Juez-Larre, J., 2005. Oligocene-Miocene age of aridity in the Atacama Desert revealed by exposure dating of erosion-sensitive landforms. Geology 33, 321-324.

Evenstar, L.A., Hartley, A.J., Stuart, F.M., Mather, A.E., Rice, C.M., Chong, G., 2009. Multiphase development of the Atacama Planation Surface recorded by cosmogenic He-3 exposure ages: Implications for uplift and Cenozoic climate change in western South America. Geology 37, 27-30.

Ewing, S.A., Michalski, G., Thiemens, M., Quinn, R.C., Macalady, J.L., Kohl, S., Wankel, S.D., Kendall, C., McKay, C.P., Amundson, R., 2007. Rainfall limit of the N cycle on Earth. Global Biogeochemical Cycles 21.

Ewing, S.A., Yang, W., DePaolo, D.J., Michalski, G., Kendall, C., Stewart, B.W., Thiemens, M., Amundson, R., 2008. Non-biological fractionation of stable Ca isotopes in soils of the Atacama Desert, Chile. Geochimica Et Cosmochimica Acta 72, 1096-1110.

Gonzalez, G., Dunai, T., Carrizo, D., Allmendinger, R., 2006. Young displacements on the Atacama Fault System, northern Chile from field observations and cosmogenic Ne-21 concentrations. Tectonics 25.

Granger, D., Riebe, C., 2007. Cosmogenic nuclides in weathering and erosion. Treatise on Geochemistry: Oxford, Pergamon, 1-42.

Heusser, L., Heusser, C., Mix, A., McManus, J., 2006. Chilean and Southeast Pacific paleoclimate variations during the last glacial cycle: directly correlated pollen and delta 18O records from ODP Site 1234. Quaternary Science Reviews 25, 3404-3415.

Houston, J., 2006. Variability of precipitation in the Atacama desert: Its causes and hydrological impact. International Journal of Climatology 26, 2181-2198.

Jungers, M.C., Bierman, P.R., Matmon, A., Nichols, K., Larsen, J., Finkel, R., 2009. Tracing hillslope sediment production and transport with in situ and meteoric Be-10. Journal of Geophysical Research-Earth Surface 114.

Kober, F., Ivy-Ochs, S., Zeilinger, G., Schlunegger, F., Kubik, P.W., Baur, H., Wieler, R., 2009. Complex multiple cosmogenic nuclide concentration and histories in the arid Rio Lluta catchment, northern Chile. Earth Surface Processes and Landforms 34, 398-412.

Lal, D., Arnold, J., 1985. Tracing quartz through the environment. Journal of Earth System Science 94, 1-5.

Lamy, F., Hebbeln, D., Wefer, G., 1998. Late quaternary precessional cycles of terrigenous sediment input off the Norte Chico, Chile (27.5 degrees S) and palaeoclimatic implications. Palaeogeography Palaeoclimatology Palaeoecology 141, 233-251.

Lamy, F., Klump, J., Hebbeln, D., Wefer, G., 2000. Late Quaternary rapid climate change in northern Chile. Terra Nova 12, 8-13.

Latorre, C., Betancourt, J.L., Arroyo, M.T.K., 2006. Late Quaternary vegetation and climate history of a perennial river canyon in the Rio Salado basin (22 degrees S) of Northern Chile. Quaternary Research 65, 450-466.

Maldonado, A., Betancourt, J.L., Latorre, C., Villagran, C., 2005. Pollen analyses from a 50 000-yr rodent midden series in the southern Atacama Desert (25 degrees 30 ' S). Journal of Quaternary Science 20, 493-507.

Navarro-Gonzalez, R., Rainey, F.A., Molina, P., Bagaley, D.R., Hollen, B.J., de la Rosa, J., Small, A.M., Quinn, R.C., Grunthaner, F.J., Caceres, L., Gomez-Silva, B., McKay, C.P., 2003.

Mars-like soils in the Atacama Desert, Chile, and the dry limit of microbial life. Science 302, 1018-1021.

Nichols, K.K., Bierman, P.R., Hooke, R.L., Clapp, E.M., Caffee, M., 2002. Quantifying sediment transport on desert piedmonts using Be-10 and Al-26. Geomorphology 45, 105-125.

Nishiizumi, K., Caffee, M.W., Finkel, R.C., Brimhall, G., Mote, T., 2005. Remnants of a fossil alluvial fan landscape of Miocene age in the Atacama Desert of northern Chile using cosmogenic nuclide exposure age dating. Earth and Planetary Science Letters 237, 499-507.

Owen, J.J., Amundson, R., Dietrich, W.E., Nishiizumi, K., Sutter, B., Chong, G., 2011. The sensitivity of hillslope bedrock erosion to precipitation. Earth Surface Processes and Landforms 36, 117-135.

Perg, L.A., Anderson, R.S., Finkel, R.C., 2001. Use of a new Be-10 and Al-26 inventory method to date marine terraces, Santa Cruz, California, USA. Geology 29, 879-882.

Phillips, W.M., McDonald, E.V., Reneau, S.L., Poths, J., 1998. Dating soils and alluvium with cosmogenic Ne-21 depth profiles: case studies from the Pajarito Plateau, New Mexico, USA. Earth and Planetary Science Letters 160, 209-223.

Placzek, C.J., Matmon, A., Granger, D.E., Quade, J., Niedermann, S., 2010. Evidence for active landscape evolution in the hyperarid Atacama from multiple terrestrial cosmogenic nuclides. Earth and Planetary Science Letters 295, 12-20.

Putkonen, J., Balco, G., Morgan, D., 2008. Slow regolith degradation without creep determined by cosmogenic nuclide measurements in Arena Valley, Antarctica. Quaternary Research 69.

Quade, J., Rech, J.A., Betancourt, J.L., Latorre, C., Quade, B., Rylander, K.A., Fisher, T., 2008. Paleowetlands and regional climate change in the central Atacama Desert, northern Chile. Quaternary Research 69, 343-360.

Rech, J.A., Currie, B.S., Michalski, G., Cowan, A.M., 2006. Neogene climate change and uplift in the Atacama Desert, Chile. Geology 34, 761-764.

Rundel, P.W., Dillon, M.O., Palma, B., Mooney, H.A., Gulmon, S.L., Ehleringer, J.R., 1991. The Phytogeography and Ecology of the Coastal Atacama and Peruvian Deserts. Aliso 13, 1-50.

Stuut, J.B.W., Lamy, F., 2004. Climate variability at the southern boundaries of the Namib (Southwestern Africa) and Atacama (northern Chile) coastal deserts during the last 120,000 yr. Quaternary Research 62, 301-309.

Stuut, J.B.W., Lamy, F., 2004. Climate variability at the southern boundaries of the Namib (Southwestern Africa) and Atacama (northern Chile) coastal deserts during the last 120,000 yr. Quaternary Research 62, 301-309.

Wara, M.W., Ravelo, A.C., Delaney, M.L., 2005. Permanent El Nino-like conditions during the Pliocene warm period. Science 309, 758-761.

Zhou, J.Y., Lau, K.M., 1998. Does a monsoon climate exist over South America? Journal of Climate 11, 1020-1040.

Table

Table 2.1. Sample locations and cosmogenic nuclide concentrations

Sample ID	Latitude	Longitude	Elevation	Depth	[^{10}Be]	+/-	[^{21}Ne]	+/-
			m	cm	atoms/g_{qtz}		atoms/g_{qtz}	
CH-DB-000cm	-23.76426	-70.26296	566	0	4.38E+06	1.28E+05	4.94E+07	1.49E+06
CH-DB-050cm	-23.76426	-70.26296	566	50	4.21E+06	1.88E+05	6.97E+07	3.31E+06
CH-DB-100cm	-23.76426	-70.26296	566	100	4.20E+06	6.02E+04	6.50E+07	3.03E+06
CH-DB-150cm	-23.76426	-70.26296	566	150	4.27E+06	2.01E+05	5.57E+07	2.05E+06
CH-FM-000cm	-23.76484	-70.24759	614	0	3.73E+06	8.12E+04	5.72E+07	3.84E+06
CH-FM-025cm	-23.76484	-70.24759	614	25	3.96E+06	1.15E+05	6.24E+07	3.06E+06
CH-FM-050cm	-23.76484	-70.24759	614	50	4.27E+06	1.29E+05	6.41E+07	3.21E+06
CH-FM-075cm	-23.76484	-70.24759	614	75	4.66E+06	2.04E+05	5.30E+07	2.25E+06
CH-YG-000cm	-24.10161	-70.01829	1009	0	6.98E+06	2.41E+05	8.33E+07	4.21E+06
CH-YG-050cm	-24.10161	-70.01829	1009	50	8.31E+06	1.66E+05	8.97E+07	3.99E+06
CH-YG-100cm	-24.10161	-70.01829	1009	100	7.92E+06	1.58E+05	9.66E+07	4.09E+06
CH-YG-200cm	-24.10161	-70.01829	1009	200	7.54E+06	1.61E+05	n/a	n/a

Figure Captions

Figure 2.1. Sample sites in the hyperarid Atacama Desert of northern Chile. Modern channel and low terrace profiles are east of Antofagasta in the Central Depression. The alluvial fan profile is farther south but within the same geological framework. Inset photographs show field setting for each sample site: modern channel ('Floating Man'), low terrace ('Dancing Bag'), and alluvial fan ('Yungay'). Please see supplementary Figure S1 and the supplementary KMZ file to view higher resolution imagery of each site.

Figure 2.2. Transition from a ^{10}Be depth profile that is a function of deposition rate to a profile that is a function of exposure time and erosion rate. If sediment is steadily accumulating at a site, then ^{10}Be concentrations increase with depth according to a characteristic depositional profile defined by equation 2. If an aggrading stream incises into its alluvial bed, previously aggrading sediment becomes stable, and ^{10}Be concentrations will begin to transition toward the more familiar attenuation profile, defined by equation 1, associated with surface exposure dating of alluvial deposits (e.g., Anderson et al., 1996).

Figure 2.3. ^{10}Be depth profile for Yungay soil (error bars are 1σ analytical error) with soil profile sketch and description (Ewing et al., 2006) for context. ^{10}Be concentrations jump to higher concentrations at 50 cm below the surface, and then decay with depth. Surface concentrations are similar to those reported by Ewing et al. (2006). A best-fit exposure age for this profile using equation 1 suggests an apparent exposure age of 300,000 years.

Figure 2.4. Lal 'erosion island' plot for ^{10}Be/^{21}Ne ratios of modern channel, low terrace, and alluvial fan samples. Concentrations above the simple exposure (i.e., no erosion) line are not

possible. Steady erosion line is a continuum of steady-state erosion endpoints. Concentrations between the simple exposure curve and the steady erosion curve are within the 'island' of simple exposure and erosion. Concentrations below the steady erosion continuum are the result of repeated burial and re-exposure or constant burial. Samples from the modern channel and low terrace profiles have undergone a complex exposure history during transport within the Central Depression. Samples from the alluvial fan profile appear to have undergone only one cycle of erosion and deposition. 68% confidence ellipses for analytical error.

Figure 2.5. ^{10}Be and ^{21}Ne depth profiles for modern channel site ('Floating Man'). Cosmogenic nuclide concentrations increase as a function of depth suggesting a depositional profile (error bars are 1σ analytical error and smaller than the symbols for the ^{10}Be data). We infer a best-fit deposition rate of 2.1 ± 1.0 m Myr^{-1} for both nuclide profiles. This rate requires a minimum period of aggradation of 250,000 years for this site (i.e., 0.5 m * Myr/2.1 m). Error bars are 1σ analytical uncertainty.

Figure 2.6. The initial condition (pre-abandonment) for sediment at our low terrace site is determined by leveraging our knowledge of how long the adjacent channel has been aggrading subsequent to its incision below the terrace level. Solving equation 1 for N_0 finds the pre-incision ^{10}Be concentrations for each sample depth (C). This initial condition is essentially the result of subtracting the amount of ^{10}Be produced during terrace stability (B) from the observed ^{10}Be profile (A). Since 250,000 years of exposure is a minimum estimate derived from the modern channel cosmogenic nuclide depth profile, we also include two longer exposure scenarios. However, initial conditions inferred from the 500,000 and

750,000 year exposure scenarios suggest deposition profiles that are not reasonably explained by equation 2 – i.e., they would require deposition rates one to two orders of magnitude slower than even the very slow rates we observe at our modern channel site. The best fit deposition rate for the initial condition inferred from the 250,000 year exposure scenario is 2 m Myr^{-1}.

Figure 2.7. Process model for the relationship between the modern channel site ('Floating Man' or FM) and the adjacent low terrace ('Dancing Bag' or DB). Note that for this model we include the deepest sample from the FM profile, so aggradation in the modern channel begins at 375,000 years before present. Prior to 375,000 years, the fluvial system had incised into Tertiary fill deposits, and subsequently aggraded for as long as 750,000 years to produce the initial condition for the DB ^{10}Be profile (A). At 375,000 years, the fluvial system incised below the DB terrace, and aggradation began. By 250,000 years b.p. (B), 25 cm of sediment has aggraded in the modern channel and a steady-state deposition profile is developing for ^{10}Be in the FM sediment (dashed line). ^{10}Be concentrations in the terrace sediment (solid line) are transitioning from a deposition profile to an attenuation profile following 125,000 years of stability. At present (C), 75 cm of sediment has accumulated in the modern channel, and continued deposition maintains a deposition profile for the ^{10}Be in the FM sediment (open boxes are observed concentrations, dashed line is modeled concentrations). ^{10}Be concentrations in the low terrace sediment (DB) continues transitioning toward an attenuation profile diagnostic of surface stability (closed boxes are observed concentrations, solid line is modeled concentrations). Error bars represent 1σ analytical uncertainty.

Figures

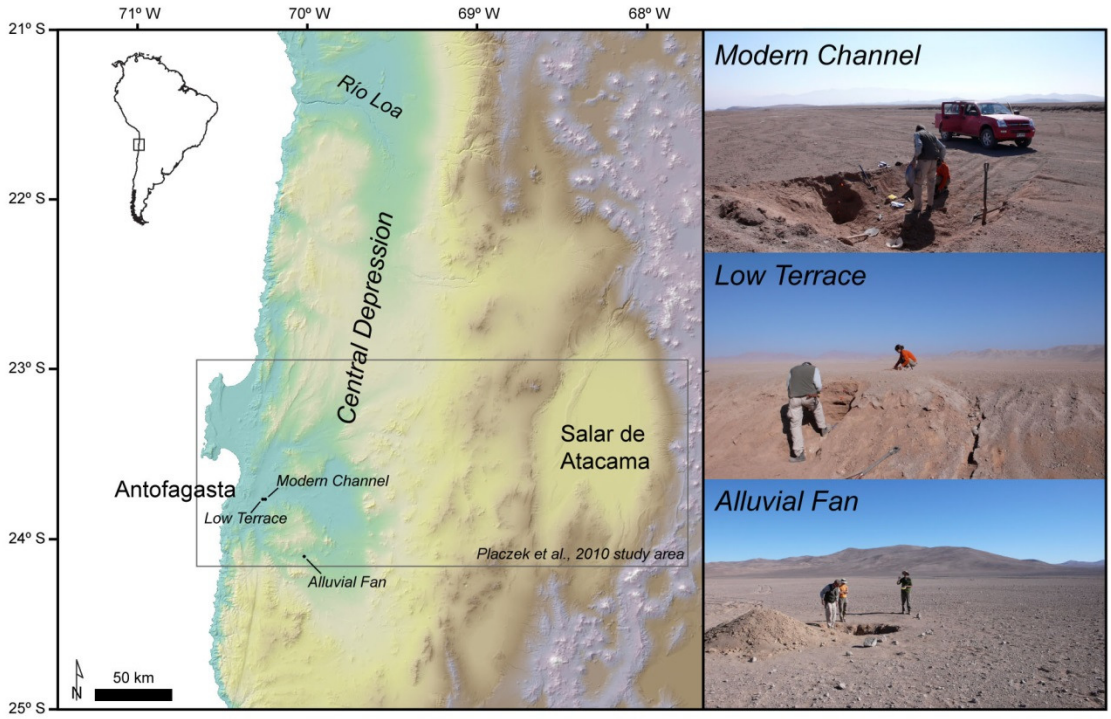

Figure 2.1

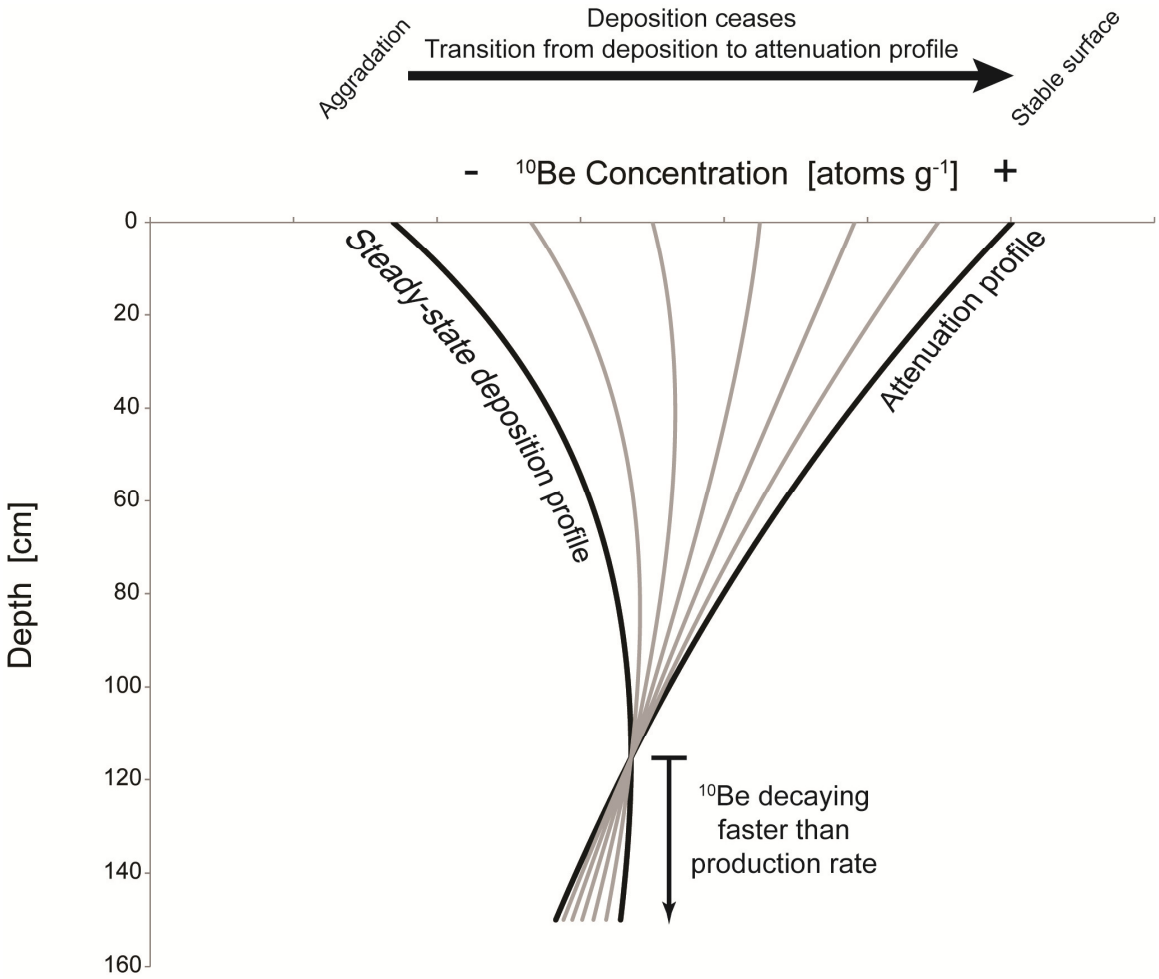
Aggradation
Deposition ceases
Transition from deposition to attenuation profile
Stable surface
- ^{10}Be Concentration [atoms g^{-1}] +
Depth [cm]
0
20
40
60
80
100
120
140
160
Steady-state deposition profile
Attenuation profile
^{10}Be decaying faster than production rate

Figure 2.2

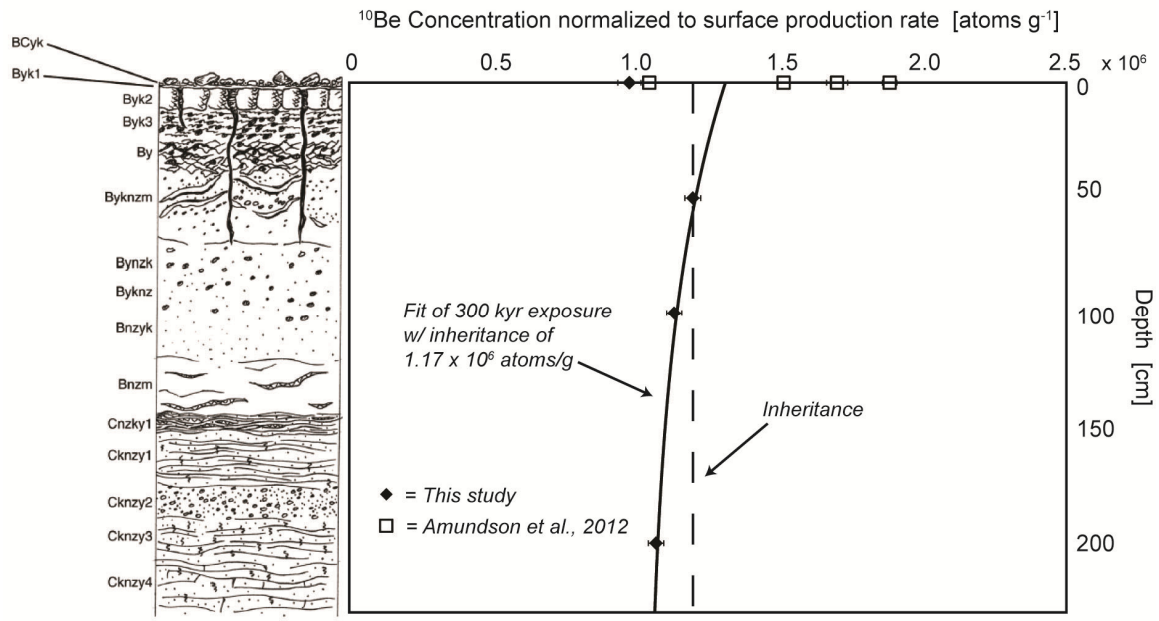
^{10}Be Concentration normalized to surface production rate [atoms g^{-1}]
0
0.5
1.0
1.5
2.0
2.5
x 10^6
0
50
100
150
200
Depth [cm]
BCyk
Byk1
Byk2
Byk3
By
Byknzm
Bynzk
Byknz
Bnzyk
Bnzm
Cnzky1
Cknzy1
Cknzy2
Cknzy3
Cknzy4
Fit of 300 kyr exposure w/ inheritance of 1.17 x 10^6 atoms/g
Inheritance
= This study
= Amundson et al., 2012

Figure 2.3

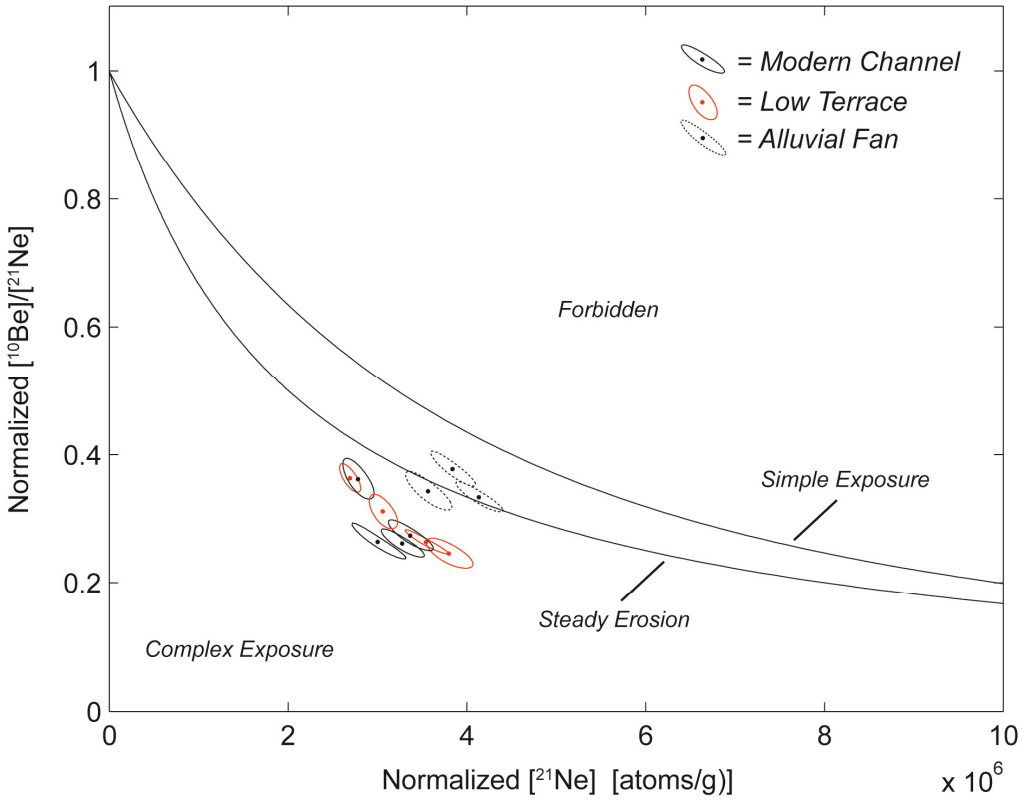
= Modern Channel
= Low Terrace
= Alluvial Fan
Forbidden
Simple Exposure
Steady Erosion
Complex Exposure
Normalized [10Be]/[21Ne]
Normalized [21Ne] [atoms/g)]
x 10^6
0
0.2
0.4
0.6
0.8
1
0
2
4
6
8
10

Figure 2.4

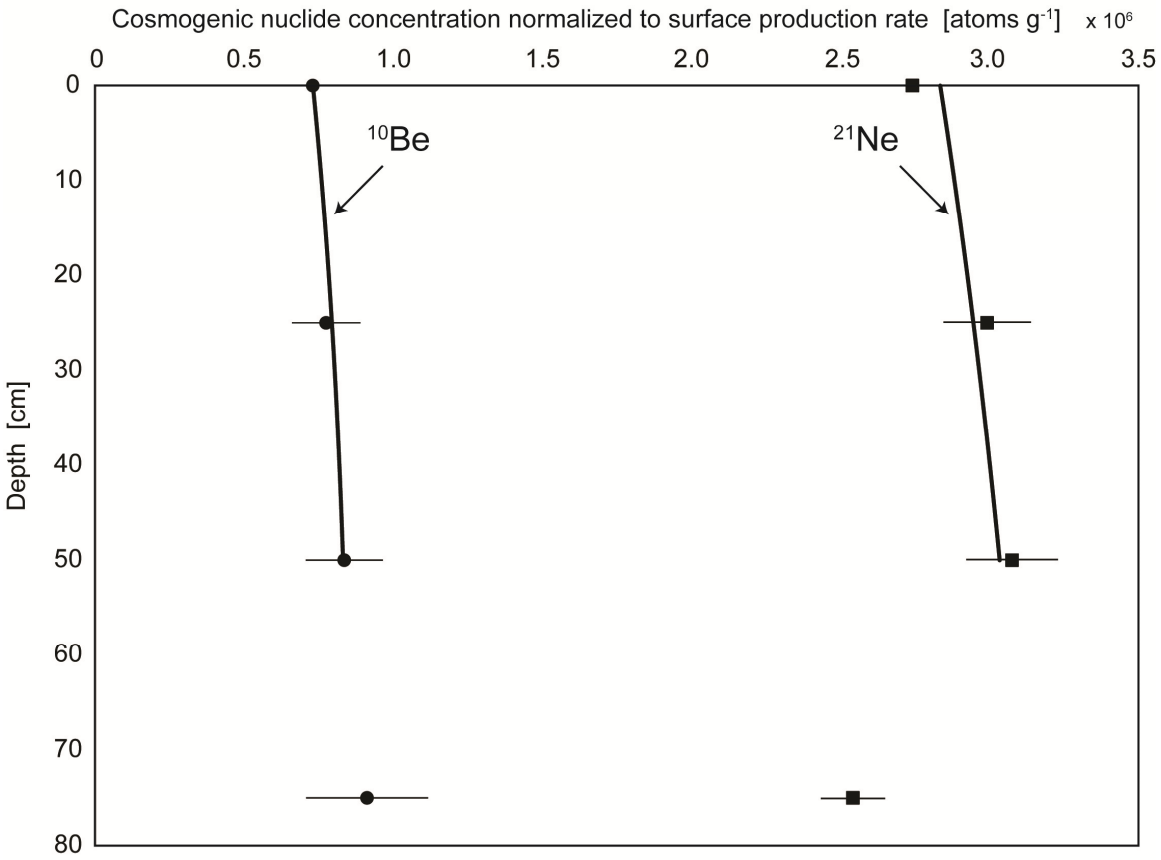
Cosmogenic nuclide concentration normalized to surface production rate [atoms g-1] x 10^6
0
0.5
1.0
1.5
2.0
2.5
3.0
3.5
Depth [cm]
0
10
20
30
40
50
60
70
80
10Be
21Ne
Figure 2.5

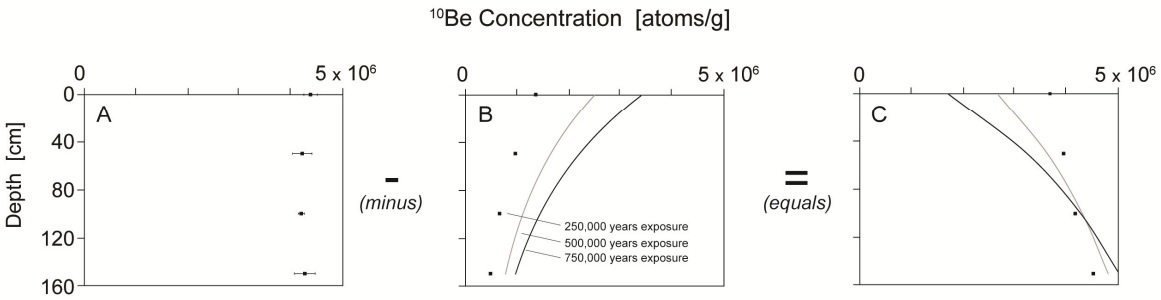
^{10}Be Concentration [atoms/g]
0
5 x 10^6
Depth [cm]
0
40
80
120
160
A
(minus)
B
250,000 years exposure
500,000 years exposure
750,000 years exposure
(equals)
C
Figure 2.6

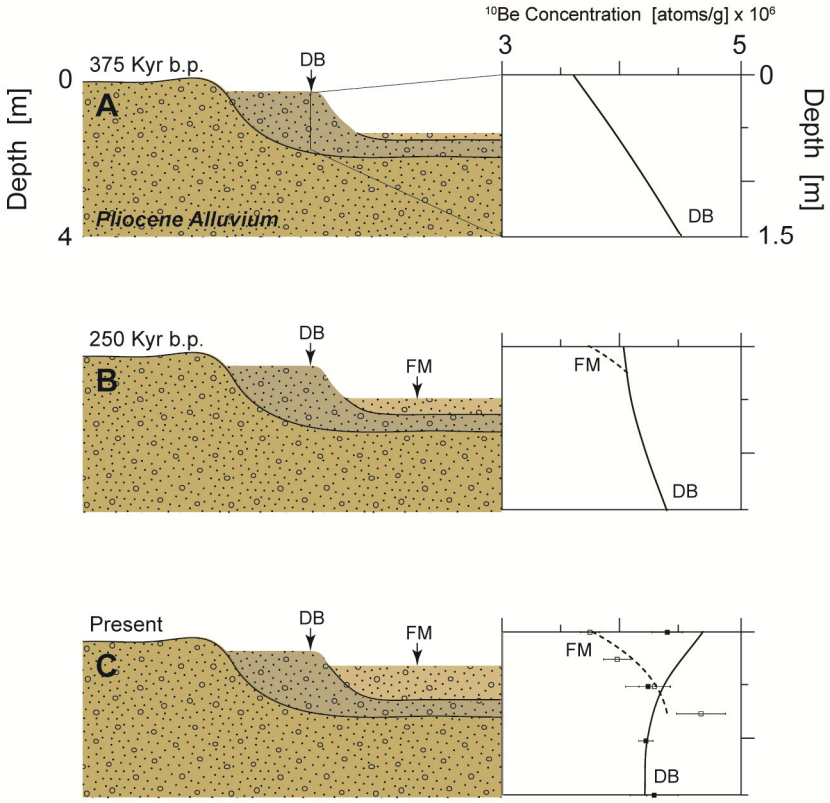
^{10}Be Concentration [atoms/g] x 10^6
3
5
0
0
Depth [m]
Depth [m]
375 Kyr b.p.
DB
A
Pliocene Alluvium
4
1.5
DB
250 Kyr b.p.
DB
FM
B
FM
DB
Present
DB
FM
C
FM
DB

Figure 2.7

CHAPTER 3

Complex Exposure Histories in Alluvial Deposits of the Atacama Desert, Northern Chile

Matthew C. Jungers, Arjun M. Heimsath, Ronald Amundson, Greg Balco, David Shuster

Abstract

The climate history of the Atacama Desert of northern Chile is intimately linked to geologic questions such as the tectonic history of the Andes, and to economic interests such as the formation and preservation of rich supergene copper deposits. As a result, there have been several recent efforts to constrain the age of relict landforms in the Atacama Desert using terrestrial cosmogenic nuclides in the hope that these dates will help clarify the climate history of the region. These studies report some of the oldest dates and slowest erosion rates ever quantified using cosmogenic nuclides, which calls into question whether any fundamental assumptions behind the application of cosmogenic nuclides are being violated. We report a suite of ^{10}Be and ^{21}Ne abundances in alluvial sediment that record a history of complex exposure and significant inheritance of stable cosmogenic nuclides that complicates any simple interpretation of nuclide abundances in terms of surface process rates or landform dates. We evaluate the magnitude of inheritance at each of our sample sites, and we offer a first order attempt to quantify how many cycles of burial and re-exposure each sample may have undergone. We strongly recommend that any future studies of landscape evolution in the Atacama Desert use a multiple nuclide approach and explicitly account for inherited cosmogenic nuclide abundances if calculating surface exposure dates.

1.0 Introduction and Motivation

The Atacama Desert of northern Chile is a landscape developing under one of the driest climates on Earth, adjacent to one of the planet's largest, actively deforming mountain ranges, the Andes. The desert is also host to rich mineral deposits – the nitrate mines of the 19th and 20th centuries, and some of the largest active copper mines globally – which owe their origin to feedbacks between the region's active tectonics and a climate that transitioned to hyperarid sometime in the last 30 Myr (Mortimer, 1980; Alpers and Brimhall, 1988; Hartley and Chong, 2002; Amundson et al., 2012). Since the timing of the onset of hyperaridity has potentially important implications for the continental scale tectonics of the Andes, global atmospheric and oceanic circulation patterns, and the emplacement and preservation of economic deposits, much work strives to refine the ages of deposits that bracket the timing of climate change in the Atacama Desert. Studies of landscape evolution in the Atacama Desert also enrich our understanding of how hillslope and fluvial processes produce and transport sediment under such dry conditions, with potential implications for landscape evolution models, geomorphic transport laws, and analogies between surface processes on Earth vs. Mars. Over the last 10-15 years numerous studies employing both radio- and stable terrestrial cosmogenic nuclides (TCN) have sought to date relict landforms of the desert that potentially preserve past response to shifting climate while at the same time quantifying rates of surface processes in a hyperarid climate (Nishiizumi et al., 2005; Dunai et al., 2005; Gonzalez et al., 2006; Kober et al., 2007; Carrizo et al., 2008; Hall et al., 2008; Evenstar et al., 2009; Placzek et al., 2010; Owen et al., 2011; Jungers et al., 2013; Rodriguez et al., 2013). TCN-derived erosion rates from the Atacama Desert are some of the slowest measured on Earth, and apparent exposure ages

reach back to the Oligocene, reflecting the potential for the preservation of very old landforms under such slow erosion rates (Dunai et al., 2005). However, these intriguingly slow rates and old dates do suggest the possibility that some necessary assumptions for the application of TCN techniques – both the use of TCN for geochronology and as a tracer for rates of surface processes (Gosse and Phillips, 2001) – may be violated in the Atacama Desert, and extra care should be taken by anyone endeavoring to apply 'standard techniques' to this important landscape.

We collected both surface samples and samples at depth to evaluate the potential for complex exposure for alluvial deposits and the significance of inherited TCN abundances in interpreting surface concentrations. Based on complicated ^{21}Ne and ^{10}Be ratios from suites of samples collected between latitudes 21-24°S, we argue that a multiple nuclide approach to TCN studies is most appropriate for work in the Atacama Desert, with a special emphasis on the need for multiple nuclides if a stable TCN such as ^{21}Ne or ^{3}He is to be employed. We contextualize our results with the multiple nuclide approaches of others (e.g., Nishiizumi et al., 2005; Kober et al., 2007; Kober et al., 2009), and evaluate the potential pitfalls of past and future studies that make no attempt to evaluate the pre-deposition exposure history of alluvial deposits. An understanding of landscape evolution in the Atacama Desert from the Miocene to the present has significant implications for our models of global tectonics and climate, as well as economic implications. Extra care should be taken when applying cutting edge TCN methodologies to sites that are not ideal for the techniques.

2.0 Background

2.1 Geologic and Climatic Setting

The Atacama Desert spans approximately 8-10 degrees of latitude within the structurally defined Central Depression of Northern Chile. Three factors are commonly cited as the cause for the region's extreme lack of precipitation: (1) the rain shadow of the Andes to the east, blocking moisture from the Atlantic Ocean; (2) the region's position within the subtropical high-pressure belt; and (3) the upwelling of cold water to the west related to the Pacific Ocean's Humboldt current (e.g., Houston, 2006). Additionally, the Coastal Cordillera between the Central Depression and the Pacific Ocean minimizes the amount of moisture that can reach the Atacama. A north-south gradient in mean annual precipitation sets the boundaries of ecosystems. The hyperarid north (19°-23°S) is largely abiotic, and increasing fog and precipitation from 26°-29°S enables vegetation to begin taking hold near the southern extent of the desert (Navarro-González et al., 2003; Rundel et al., 1991; Owen et al., 2010).

Our study is focused within the hyperarid central Atacama Desert, between 21°-24°S (Figure 1), an area that now experiences minimal winter rainfall (< 3 mm yr^{-1}) sourced from the Pacific Ocean. Specifically, we centered our study around 24°S latitude, near a boundary between moisture effects from two wind belts, the southern westerlies and the tropical easterlies (Maldonado et al., 2005). North of 24°S, most of the moisture carried by the tropical easterlies is excluded from the northern Atacama Desert by the rain shadow of the Andes. During the summer, however, convective precipitation related to the South American Summer Monsoon can deliver moisture to the eastern edge of the northern Atacama Desert (Zhou and Lau, 1998; Ammann et al., 2001; Placzek et al., 2010). South of 24°S, precipitation thus increases with latitude and is delivered

primarily in the form of winter precipitation from Pacific fronts and cutoff lows (Vuille and Ammann, 1997; Latorre et al., 2006; Placzek et al., 2010). The rare precipitation events that have delivered the minimal rainfall recorded near 24°S are most likely attributed to the interception of these cold air masses by increasingly high topography to the east of the Central Depression (Vuille and Ammann, 1997; Placzek et al., 2010). Any past shift in the boundary between these two moisture regimes would be significant to processes active across our study sites since they are near the modern boundary. Independent studies of the late Quaternary paleoclimate of northern Chile suggest that the northernmost boundary of Pacific-derived moisture has shifted toward the equator during recent glacial periods (Lamy et al., 1998; Lamy et al., 2000; Stuut and Lamy, 2004; Maldonado et al., 2005; Heusser et al., 2006). It is therefore possible that the magnitude of precipitation fluctuated to levels higher than the present for hyperarid sites located from 22-24°S, including our study area.

2.2 Apparent Exposure Ages and Erosion Rates from TCN in the Atacama Desert

A detailed chronology for Miocene development of the Western Cordillera bounding the eastern edge of the Atacama Desert is derived from detailed geochronologic and stratigraphic studies of ignimbrites that ramp down from the edge of the Altiplano to the margin of the Central Depression (e.g., Mortimer, 1973). Early studies employing TCN in the Atacama Desert (Nishiizumim et al., 2005) focused on Plio-Pleistocene alluvial deposits and their relationship to planation surfaces (Mortimer, 1973) developed into the aforementioned Miocene stratigraphy.

Nishiizumi et al. (2005) used as multiple nuclide approach, measuring ^{10}Be, ^{26}Al, and ^{21}Ne in quartz-rich cobbles on the surface of alluvial fan remnants in the southern Atacama Desert (~26°S).

Their measurements are the first terrestrial application of a multiple nuclide approach although the technique had been previously applied to meteorites (Herzog et al., 1997). The inclusion of a stable nuclide such as ^{21}Ne in such an approach is especially appealing for a landscape evolving as slowly as the Atacama Desert since the stable nuclide can theoretically record an infinite duration of exposure since TCN production will never reach secular equilibrium with some rate of nuclide decay (Niedermann, 2002). However, in practice, exposure dating with stable nuclides does have an upper practical age limit that is a function of local TCN production rates and even minimal surface denudation which will produce an equilibrium concentration (and an associated minimum apparent exposure age and maximum denudation rate). Importantly, because stable TCN do not decay once they are produced in mineral grain, they can record the production of TCN over several episodes of exposure-burial-exposure while radionuclides will decay away to lower abundances once shielded from TCN production. Nishiizumi et al., report some of the slowest surface erosion rates determined up to the date of their publication, uniformly <0.1 m/Myr. The oldest date that they report is for a cobble is 9 Myr based on its ^{21}Ne/^{26}Al , and they assert that this supports previous assertions for a Mid-Miocene onset of hyperaridity. One other sample had a ^{21}Ne/^{26}Al that required some degree of complex exposure, so the authors do not assign it a simple apparent exposure age. For these alluvial fan remnants, the authors did not quantify what proportion of measured TCN abundances were produced prior to the deposition of the cobbles (commonly referred to as the 'inherited' concentration; Anderson et al., 1996). Therefore, we cannot evaluate whether their apparent exposure ages overestimate the antiquity of the landforms.

A suite of samples collected in the northern Atacama Desert (19.5°S), on the surface of landforms interpreted to be abandoned alluvial fan surfaces perched above the Quebrada de

Tiliviche, analyzed for only ^{21}Ne yielded apparent exposure ages ranging from 9 – 37 Myr, with populations of amalgamated samples clustering at 25, 24, and 14 Myr (Dunai et al., 2005). The authors suggest that these results support a potential Oligocene onset for the transition of hyperaridity in the Atacama Desert, and further assert that this may support the hypothesis that arid conditions helped initiate the uplift of the Andes (Lamb and Davis, 2003). The authors did not measure multiple nuclides, so there is no potential to assess whether the highest measured ^{21}Ne concentrations are the cumulative result of several generations of exposure during sediment transport, storage, and remobilization prior to deposition. Dunai et al. do include a discussion of their attempt to account for inheritance from pre-exposure. At one of their four sites, they collected a surface sample and a sample at depth (90 cm) in order to quantify how much inheritance needed to be corrected for at that site. Inheritance accounted for ~52% of the surface concentration, although in reporting an apparent exposure age for the site in their Data Repository, they do not seem to correct for inheritance before modeling an exposure age. With no correction, the site is appears to have been stable for 120 kyr, but if inheritance is included then the site's apparent exposure age is closer to 67 kyr. The authors do not include this 67-120 kyr site in their discussion of the landscape evolution surrounding Quebrada de Tiliviche, but they do state that if they apply this inheritance to all their sites it does not significantly affect the distribution of predominantly Miocene dates. This approach is good in the sense that they make an effort to account for inheritance, but it is flawed since they do not have site specific estimates for inheritance. If inheritance scaled similarly at each site – i.e., ~50% of surface concentrations – then the implications for this work would be significantly different in terms of feedbacks between climate and the uplift of the Andes. The authors clearly state that they don't believe that inheritance at other sites would

exceed >1 Myr of exposure equivalent, but without at least one other nuclide, there is no way to assess the potential for multiple rounds of pre-exposure.

Evenstar et al. (2009) conducted another important study of Atacama Desert landscape evolution slightly south (19.7°S) and east from Dunai et al.'s Tiliviche site, investigating the potential for different stages of planation along the western flank of the Western Cordillera. These authors sampled populations of boulders for surface exposure date derived from ^{3}He in mafic minerals. Apparent exposure ages range from 1.2 – 22 Myr, with what the authors identify as clusters of ages at ~14.6, 7, and 3 Myr. The 22 Myr date is older than the stratigraphy into which the planation surface is developed, so it is discarded from the discussion of a multi-stage development of the Atacama Planation Surface at this latitude. The authors conclude that initial abandonment of the planation surface initiated at 14.6 Myr, coincident with the onset of hyperaridity, and subsequent younger portions of the planation surface are related to climate shifts driven by ice sheet development in Antarctica. In addition to relating the multiple phases of planation surface development to climate forcing, the authors assert that due to the multi-phase nature of the planation surface it should not be used as a chronostratigraphic datum for studies investigating the uplift history of the Western Cordillera (e.g., Hoke et al., 2007). Evenstar et al. only mention the potential for inheritance in samples that they discard as stratigraphically unreasonable. As mentioned previously, dates older than 16.5 are not possible since they are apparently older than the underlying ignimbrites. Other populations of dates are not corrected for inheritance despite this apparent potential for up to 6 Myr of exposure equivalent inheritance. Considering the enhanced potential for multiple stages of inheritance in the development of stable TCN abundances like ^{3}He, the apparent

exposure ages reported for this study could be overestimates by several million years, and their relationship to global climate forcing would be more complicated than the authors present.

Other studies in northern Chile do make an effort to carefully account for the potential of complex transport histories and the associated significant inheritance that must be taken into consideration when modeling apparent exposure ages from stable TCN (Gonzalez et al., 2006; Kober et al., 2007; Kober et al., 2009). Gonzalez et al. focused on dating offset alluvial fans to constrain the Pleistocene activity along the Atacama Fault System (AFS) that bounds the Central Depression at ~23.5°S, while Kober et al. focus on rates of landscape evolution in the Rio Lluta catchment at ~19°S.

At their sites, Gonzalez et al. report difficulty in collecting enough quartz-rich material at depth to quantify inheritance via a concentration depth profile (Anderson et al., 1996). The authors remedy this problem by collecting modern sands and clasts from channels that incise the offset, abandonded fans, and making the assumption that upland erosion rates have likely been slow and steady at these sites such that modern, catchment-averaged ^{21}Ne abundances serve as a good proxy for pre-deposition inheritance in fan sediment. Using this approximation for inheritance, Gonzalez et al., correct ^{21}Ne abundances in surface clasts for pre-deposition exposure and apparent exposure ages are shifted from >1 Myr to much younger inferred ages of 0.1-0.4 Myr with significant implications regarding the timing and magnitude of displacement along the AFS.

When considered in conjunction with one another, the 2007 and 2009 studies of Kober et al. in the Rio Lluta catchment represent the most fully integrated investigation of landscape evolution utilizing TCN yet published for northern Chile. First, the authors use ^{21}Ne, ^{26}Al, and ^{10}Be to quantify bedrock erosion rates of headwater interluves. The authors find that in general, erosion rates are

lowest (<0.1 m/Myr) at lower elevations in the Atacama Desert, and rates increase to a maximum rate of 4.6 m/Myr at higher altitudes in the Western Cordillera. This increase in erosion rates with altitude is taken to be a function of increasing precipitation across the transition from the hyperarid lower elevations to semi-arid conditions in the Western Cordillera. Kober et al. (2007) also report a ^{10}Be and ^{21}Ne concentration depth profile into an ignimbrite, one of three studies that report TCN concentrations at depth for any sites in northern Chile (Dunai et al., 2005; Kober et al., 2007; Jungers et al., 2013). In their 2007 study, Kober et al. effectively define a baseline for background rates of sediment generation in the headwaters of their site, and the associate single nuclide TCN abundances and TCN ratios. Kober et al. (2009) report catchment-averaged erosion rates from the Rio Lluta catchment derived from ^{21}Ne, ^{26}Al, and ^{10}Be as well as TCN ratios from multiple nuclide analyses in individual sample. The authors find a range of erosion rates from 12-75 m/Myr with an apparent trend of increasing erosion rate downstream. TCN ratios reveal complex exposure histories that may be attributed to increasing likelihood of 1ong term sediment storage in fill terraces at greater distances downstream within the Rio Lluta. Since ^{21}Ne does not decay during these periods of storage the authors infer infer that it maintains the most representative TCN abundance with respect to upland erosion rates. The radionuclides decay significantly during storage, and then when reworked into the Rio Lluta's active sediment load, they dilute the overall ^{10}Be and ^{26}Al abundances generating an apparently faster TCN-derived upland erosion rate. Both studies in the Rio Lluta provide important lessons for the application of TCN to the study of landscape evolution in northern Chile. First, complex exposure of sediment must be accounted for when attempting to quantify catchment-averaged erosion rates from sand transported by large rivers that head in the Western Cordillera and drain across the Central Depression into the Pacific Ocean. Studies that rely

on just ^{10}Be and ^{26}Al are especially susceptible to overestimating erosion rates in this setting. Second, the relatively constant ^{21}Ne abundances in sediment that have experience several generations of exposure-burial-exposure suggest that complex exposure does not necessarily produce a monotonic increase in stable nuclides as a function of increasing number of re-exposure cycles. This last point should temper some of the concerns mentioned above regarding incomplete considerations of inheritance by Dunai et al. (2005) and Evenstar et al. (2009). However, other recent work in the Central Depression report ^{21}Ne/^{10}Be that suggest significant accumulation of stable TCN over several generations of complex exposure during still active erosion-deposition cycles (Jungers et al., 2013). New data reported in this paper build off the results of Jungers et al., and underscore some of the pitfalls of using single nuclide analysis of stable nuclides to model apparent exposure ages.

3.0 Methods

At each site, we collected sediment and clasts at the surface, and, when possible, at regular intervals from the surface to depths of up to 500 cm. The CH-09-xx sample series are suites of surface clasts (>45 clasts per suite) collected from subtle, abandoned surfaces adjacent to the incised Rio Loa (analogous to the sites sampled by Dunai et al., 2005, adjacent to Quebrada de Tiliviche). CH-DB, CH-FM, and CH-YG are concentration depth profiles from a chronosequence of landforms southeast of Antofagasta. The specific motivation for these three sample suites are explained in great deal by Jungers et al. (2013). The CH-R and CH-R2 samples represent two suites of samples collected at depth, exploiting a railroad cut. CH-SQ1 and CH-SQ2 are two concentration depth profiles collected within meters of one another within a gravel quarry. Samples were first sieved to extract the 250-1000 μm fraction, and pebbles larger than 1000 μm were then crushed and

sieved to bulk up the total amount of sample in the 250-1000 μm range since samples were not quartz-rich. We then isolated quartz via cleaning in aqua regia and subsequent etching in HF and HNO_3. We extracted ^{10}Be through column chromatography, and $^{10}Be/^{9}Be$ ratios were measured via accelerator mass spectrometry at the Purdue Rare Isotope Measurement Laboratory at Purdue University. Table 3.1 shows complete results. Note that the concentration depth profiles for CH-R, CH-R2, CH-SQ1, and CH-SQ2 are incomplete because some depth intervals from each sample suite did not yield enough quartz for measurement. Other researchers in this region of the Atacama Desert have reported similar difficulties with quartz yield (Gonzalez et al., 2006).

We measured cosmogenic ^{21}Ne at the Berkeley Geochronology Center by encapsulating 150 mg aliquots (of the same purified quartz analyzed for ^{10}Be) in a Ta packet, heating them under vacuum using a 150 W diode laser, purifying the released gas by reaction with hot and/or cold getters and cryoseparation of Ne from other noble gases, and analyzing the resulting Ne in a MAP-215-50 mass spectrometer. Balco and Shuster (2009) describe analytical details. Ne isotope ratios in all steps were indistinguishable from a two-component mixture of atmospheric and cosmogenic neon, so we computed cosmogenic Ne concentrations on this basis. Analyses of the CRONUS-A quartz standard during the period of these measurements yielded a cosmogenic ^{21}Ne concentration of $338.9 \pm 3.8 \times 10^{6}$ atoms g^{-1}.

4.0 Results

Nearly all of our samples have higher $^{21}Ne/^{10}Be$ ratios than can be explained by simple exposure or steady erosion (Figure 3.2). Therefore, ^{10}Be concentrations may be representative of a most recent round of exposure to TCN production, but ^{21}Ne abundances are the product of an

unconstrained number of exposure events (Lal, 1991). Concentration depth profiles for CH-SQ1, CH-SQ2, CH-R, and CH-R2 are incomplete due to low quartz yields, and thus they cannot be used to model surface exposure ages (Figure 3.4). Concentration depth profiles for CH-DB, CH-FM, and CH-YG can be interpreted via TCN and process models, the details of which are presented in Jungers et al., 2013 (Chapter 2 above). One sample, CH-09-06, collected from a surface that grades to the degraded shoreline of a Miocene salt flat, does plot along the continuum of steady-erosion (Figure 3.2). This sample cannot be interpreted in terms of an apparent exposure age, but it does suggest an incredibly slow surface denudation rate of 0.07 m/Myr (^{10}Be) or 0.06 m/Myr (^{21}Ne).

Despite the complexity revealed by ^{21}Ne/^{10}Be ratios and poor quartz yields our samples from depth still represent some of only a very few measurements of potential TCN inheritance in alluvial deposits of the Atacama Desert (Dunai et al., 2005; Kober et al., 2007; Jungers et al., 2013). Although the concentration depth profiles do not follow an exponential relationship with depth expected from the attenuation of TCN production beneath Earth's surface, we believe it is nonetheless useful to still report how ^{10}Be concentrations at depth compare to surface concentrations. For CH-SQ, samples from depth range from ~25-75% of the surface concentrations with one sample, CH-SQ-500cm-2, containing 150% of the surface concentration. This very high concentration at 500 cm depth likely represents either contamination of the sampled strata by sediment from above, or unintentional sampling of the top of some buried deposit (cf., Nichols et al., 2002) rather than a measure of inheritance. For the CH-R samples, ^{10}Be concentrations at depth are 72-96% of the surface concentrations. These results suggest the potential for significant inheritance of radionuclides such as ^{10}Be in Atacama Desert sediments, and the evidence for

cumulative stable TCN production revealed by our $^{21}Ne/^{10}Be$ suggests that inheritance of stable TCN is an even more significant concern. The implications for our results are discussed below.

5.0 Discussion

Our samples from the Central Depression of northern Chile's Atacama Desert between the latitudes of 21-24°, record a story of complex exposure to TCN production that makes it impossible to interpret the results using any standard assumptions of simple exposure or steady erosion commonly used in the inversion of TCN abundances for dates and process rates. Our results are significantly more complex than the results of other studies that analyzed rock and sediment for $^{21}Ne/^{10}Be$ in the Atacama Desert (Figure 3.3). We cannot directly compare our results to studies that report just one nuclide (e.g., Dunai et al., 2005). Previous work in other landscapes successfully explained complex TCN exposure histories using relatively simple process models such as intermittent shielding by ice (Bierman et al., 1999) or long-term shielding by loess that is then quickly stripped away (Riihimaki et al., 2006). Although individual suites of our samples do have roughly similar $^{21}Ne/^{10}Be$ (Figure 3.2), we cannot in good conscience invoke some simple process of shielding or predictably periodic burial and re-exposure. Even our concentration depth profiles that record active erosion-deposition cycles (CH-FM and CH-DB) have $^{21}Ne/^{10}Be$ ratios that are as much a function of sediment sourcing as they are a function of cyclic burial and reworking. However, we can present a simple approach to compare the magnitude of complex exposure from sample to sample, and give a rough estimate of how many cycles of re-exposure a sample may have experienced.

The $^{21}Ne/^{10}Be$ ratios that we find for our samples are the result of ^{10}Be decay during any period of shielding from TCN production. ^{21}Ne is stable and thus abundances of this TCN can only cumulatively increase through time. Kober et al. (2009) experienced similar results with alluvium collected from the Rio Lluta where radionuclides were decaying during storage of sediment in fill terraces leading to a decrease in ^{10}Be concentrations down system. The resulting $^{21}Ne/^{10}Be$ ratios can be seen in Figure 3.3. If we make the assumption that nearly all ^{10}Be decays away during each deposition event (an assumption difficult to fully support or refute), then the ^{10}Be that we measure in our samples is the product of just the most recent exposure event. If we use our measured ^{10}Be to solve for an erosion rate associated with that TCN abundance (Equation 1 below), then we can subsequently calculate how much ^{21}Ne should have been produced during the most recent exposure event (Equation 2):

$$\varepsilon = \frac{\Lambda}{\rho}\left(\frac{P_{10}}{N_{10}} - \lambda_{10}\right), \qquad (1)$$

$$N_{21} = \frac{P_{21}}{\frac{\rho\varepsilon}{\Lambda}}\ , \qquad (2)$$

where ε is erosion rate [cm/yr], Λ is attenuation length for TCN production [g/cm^2], ρ is density [g/cm^3], P_{10} is the site-specific surface production rate for ^{10}Be [atoms/g yr^{-1}], N_{10} is measure ^{10}Be concentration [atoms/g], λ_{10} is the decay constant for ^{10}Be [yr^{-1}], N_{21} is the inferred ^{21}Ne concentration for the recent round of exposure [atoms/g], and P_{21} is the site-specific surface production rate for ^{21}Ne [atoms/g yr^{-1}]. It is incredibly important to note that the erosion rate we calculate with Equation 1 using this approach does not have any true relationship to modern upland erosion rates since we don't know how much ^{10}Be decayed away during the last burial event. We are

simply using this erosion rate as a proxy to predict how much ^{21}Ne we would have expected to find in our sample. The difference between this predicted ^{21}Ne and our measured ^{21}Ne we will call 'excess' ^{21}Ne, and it is the cumulative product of earlier exposure events. Dividing each sample's excess abundance of ^{21}Ne by the predicted ^{21}Ne from one round of exposure (Equation 2) gives a first order approximation for how many rounds of exposure a given sample of sediment has undergone. We conducted this analysis for our samples that we infer have experienced complex exposure histories and found that our samples have undergone a range of previous exposure cycles from one previous exposure up to eight. CH-SQ-300cm-2 has an excess abundance of ^{21}Ne that suggests 28 previous cycles of exposure, which strikes as us as unlikely given the other samples' histories. The full results of our analysis can be found in Table 2. Given the complexity of our data, we feel that this approach is the most transparent translation of somewhat confounding exposure histories into a meaningful context with respect to geomorphic processes. It is not possible to perfectly constrain what ratio of exposure time to burial duration produced the nuclide abundances we measured, but we can leverage our results from CH-DB and CH-FM to approximate complex exposure paths (Jungers et al., 2013). The active erosion deposition cycles that these samples are undergoing take place on the timescale of 0.25-1.0 Myr, and if we plot several cycles of burial:exposure across that time frame, we develop complex exposure paths that capture our measured abundances (Figure 3.5).

6.0 Conclusions

Our suite of confoundingly complex ^{21}Ne/^{10}Be ratios and ^{10}Be concentrations at 100-400 cm depth that are >50% surface concentrations underscore the necessity for multiple TCN approaches

to questions of landscape evolution in the Atacama Desert, and attempts to use TCN for surface exposure dating must explicitly account for inherited TCN abundances. This last point is especially important for surface exposure dates determined via stable TCN. For our samples, it was common for samples to undergo at least one previous cycle of burial and re-exposure, and ^{21}Ne abundances are the cumulative product of these sediment cycles. If we had taken our ^{21}Ne data at face value with no additional context provided by ^{10}Be, we would have incorrectly reported apparent exposure ages for some of our dated surfaces suggesting stability since the Mid-to-Late Miocene.

References

Alpers, Charles N., and George H. Brimhall. "Middle Miocene climatic change in the Atacama Desert, northern Chile: Evidence from supergene mineralization at La Escondida." *Geological Society of America Bulletin* 100.10 (1988): 1640-1656.

Ammann, C., Jenny, B., Kammer, K., Messerli, B., 2001. Late Quaternary Glacier response to humidity changes in the arid Andes of Chile (18-29 degrees S). Palaeogeography Palaeoclimatology Palaeoecology 172, 313-326.

Amundson, R., Dietrich, W., Bellugi, D., Ewing, S., Nishiizumi, K., Chong, G., Owen, J., Finkel, R., Heimsath, A., Stewart, B., 2012. Geomorphologic evidence for the late Pliocene onset of hyperaridity in the Atacama Desert. Geological Society of America Bulletin 124, 1048-1070.

Anderson, R.S., Repka, J.L., Dick, G.S., 1996. Explicit treatment of inheritance in dating depositional surfaces using in situ Be-10 and Al-26. Geology 24, 47-51.

Balco, G., Shuster, D.L., 2009. Production rate of cosmogenic Ne-21 in quartz estimated from Be-10, Al-26, and Ne-21 concentrations in slowly eroding Antarctic bedrock surfaces. Earth and Planetary Science Letters 281, 48-58.

Bard, E., Rickaby, R.E.M., 2009. Migration of the subtropical front as a modulator of glacial climate. Nature 460, 380-U393.

Bierman, P. R., Marsella, K. A., Patterson, C., Davis, P. T., & Caffee, M. (1999). Mid-Pleistocene cosmogenic minimum-age limits for pre-Wisconsinan glacial surfaces in southwestern Minnesota and southern Baffin Island: a multiple nuclide approach. *Geomorphology*, *27*(1), 25-39.

Carrizo, D., Gonzalez, G., Dunai, T., 2008. Neogene constriction in the northern Chilean Coastal Cordillera: Neotectonics and surface dating using cosmogenic Ne-21. Revista Geologica De Chile 35, 1-38.

Dunai, T.J., Lopez, G.A.G., Juez-Larre, J., 2005. Oligocene-Miocene age of aridity in the Atacama Desert revealed by exposure dating of erosion-sensitive landforms. Geology 33, 321-324.

Evenstar, L.A., Hartley, A.J., Stuart, F.M., Mather, A.E., Rice, C.M., Chong, G., 2009. Multiphase development of the Atacama Planation Surface recorded by cosmogenic He-3 exposure ages: Implications for uplift and Cenozoic climate change in western South America. Geology 37, 27-30.

Gonzalez, G., Dunai, T., Carrizo, D., Allmendinger, R., 2006. Young displacements on the Atacama Fault System, northern Chile from field observations and cosmogenic Ne-21 concentrations. Tectonics 25.

Gosse, J. C., & Phillips, F. M. (2001). Terrestrial in situ cosmogenic nuclides: theory and application. *Quaternary Science Reviews*, *20*(14), 1475-1560.

Hartley, A. J., & Chong, G. (2002). Late Pliocene age for the Atacama Desert: Implications for the desertification of western South America. *Geology*, *30*(1), 43-46.

Herzog, G. F., Vogt, S., Albrecht, A., Xue, S., Fink, D., Klein, J., ... & Schultz, L. (1997). Complex exposure histories for meteorites with "short" exposure ages. *Meteoritics & Planetary Science*, *32*(3), 413-422.

Heusser, L., Heusser, C., Mix, A., McManus, J., 2006. Chilean and Southeast Pacific paleoclimate variations during the last glacial cycle: directly correlated pollen and delta 18O records from ODP Site 1234. Quaternary Science Reviews 25, 3404-3415.

Hoke, G. D., Isacks, B. L., Jordan, T. E., Blanco, N., Tomlinson, A. J., & Ramezani, J. (2007). Geomorphic evidence for post-10 Ma uplift of the western flank of the central Andes 18 30'–22 S. *Tectonics*, *26*(5).

Houston, J., 2006. Variability of precipitation in the Atacama desert: Its causes and hydrological impact. International Journal of Climatology 26, 2181-2198.

Jungers, M. C., Heimsath, A. M., Amundson, R., Balco, G., Shuster, D., & Chong, G. (2013). Active erosion–deposition cycles in the hyperarid Atacama Desert of Northern Chile. *Earth and Planetary Science Letters*, *371*, 125-133.

Kober, F., Ivy-Ochs, S., Schlunegger, F., Baur, H., Kubik, P. W., & Wieler, R. (2007). Denudation rates and a topography-driven rainfall threshold in northern Chile: Multiple cosmogenic nuclide data and sediment yield budgets.*Geomorphology*, *83*(1), 97-120.

Kober, F., Ivy-Ochs, S., Zeilinger, G., Schlunegger, F., Kubik, P.W., Baur, H., Wieler, R., 2009. Complex multiple cosmogenic nuclide concentration and histories in the arid Rio Lluta catchment, northern Chile. Earth Surface Processes and Landforms 34, 398-412.

Lal, D. (1991). Cosmic ray labeling of erosion surfaces:< i> in situ</i> nuclide production rates and erosion models. *Earth and Planetary Science Letters*,*104*(2), 424-439.

Lamb, S., & Davis, P. (2003). Cenozoic climate change as a possible cause for the rise of the Andes. *Nature*, *425*(6960), 792-797.

Lamy, F., Hebbeln, D., Wefer, G., 1998. Late quaternary precessional cycles of terrigenous sediment input off the Norte Chico, Chile (27.5 degrees S) and palaeoclimatic implications. Palaeogeography Palaeoclimatology Palaeoecology 141, 233-251.

Lamy, F., Klump, J., Hebbeln, D., Wefer, G., 2000. Late Quaternary rapid climate change in northern Chile. Terra Nova 12, 8-13.

Latorre, C., Betancourt, J.L., Arroyo, M.T.K., 2006. Late Quaternary vegetation and climate history of a perennial river canyon in the Rio Salado basin (22 degrees S) of Northern Chile. Quaternary Research 65, 450-466.

Maldonado, A., Betancourt, J.L., Latorre, C., Villagran, C., 2005. Pollen analyses from a 50 000-yr rodent midden series in the southern Atacama Desert (25 degrees 30 ' S). Journal of Quaternary Science 20, 493-507.

Mortimer, C. (1973). The Cenozoic history of the southern Atacama desert, Chile. *Journal of the Geological Society*, *129*(5), 505-526.

Mortimer, C. (1980). Drainage evolution in the Atacama Desert of northernmost Chile. *Andean Geology*, (11).

Navarro-Gonzalez, R., Rainey, F.A., Molina, P., Bagaley, D.R., Hollen, B.J., de la Rosa, J., Small, A.M., Quinn, R.C., Grunthaner, F.J., Caceres, L., Gomez-Silva, B., McKay, C.P., 2003. Mars-like soils in the Atacama Desert, Chile, and the dry limit of microbial life. Science 302, 1018-1021.

Nichols, K.K., Bierman, P.R., Hooke, R.L., Clapp, E.M., Caffee, M., 2002. Quantifying sediment transport on desert piedmonts using Be-10 and Al-26. Geomorphology 45, 105-125.

Niedermann, S. (2002). Cosmic-ray-produced noble gases in terrestrial rocks: dating tools for surface processes. *Reviews in Mineralogy and Geochemistry*,*47*(1), 731-784.

Nishiizumi, K., Caffee, M.W., Finkel, R.C., Brimhall, G., Mote, T., 2005. Remnants of a fossil alluvial fan landscape of Miocene age in the Atacama Desert of northern Chile using cosmogenic nuclide exposure age dating. Earth and Planetary Science Letters 237, 499-507.

Owen, J.J., Amundson, R., Dietrich, W.E., Nishiizumi, K., Sutter, B., Chong, G., 2011. The sensitivity of hillslope bedrock erosion to precipitation. Earth Surface Processes and Landforms 36, 117-135.

Placzek, C.J., Matmon, A., Granger, D.E., Quade, J., Niedermann, S., 2010. Evidence for active landscape evolution in the hyperarid Atacama from multiple terrestrial cosmogenic nuclides. Earth and Planetary Science Letters 295, 12-20.

Quade, J., Rech, J.A., Betancourt, J.L., Latorre, C., Quade, B., Rylander, K.A., Fisher, T., 2008. Paleowetlands and regional climate change in the central Atacama Desert, northern Chile. Quaternary Research 69, 343-360.

Rech, J.A., Currie, B.S., Michalski, G., Cowan, A.M., 2006. Neogene climate change and uplift in the Atacama Desert, Chile. Geology 34, 761-764.

Riihimaki, C. A., Anderson, R. S., Safran, E. B., Dethier, D. P., Finkel, R. C., & Bierman, P. R. (2006). Longevity and progressive abandonment of the Rocky Flats surface, Front Range, Colorado. *Geomorphology*, *78*(3), 265-278.

Rodríguez, M. P., Carretier, S., Charrier, R., Saillard, M., Regard, V., Hérail, G., ... & Audin, L. (2013). Geochronology of pediments and marine terraces in north-central Chile and their implications for Quaternary uplift in the Western Andes. *Geomorphology*, *180*, 33-46.

Rundel, P.W., Dillon, M.O., Palma, B., Mooney, H.A., Gulmon, S.L., Ehleringer, J.R., 1991. The Phytogeography and Ecology of the Coastal Atacama and Peruvian Deserts. Aliso 13, 1-50.

Stuut, J.B.W., Lamy, F., 2004. Climate variability at the southern boundaries of the Namib (Southwestern Africa) and Atacama (northern Chile) coastal deserts during the last 120,000 yr. Quaternary Research 62, 301-309.

Stuut, J.B.W., Lamy, F., 2004. Climate variability at the southern boundaries of the Namib (Southwestern Africa) and Atacama (northern Chile) coastal deserts during the last 120,000 yr. Quaternary Research 62, 301-309.

Wara, M.W., Ravelo, A.C., Delaney, M.L., 2005. Permanent El Nino-like conditions during the Pliocene warm period. Science 309, 758-761.

Zhou, J.Y., Lau, K.M., 1998. Does a monsoon climate exist over South America? Journal of Climate 11, 1020-1040.

Tables

Table 3.1 Sample locations and TCN abundances

Sample ID	Latitude	Longitude	Elevation	Depth	[^{10}Be]	±	[^{21}Ne]	±
			m	cm	atoms/g_{qtz}		atoms/g_{qtz}	
CH-09-06	-21.05000	-69.64100	895	0	9.52E+06	3.15E+05	2.30E+08	3.57E+06
CH-09-07	-21.40450	-70.03730	493	0	2.02E+06	4.66E+04	2.21E+07	3.66E+06
CH-09-09	-21.59340	-69.56870	892	0	2.55E+06	6.74E+04	4.09E+07	1.88E+06
CH-09-12	-21.16215	-70.03690	746	0	5.25E+06	1.05E+05	9.02E+07	3.10E+06
CH-DB-000cm	-23.76426	-70.26296	566	0	4.38E+06	1.28E+05	4.94E+07	1.49E+06
CH-DB-050cm	-23.76426	-70.26296	566	50	4.21E+06	1.88E+05	6.97E+07	3.31E+06
CH-DB-100cm	-23.76426	-70.26296	566	100	4.20E+06	6.02E+04	6.50E+07	3.03E+06
CH-DB-150cm	-23.76426	-70.26296	566	150	4.27E+06	2.01E+05	5.57E+07	2.05E+06
CH-FM-000cm	-23.76484	-70.24759	614	0	3.73E+06	8.12E+04	5.72E+07	3.84E+06
CH-FM-025cm	-23.76484	-70.24759	614	25	3.96E+06	1.15E+05	6.24E+07	3.06E+06
CH-FM-050cm	-23.76484	-70.24759	614	50	4.27E+06	1.29E+05	6.41E+07	3.21E+06
CH-FM-075cm	-23.76484	-70.24759	614	75	4.66E+06	2.04E+05	5.30E+07	2.25E+06
CH-R-000cm	-24.02200	-69.77260	1011	0	8.16E+06	2.06E+05	1.95E+08	3.94E+06
CH-R-075cm	-24.02200	-69.77260	1011	75	7.81E+06	2.78E+05	2.36E+08	3.94E+06
CH-R2-100cm	-24.02200	-69.77260	1011	100	7.69E+06	2.02E+05	2.23E+08	3.79E+06
CH-R2-150cm	-24.02200	-69.77260	1011	150	5.91E+06	1.76E+05	1.98E+08	4.16E+06
CH-SQ-000cm #1	-21.36193	-69.44540	870	0	8.88E+05	2.62E+04	2.11E+07	2.40E+06
CH-SQ-050cm #1	-21.36193	-69.44540	870	50	6.28E+05	1.26E+04	2.46E+07	3.27E+06
CH-SQ-050cm #2	-21.36193	-69.44540	870	50	6.43E+05	1.29E+04	1.48E+07	2.87E+06
CH-SQ-100cm #2	-21.36193	-69.44540	870	100	6.43E+05	1.29E+04	1.47E+07	2.40E+06
CH-SQ-300cm #2	-21.36193	-69.44540	870	300	2.33E+05	8.87E+03	2.71E+07	3.06E+06
CH-SQ-400cm #1	-21.36193	-69.44540	870	400	4.15E+05	1.40E+04	9.02E+06	2.09E+06
CH-SQ-400cm #2	-21.36193	-69.44540	870	400	6.81E+05	2.09E+04	1.55E+07	2.99E+06
CH-SQ-500cm #2	-21.36193	-69.44540	870	500	1.37E+06	2.74E+04	2.44E+07	3.73E+06
CH-YG-000cm	-24.10161	-70.01829	1009	0	6.98E+06	2.41E+05	8.33E+07	4.21E+06
CH-YG-050cm	-24.10161	-70.01829	1009	50	8.31E+06	1.66E+05	8.97E+07	3.99E+06
CH-YG-100cm	-24.10161	-70.01829	1009	100	7.92E+06	1.58E+05	9.66E+07	4.09E+06

Table 3.2 Excess ^{21}Ne and Estimates of Previous Exposure Cycles

Sample ID	Predicted ^{21}Ne atoms/g	Excess ^{21}Ne atoms/g	Previous exposure cycles
CH-09-07	1.06E+07	1.16E+07	1
CH-09-09	1.31E+07	2.78E+07	2
CH-09-12	4.25E+07	4.77E+07	1
CH-DB-000cm	3.10E+07	1.85E+07	1
CH-DB-050cm	2.90E+07	4.07E+07	1
CH-DB-100cm	2.88E+07	3.61E+07	1
CH-DB-150cm	2.96E+07	2.61E+07	1
CH-FM-000cm	2.32E+07	3.39E+07	1
CH-FM-025cm	2.55E+07	3.69E+07	1
CH-FM-050cm	2.89E+07	3.52E+07	1
CH-FM-075cm	3.37E+07	1.93E+07	1
CH-R-000cm	8.90E+07	1.06E+08	1
CH-R-075cm	7.94E+07	1.57E+08	2
CH-R2-100cm	7.63E+07	1.46E+08	2
CH-R2-150cm	4.36E+07	1.55E+08	4
CH-SQ-000cm #1	3.85E+06	1.72E+07	4
CH-SQ-050cm #1	2.66E+06	2.19E+07	8
CH-SQ-050cm #2	2.72E+06	1.20E+07	4
CH-SQ-100cm #2	2.72E+06	1.19E+07	4
CH-SQ-300cm #2	9.52E+05	2.61E+07	27
CH-SQ-400cm #1	1.72E+06	7.30E+06	4
CH-SQ-400cm #2	2.90E+06	1.26E+07	4
CH-SQ-500cm #2	6.22E+06	1.82E+07	3

Figure Captions

Figure 3.1. Overview of northern Chile highlighting where samples were collected for this study, and the locations of several studies mentioned in the text.

Figure 3.2. Erosion island plot showing that most of our data plot outside the realm of simple exposure or steady erosion, requiring a history of complex exposure including periods of complete or partial shielding from TCN production. Data are normalized by site-specific surface production rate to ease comparison. Errors are smaller than symbols at this scale.

Figure 3.3. Erosion island plot showing our results in the context of other studies from the region that report $^{21}Ne/^{10}Be$ data. Kober et al., 2009, infer complex exposure histories in the Rio Lluta related to long term storage of sediment in fill terraces. Data are normalized by site-specific surface production rate to ease comparison. Errors are smaller than symbols at this scale.

Figure 3.4. ^{10}Be concentration depth profiles for each sample suite. CH-R1 and CH-R2 are combined into one symbol (CH-R) as a summary of surface and depth concentrations at that site. Analytical errors are smaller than symbols at this scale.

Figure 3.5. Complex exposure paths for CH-DB and CH-FM. Based on exposure and burial durations inferred from the duration of previously modeled erosion deposition cycles (Jungers et al., 2013) we explore how different exposure:burial pathways compare to our data. A scenario of 2-4

cycles of 0.5 Myr of burial with 0.25 Myr of exposure produces complex exposure paths that pass through our data. This model example assumes an initial TCN abundance associated with an upland erosion rate of 0.25 m/Myr, and the fit of any complex exposure paths to measured abundances is strongly dependent on this initial condition.

Figures

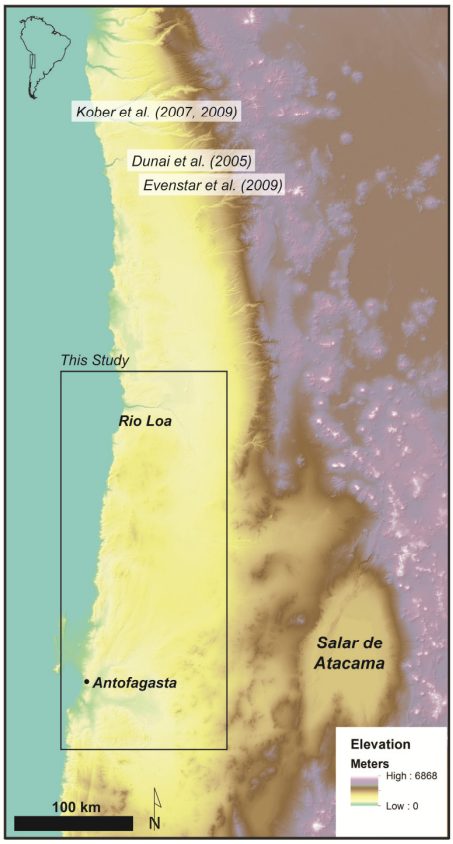

Figure 3.1.

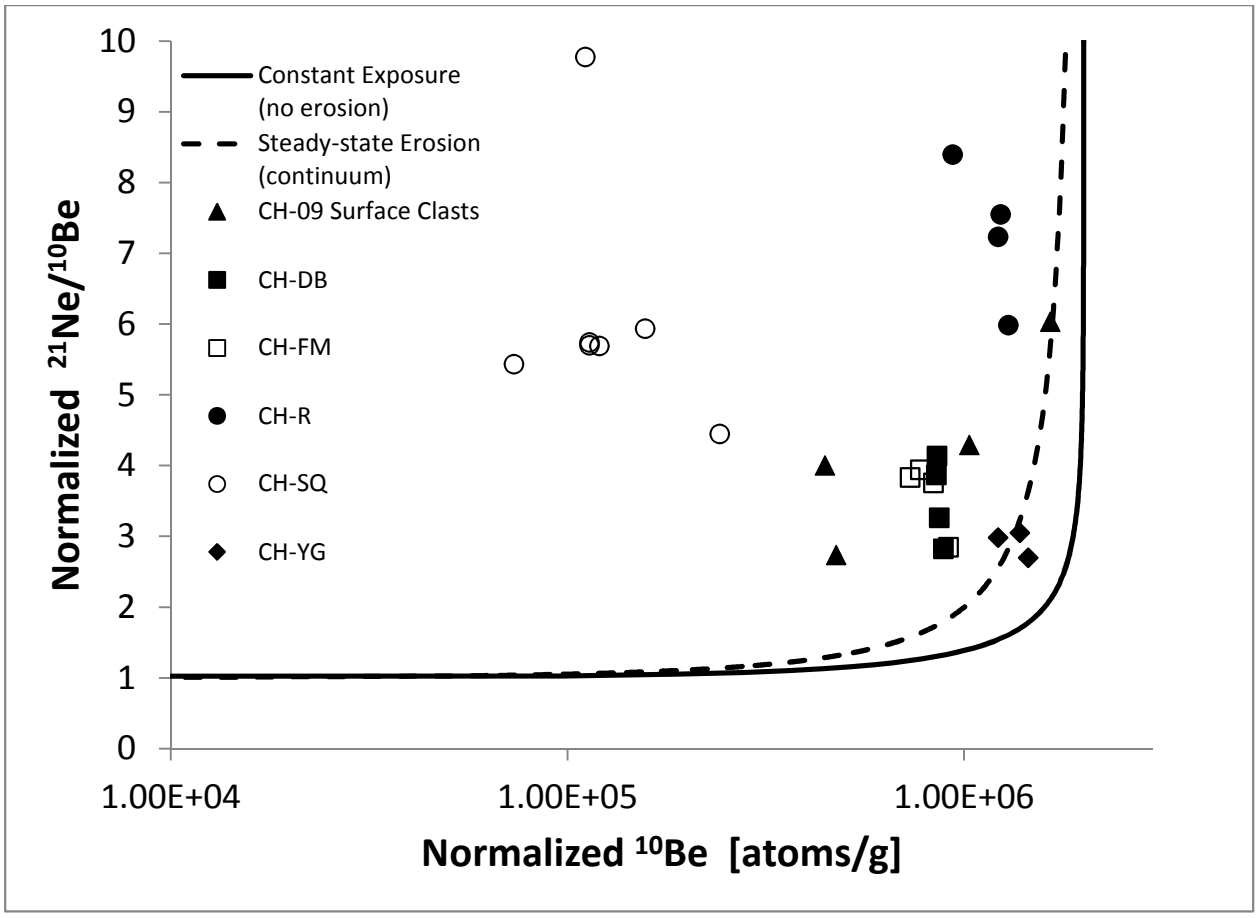
Constant Exposure
(no erosion)
Steady-state Erosion
(continuum)
CH-09 Surface Clasts
CH-DB
CH-FM
CH-R
CH-SQ
CH-YG
Normalized 21Ne/10Be
Normalized 10Be [atoms/g]
0
1
2
3
4
5
6
7
8
9
10
1.00E+04
1.00E+05
1.00E+06

Figure 3.2.

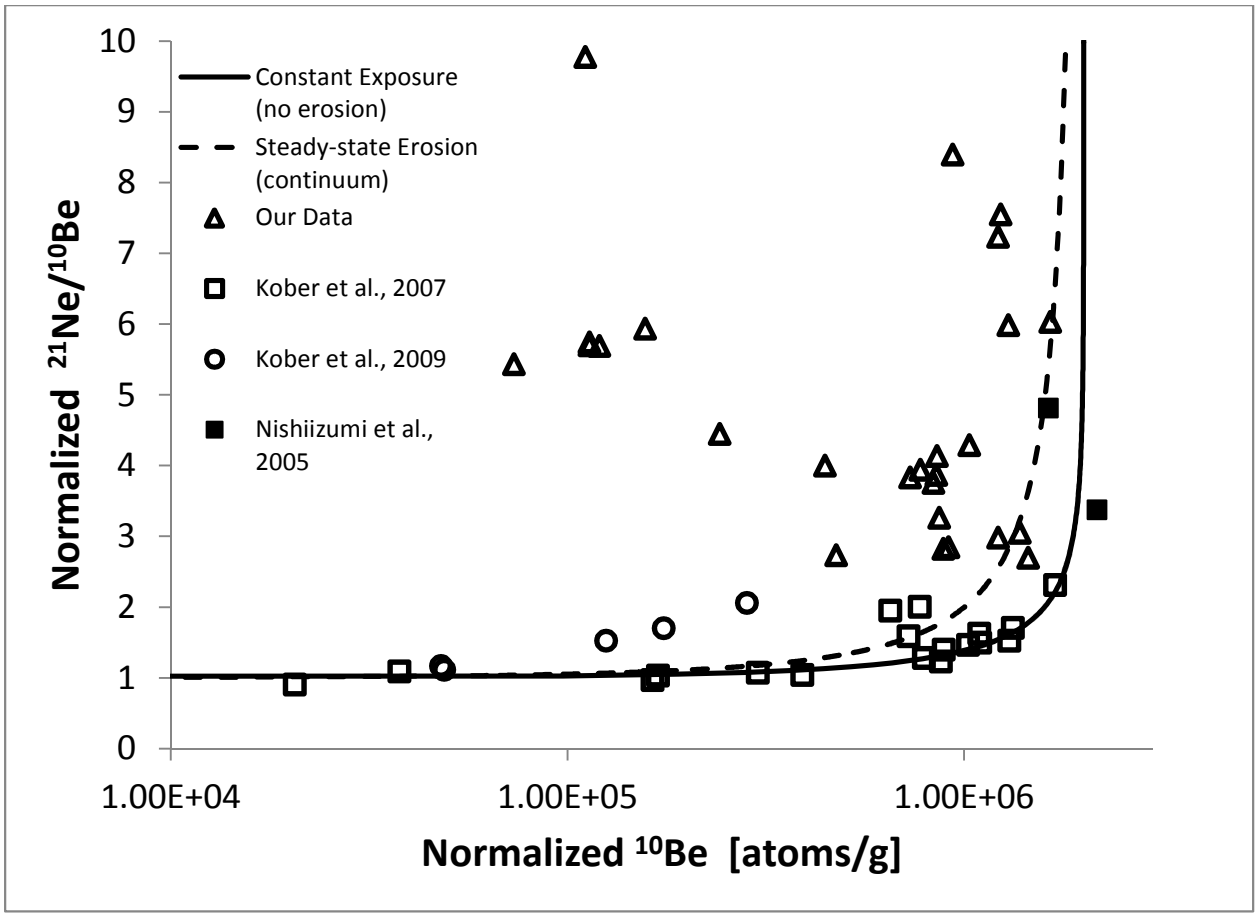
Constant Exposure
(no erosion)
Steady-state Erosion
(continuum)
Our Data
Kober et al., 2007
Kober et al., 2009
Nishiizumi et al.,
2005
Normalized 21Ne/10Be
Normalized 10Be [atoms/g]
0
1
2
3
4
5
6
7
8
9
10
1.00E+04
1.00E+05
1.00E+06

Figure 3.3.

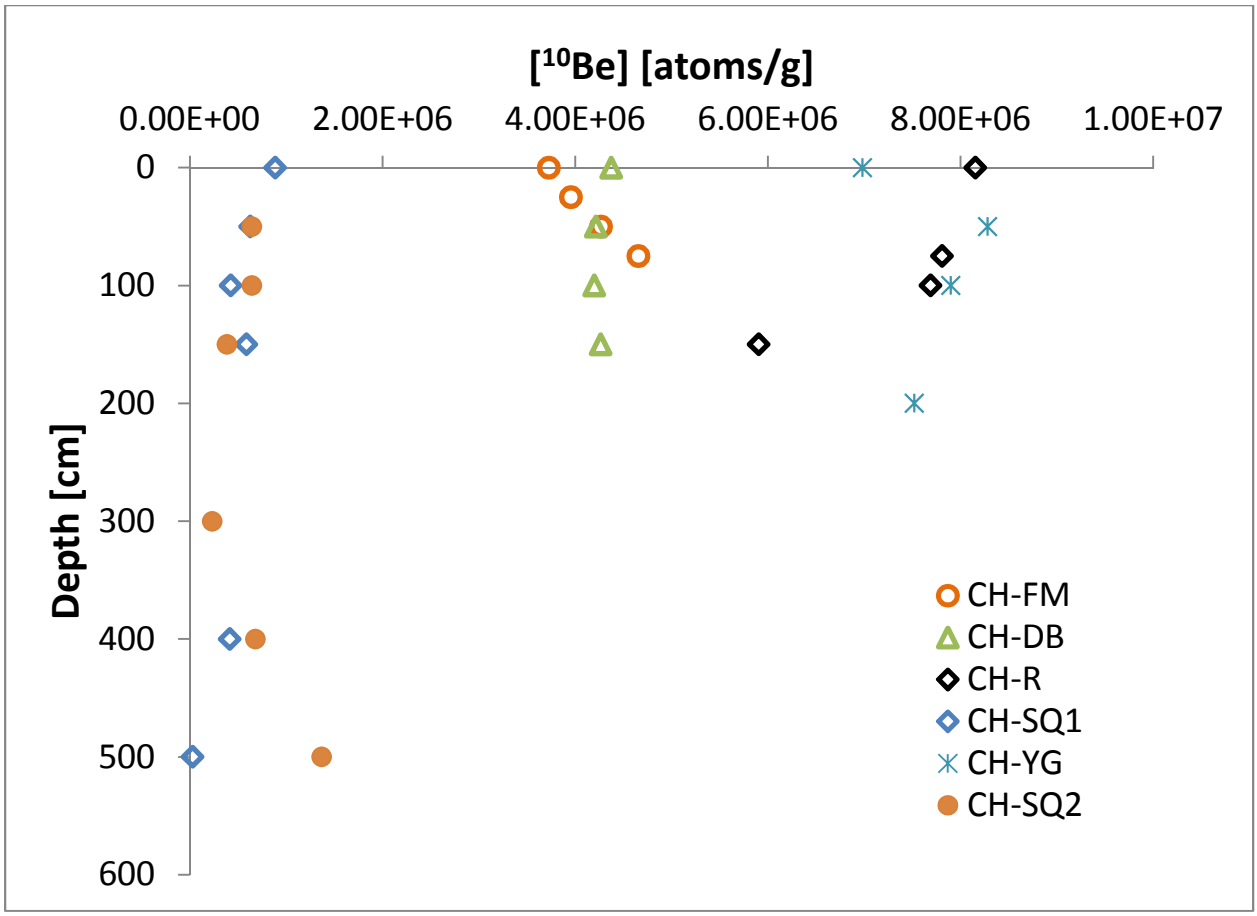
[10Be] [atoms/g]
0.00E+00
2.00E+06
4.00E+06
6.00E+06
8.00E+06
1.00E+07
0
100
200
300
400
500
600
Depth [cm]
CH-FM
CH-DB
CH-R
CH-SQ1
CH-YG
CH-SQ2

Figure 3.4

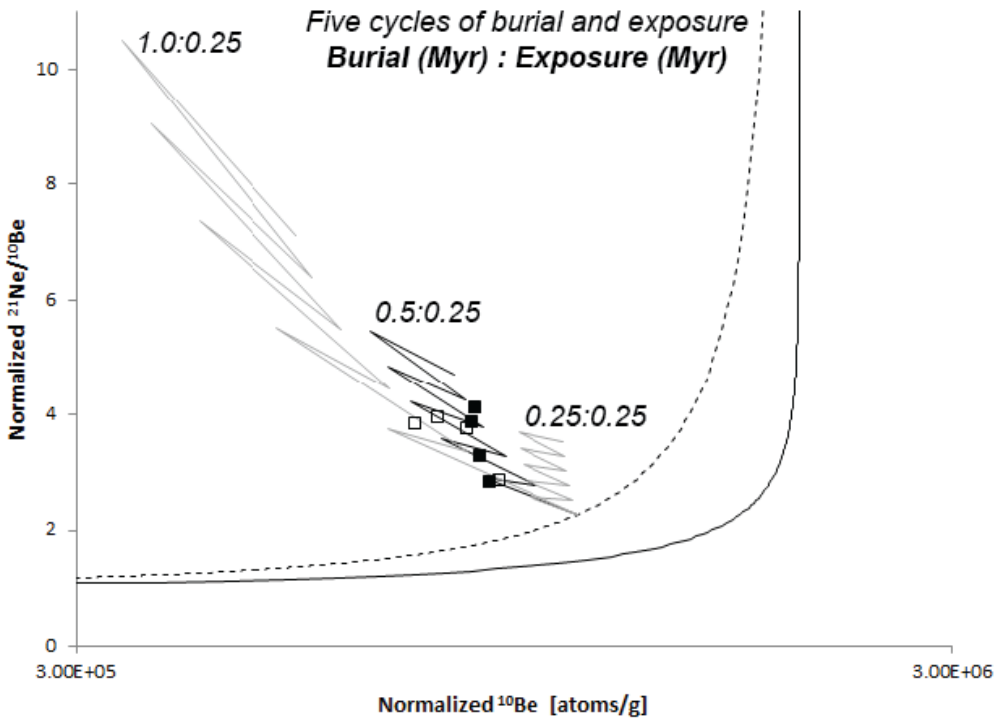
Five cycles of burial and exposure
Burial (Myr) : Exposure (Myr)
1.0:0.25
0.5:0.25
0.25:0.25
Normalized 21Ne/10Be
Normalized 10Be [atoms/g]
0
2
4
6
8
10
3.00E+05
3.00E+06

Figure 3.5.

CHAPTER 4

Transverse Canyon Incision and Sedimentary Basin Excavation Driven by Drainage Integration, Aravaipa Creek, AZ

Matthew C. Jungers and Arjun M. Heimsath

School of Earth and Space Exploration, Arizona State University

For submission to *Earth Surface Processes and Landforms*

Abstract

Drainage reorganization events have the potential to drive incision and erosion at rates normally attributed to tectonic or climatic forcing. However, it can be difficult to isolate the signal of transient events driven by drainage integration from longer term tectonic or climatic forcing. We exploit an ideal field setting in Aravaipa Creek basin of southeastern Arizona to isolate just such a signal. Aravaipa Creek basin underwent a period of transient incision that formed Aravaipa Canyon, its connection to the Lower San Pedro basin downstream, and this sudden lowering of base level evacuated a significant volume of sedimentary basin fill from the previously internally drained basin. We use digital terrain analyses to reconstruct the pre-incision landscape, and we then quantify the magnitude of incision and erosion that have occurred since drainage integration. Terrestrial cosmogenic nuclide burial dates for latest stage basin fill in Aravaipa Creek basin provide a maximum age constraint for the timing of incision, and allow us to calculate long term incision and erosion rates from 3 Myr to the present. Transient rates of incision that created Aravaipa Canyon

were fast, 150 m/Myr or more, but the background rate of erosion since integration is quite low, between 10-20 m/Myr.

1.0 Introduction and Motivation

Periods of transient erosion during landscape evolution are commonly attributed to fluvial systems' responses to changes in tectonic or climatic forcing (e.g., Whipple and Meade, 2006). However, dramatic changes in base level and sudden increases in drainage area associated with drainage reorganization can drive punctuated events of incision and erosion of equal magnitude to those driven by tectonics or climate (Meek, 1989; Meek and Douglass, 2001; Prince et al., 2011; Yanites et al., 2013). Investigations linking incision rates to tectonic or climatic forcing must be able to identify and resolve the component of landscape evolution attributable to drainage reorganization alone, or inferences of uplift rates and climate shifts will be incorrect. Cycles of uplift, sedimentary basin filling, and incision in actively uplifting orogens can bring additional complexity to this problem (Hilley and Strecker, 2005). Dramatic transverse gorges can form between structural basins as a result of both antecedence to uplift or from drainage integration events (Douglass et al., 2009), and distinguishing between the two processes is of fundamental importance to tectonic geomorphology. The clearest setting to quantify the magnitude of bedrock canyon incision and sedimentary basin fill evacuation attributable to drainage integration is a tectonically quiescent landscape with a moderately well constrained paleoclimate. We exploit just such an ideal field setting in Aravaipa Creek basin of southeastern Arizona. Aravaipa Creek basin underwent a period of transient incision that formed Aravaipa Canyon, its connection to the Lower San Pedro basin downstream, and this sudden lowering of base level evacuated a significant volume of sedimentary

basin fill from the previously internally drained basin. We use a series of digital terrain analyses to reconstruct the paleo-topography of the pre-incision basin surface, and we then calculate the magnitude of incision and the volume of material eroded driven by drainage integration. Cosmogenic nuclide derived burial dates for latest stage basin fill deposits in Aravaipa Creek basin allow the quantification of long-term incision and erosion rates since drainage integration.

In southeastern Arizona's Basin and Range, a tectonically quiescent portion of the larger North American physiographic province, the Gila River system integrates a network of previously internally drained structural basins. One basin in particular, Aravaipa Creek, serves as an archetypal example for basins' transition from internal to external drainage. Aravaipa Creek basin's relatively small size, preservation of key components of its pre-incision high stand surface, and its juxtaposition with the adjacent, and still internally drained, Sulphur Springs basin make it an excellent site to quantify post-tectonic rates of landscape evolution driven primarily by drainage integration with the broader Gila River system. Following drainage integration, Aravaipa Creek incised to equilibrate with a new lower, base level. In doing so, it carved Aravaipa Canyon, excavated a large volume of sedimentary basin fill, and captured drainage area from the still internally drained Sulphur Springs basin to its south. Importantly, this episode of transient incision and erosion was primarily the result of drainage integration. Therefore, we can explicitly quantify the magnitude of transient incision and erosion driven by drainage reorganization.

2.0 Setting

Aravaipa Creek is a tributary to the San Pedro River, situated in southeastern Arizona's Basin and Range physiographic province (Figure 1). The region's topography is largely the result of two

stages of regional extensional tectonics. First, in the mid-Tertiary, low angle extension along detachments exhumed metamorphic core complexes – e.g., the Santa Catalina, Rincon, and Pinaleño ranges (Dickinson, 1991). Effusive volcanics were also common during the mid-Tertiary, creating ranges such as the Galiuro Mountains. Subsequently, in the mid-to-late Miocene, 12-8 Ma, steep angled normal faulting of the Basin and Range Disturbance commenced (Scarborough and Peirce, 1978). The modern pattern of rugged, high-relief ranges with intervening sedimentary basins primarily reflects uplift patterns of the Basin and Range Disturbance. Widespread extension largely ceased by 5-3 Ma, and structural basins began the transition from internal drainage to the modern, integrated Gila River drainage network (Menges and Pearthree, 1989).

We adopt the nomenclature of Simons (1964), dividing Aravaipa Creek basin into distinct sections defined by both lithology and geomorphology: 1) Aravaipa Valley and 2) Aravaipa Canyon. Aravaipa Valley is the section upstream from Stowe Gulch where Aravaipa Creek occupies a shifting floodplain several kilometers wide (Figure 2). In Aravaipa Valley, the primary lithology is late stage sedimentary basin fill (the Older Alluvium of Simons) (Figure 3). This section is bounded to the northeast by the Santa Theresa and Pinaleño ranges, and to the southwest by the Galiuro Mountains and the Black Hills. Near the range fronts, the basin fill transitions abruptly into the basement lithologies of each mountain range. The southeast extent of Aravaipa Valley is the drainage divide between Aravaipa Creek and Sulphur Springs basin, a divide 'so low and smooth that a traveler might well pass from one valley to the other without realizing it' (Ross, 1925; Davis and Brooks, 1930). Sulphur Springs basin drains internally to Willcox Playa, and thus is not yet part of the Gila River system. Aravaipa Canyon begins downstream of Stowe Gulch where Aravaipa Creek becomes entrenched in a canyon 100-200 meters deep. The canyon cuts through older Tertiary conglomerates

and the Galiuro Volcanics. Downstream of Aravaipa Canyon, Aravaipa Creek flows into the San Pedro River which soon thereafter joins the Gila River near Winkelman, AZ.

3.0 Methods

We use elements of the modern landscape to reconstruct the pre-drainage integration topography of Aravaipa Creek basin in order to quantify the magnitude of incision driven by drainage reorganization and the volume of material eroded from the basin. Key control points for our landscape reconstruction are: (1) the inferred elevation of the spillover point between Aravaipa Creek and the San Pedro River; (2) Quaternary pediment-capping gravels above Aravaipa Canyon (3) perched remnants of late stage sedimentary basin fill that preserve the slope of the pre-incision piedmonts of the Galiuro Mountains and Santa Teresa Mountains; and (4) the paleo-drainage divide between Aravaipa Creek and Sulphur Springs Valley, approximately 6 km northwest of the modern divide. The pre-incision basin surface sloped from the Sulphur Springs divide to its intersection with the point of integration between Aravaipa Creek and the San Pedro River. Maximum incision of 450 m occurred in the vicinity of Aravaipa Canyon, and more than 50 cubic kilometers of material have been eroded from Aravaipa Creek basin. Cosmogenic nuclide derived burial dates for latest stage basin fill deposits in Aravaipa Creek basin allow the quantification of long-term incision and erosion rates since drainage integration.

3.1 Reconstruction of Aravaipa Creek Basin's High Stand Geometry

We reconstruct Aravaipa Creek basin's high stand geometry by identifying features of the modern landscape that are remnants of the pre-incision landscape. The different types of features

used to inform our reconstruction of Aravaipa Creek basin's paleo-surface vary between physiographic regions of the modern basin and are explained in detail below.

In Aravaipa Canyon, we rely on modern drainage divide elevations, limited Quaternary deposits, and the preservation of low relief drainage basins within the Hell Hole Conglomerate to infer a high stand elevation near the modern mouth of Aravaipa Canyon, upstream from Aravaipa Creek's junction with the San Pedro River. North of Javalina Canyon, the drainage divide between Aravaipa Creek and Ash Creek reaches elevations as low at 1050-1100 meters. Since Aravaipa Creek did not integrate with the Gila River across this divide, we assert that a lower divide must have existed somewhere along the course of the modern Aravaipa Creek. The drainage divides between Buzan Canyon and the Lower San Pedro basin suggests that the location of Aravaipa Creek's point of integration with the Lower San Pedro was in the vicinity of Brandenburg Mountain, Periz Peak, and Flat Top Mountain (Figure 4). The headwaters of the small drainages to the south of Buzan Canyon are coincident with the pre-drainage integration divide. We conservatively estimate a maximum elevation of 1100-1200 meters for this paleo-divide.

Remnants of Quaternary pediment capping gravels support a 1100-1200 m base level for Aravaipa Canyon prior to incision. Krieger (1968) identified small patches of gravel capped pediment developed on top of the Tertiary Apsey Conglomerate Member of the Galiuro Volcanics. This pediment is best preserved adjacent to Whitewash Canyon and Hells Half Acre Canyon above the prominent bench of tuff, Hells Half Acre. The pediment caps are too eroded to allow a confident reconstruction of their original extent and depositional angle. However, the roughly accordant ridges of the eroded pediments slope from southeast to northwest from maximum elevations greater than 1310 m to minimum elevations less than 1160 m where the deposits

terminate. This geometry supports a pre-incision base level of 1100-1200 m located just northeast of our proposed integration point.

East of Stowe Gulch, in Aravaipa Valley, remnants of the pre-incision landscape comprise widespread, undeformed late stage basin fill sediments, perched patches of the basin high stand piedmont, and minimally dissected portions of the former divide between Aravaipa Creek and Sulphur Springs basin to the southeast. The mapped extent of undeformed, late stage sedimentary basin fill in Aravaipa Valley extends along the valley axis from Stowe Gulch southeast to Aravaipa Creek's drainage divide with Sulphur Springs basin. Simons (1964) maps a concealed fault west of Stowe Gulch that defines the boundary between Tertiary units to the west, including the Hell Hole Conglomerate and Galiuro Volcanics, and late stage basin fill to the east. Although Simons does not explicitly discuss activity on this fault, down to the east displacement during the Plio-Pleistocene must have contributed to the maintenance of Aravaipa Creek basin's internal drainage during that time period. Late stage basin fill deposits preserve the extent of deposition prior to drainage integration, extending from the valley axis to uncomformable contacts with basement rocks along the range fronts of the Santa Theresa Mountains, Galiuro Mountains, and Pinaleño Mountains. In some locales, most notably adjacent to Rattlesnake Creek on the north side of the Galiuro Mountains, remnants of the uppermost basin fill surface are preserved. Incision by Aravaipa Creek and its tributaries – most likely driven by drainage integration with the Lower San Pedro basin downstream – led to the abandonment of these basin high stand deposits..

We use the modern slope of uppermost basin fill piedmont remnants to determine a base level for Aravaipa Valley during its latest stage of internal drainage. We assume that the modern slopes of the remnants preserve the depositional slope of the basin's paleo-piedmont, and project

the gradients of each surface above the modern landscape to their intersection with the valley axis Figure 5). We use the most continuous surfaces of the piedmont remnants to determine a best fit slope for our projections. The two most significant limitations of our approach are: (1) we are unable to perfectly constrain what specific direction segments of the piedmont graded at the time of deposition, and (2) we do not know exactly where base level was for these piedmonts, so we truncate all our projections at the modern valley axis. Despite these limitations, we find that the projected slopes of all the piedmont remnants suggest a high stand elevation of approximately 1350 m for the axis of Aravaipa Creek basin east of Stowe Gulch.

Our goal in reconstructing the surface of Aravaipa Creek basin is to accurately represent the pre-incision landscape while avoiding overestimates of surface elevations that would misrepresent the magnitude of incision and erosion post-drainage integration. To this end, we use a linear fit to interpolate a plane through the basin axis control points described above in order to approximate a minimum estimate for the paleo-basin surface (Figure 7). Excluding additional control points such as the modern elevations of Rattlesnake , China Peak, Oak Spring, and Buford surfaces help us avoid more complex interpolation methods such as Kriging or a Spline, which we have found overestimate paleo-landscape elevations in Aravaipa Creek basin. A cross-section of our linear fit, and its relationship to our basin axis control points is presented in Figure 6. To quantify the magnitude of incision and erosion since drainage integration, we subtract the modern DEM from our DEM of the reconstructed surface. Dates for late stage basin fill outlined below allow the conversion of these magnitudes into rates of incision and erosion.

3.2 Cosmogenic Nuclide Burial and Surface Exposure Dating

3.2.1 Background

In the absence of dateable materials such as volcanic ash, the abundance of cosmogenic nuclides in alluvial sediment may be used to determine both surface exposure dates and burial dates for alluvial deposits. Cosmogenic nuclide abundances in rock and sediment record the near surface residence time of those Earth materials. TCN are produced during the bombardment of Earth's surface by secondary cosmic ray particles. When cosmic rays hit the Earth's atmosphere a cascade of secondary particles is produced, some of which reach the Earth's surface. Most of these particles are then quickly stopped by the mass of soil and rock within the first 1-3 meters of the surface (Gosse and Phillips, 2001). The accumulation of TCN in rock or sediment as a function of depth below the deposit surface, z [cm], and duration of exposure, t [yr], may be expressed as follows:

$$N(z,t) = \frac{P_0 e^{\frac{-\rho z}{\Lambda}}}{\lambda + \frac{\rho \varepsilon}{\Lambda}}\left(1 - e^{-\left(\lambda + \frac{\rho \varepsilon}{\Lambda}\right)t}\right), \qquad (1)$$

where N is cosmogenic nuclide concentration [atoms g^{-1}], ε is erosion rate[cm yr^{-1}], λ is the decay constant for a radionuclide [yr^{-1}], P_0 is the cosmogenic nuclide production rate at the surface [atoms g^{-1} yr^{-1}], Λ is the attenuation length for cosmogenic nuclide production [g cm^{-2}], and ϱ is rock or sediment density [g cm^{-3}]. This formulation is commonly used to determine apparent exposure ages and/or maximum surface erosion rates. When determining surface exposure ages for alluvial

deposits or boulders an additional term must be included to account for inherited TCN abundances accumulated prior to deposition (Anderson et al., 1996):

$$N(z,t) = N_0 e^{-\lambda t} + \frac{P_0 e^{\frac{-\rho z}{\Lambda}}}{\lambda + \frac{\rho \varepsilon}{\Lambda}}\left(1 - e^{-\left(\lambda + \frac{\rho \varepsilon}{\Lambda}\right)t}\right), \qquad (2)$$

where N_0 is the inherited concentration of the cosmogenic nuclide [atoms g^{-1}] and all other terms are as defined for Equation 1. We use Equation 2 when calculating a surface exposure age for an intermediate elevation piedmont in the Lower San Pedro basin adjacent to Aravaipa Creek basin. Equation 2 also serves as the foundation for our calculations of both catchment-averaged erosion rates and burial dates for sedimentary basin fill.

Cosmogenic nuclide abundances in sediment eroded from upland basins and deposited in downstream fill terraces, lakes, or sedimentary basins record both a paleo-upland erosion rate, and a burial duration since deposition (Granger et al., 1997; Granger and Muzikar, 2001). As a result, inverting measured TCN concentrations into a burial date requires the measurement of two cosmogenic nuclides in order to solve for those two unknowns. Importantly, at least one nuclide measured must be a radionuclide in order to determine burial duration. If using a pair of one stable cosmogenic nuclide, and one radionuclide, the stable nuclide will only provide information about the paleo-erosion rate prior to deposition. For this study, we employ two cosmogenic radionuclides, ^{26}Al and ^{10}Be, both of which have well established production rates and half-lives. A full formulation for TCN abundances in buried sediment is a combination of Equations 1 and 2, and (adapting the notation Balco and Rovey, 2008):

$$N_{10} = \frac{P_{10}}{\lambda_{10}+\frac{\rho\varepsilon}{\Lambda}} e^{-\lambda_{10} t_b} + \frac{P_{10} e^{\frac{-\rho z}{\Lambda}}}{\lambda_{10}+\frac{\rho\varepsilon}{\Lambda}} \left(1 - e^{-\left(\lambda_{10}+\frac{\rho\varepsilon}{\Lambda}\right) t_b}\right), \quad (3)$$

$$N_{26} = \frac{P_{26}}{\lambda_{26}+\frac{\rho\varepsilon}{\Lambda}} e^{-\lambda_{26} t_b} + \frac{P_{26} e^{\frac{-\rho z}{\Lambda}}}{\lambda_{26}+\frac{\rho\varepsilon}{\Lambda}} \left(1 - e^{-\left(\lambda_{26}+\frac{\rho\varepsilon}{\Lambda}\right) t_b}\right), \quad (4)$$

where *10* and *26* subscripts denote ^{10}Be and ^{26}Al, respectively, and t_b is burial duration in years. In an ideal setting, burial occurs very rapidly, and shielding from post-burial TCN production is nearly immediate. Under these conditions, the second term in the RHS of Equations 5 and 6 become insignificant, and a burial date can be determined by iterating through ε and t_b pairs to find a best fit for measured TCN abundances. We refer to this approach as conventional burial dating, and it is most appropriate for sedimentary settings where transport from eroding uplands is swift, and, once deposited, sediment is fully shielded from post-burial TCN production.

3.2.2 Sample Collection and Preparation

We used a recent road cut just below Rattlesnake Mesa to collect 15 cobbles for ^{26}Al/^{10}Be burial dating. The cobbles were shielded by several meters of basin fill prior to the construction of the road, so any post-burial TCN production was likely minimal, and would have occurred immediately after the deposition of the sediment. We crushed and sieved the cobbles to 250-1000 μm. Additionally, we collected a depth profile of samples from an intermediate elevation piedmont in the

Lower San Pedro basin to supplement our dating effort in Aravaipa Creek basin (Figure 1). We collected quartz-rich clasts from the piedmont surface and from 100 cm, 150 cm, 200 cm, and 300 cm depths. Samples for each depth contained at least 50 clasts, which were crushed and sieved to our target size.

We isolated quartz using standard methods (Kohl and Nishiizumi, 1992) by cleaning in aqua regia and subsequent etching in HF and HNO_3. Two quartz vein samples collected for burial dating Rattlesnake Mesa yielded enough material for ^{10}Be and ^{26}Al extraction. We extracted ^{10}Be and ^{26}Al through column chromatography (Ditchburn and Whitehead, 1994), and nuclide ratios were measured via accelerator mass spectrometry (AMS) at the Purdue Rare Isotope Measurement (PRIME) Laboratory at Purdue University. Samples analyzed for ^{10}Be analysis were spiked with a Be carrier produced at Arizona State University containing lower levels of background ^{10}Be than commercial carrier. We measured native Al concentrations for each sample using a Thermo iCAP6300 ICP-OES at Arizona State University's Goldwater Environmental Laboratory. Table 4.1 shows a summary of these analytical results.

3.2.3 Modeling of Burial and Surface Exposure Dates

We rely upon conventional burial dates for AZ56C and AZ56G (Granger et al., 1997). We iterate through pairs of initial $^{26}Al/^{10}Be$ and burial durations to find solutions for Equations 3 and 4 that best fit our data. Following the approach of Granger et al. (1997), we start with a guess of some paleo-erosion rate to establish an initial $^{26}Al/^{10}Be$. Using this first guess of $^{26}Al/^{10}Be$ and our measured $^{26}Al/^{10}Be$, we can calculate a first approximation of burial duration. Decay correcting our measured ^{26}Al and ^{10}Be concentrations for this burial duration provides a new initial $^{26}Al/^{10}Be$ with

which to start then next iteration. As Granger et al. (1997) state, we usually converge on a solution after just a few loops of iteration. An erosion-island plot (Figure 9) allows a visual confirmation of the solution.

To determine a surface exposure date for the set of samples collected as a depth profile from the Lower San Pedro, AZ18, we adapt the methods of Braucher et al. (2009) and Hidy et al. (2010) to determine a best fit solution to Equation 2 for our measured ^{10}Be concentration of depth profile. Reworking of the piedmont surface that we sampled is minimal based on our field observations of weakly developed desert pavement and strongly developed caliche at 50 cm (thus no samples between 0 cm and 100 cm). Since surface erosion is likely to be negligible, we fit the profile data using a range of denudation rates from 0 – 1 m/Myr and a range of exposure durations from 10^3 – 10^6 Myr. We use the concentration of ^{10}Be from our deepest (3 m) sample to approximate an initial, inherited TCN concentration (Anderson et al., 1996) due to pre-deposition exposure in an upland catchment of the Santa Catalina Mountains. Each model run compared 100 Monte Carlo simulations of our data to each depth of modeled solutions for 2000 denudation-exposure pairs. A best-fit solution for each model run is defined as the denudation-exposure pair with the lowest median chi-square. We used 1000 model runs to produce a distribution of best-fit solutions.

4.0 Results

4.1 Magnitude of Incision and Erosion in Aravaipa Creek Basin

Our reconstruction of a minimum estimate for the paleo-basin fill surface of Aravaipa Creek basin slopes from approximately 1370 m at its southeast extent (the paleo-drainage divide between Aravaipa Creek and Sulphur Spring basins) to a low point of less than 1200 m in the vicinity of our

inferred point of drainage integration (Figures 6 and 7**).** The surface slope of our reconstructed surface is 0.11°, nearly identical to the modern slope of Sulphur Springs basin from the Aravaipa Creek divide to Willcox Playa. This similarity in form to the adjacent basin suggests that our reconstruction is reasonable.

Maximum magnitudes of incision reaching nearly 450 m occurred near the downstream end of Aravaipa Canyon. Incision of 100-300 m is common near the basin axis in Aravaipa Valley and the magnitude of incision decreases to 10s of meters near the modern divide with Sulphur Springs basin (Figure 8). By subtracting today's topography from our reconstructed basin surface, we determine that the total volume of material removed from Aravaipa Creek basin since integration with the Lower San Pedro River is approximately 50 km^3.

4.2 Timing of Deposition for Latest Stage Basin Fill

Surfaces such as Rattlesnake Mesa in Aravaipa Creek basin represent the basin's high stand of aggradation before widespread dissection following downstream drainage integration (cf. Menges and McFadden, 1981). Our burial dates from samples (AZ56 series) ~10 m below the surface of Rattlesnake Mesa thus represent a maximum age constraint for the final stages of deposition and the onset of basin-wide incision. Conventional burial dates for AZ56C and AZ5G are 2.85 ± 0.8 Myr and 2.90 ± 0.9 Myr, respectively (Figure 9), suggesting the final stages of aggradation in Aravaipa Creek basin was about 3 Myr, roughly correlative to similar regional deposits such as Frye Mesa in the Safford basin to the northeast and the Martinez surface in Sonoita Creek basin to the southwest (Menges and McFadden, 1981; Jungers and Heimsath, 2014). The imprecision on these two burial dates is the result of higher than ideal concentrations of native Al in each sample, and very low ^{26}Al

concentrations leading to poor analytical precision during AMS measurements. Nonetheless, considering that no other dates exist for these deposits and that we discovered no other dateable material in Aravaipa Creek basin, we present these results as a first-order estimate for the timing of drainage integration between Aravaipa Creek and the Lower San Pedro River.

Our best-fit denudation rate-exposure age pair is for an intermediate elevation (1000 m at sample site for AZ18) 0.7 m/Myr and and 435,000 ± 43,000 years for our concentration depth profile at this site. A best fit to our data assuming zero erosion yields an apparent (minimum) exposure age of ~375,000 years (Figure 10). This requires that the Lower San Pedro basin had incised 100-150 m from its high stand by approximately 400,000 years. The modern fluvial system adjacent to our depth profile is 20 m below the elevation of the intermediate piedmont, suggesting an average incision rate of ~50 m/Myr for the Lower San Pedro basin from the Mid-Pleistocene to the present.

Our burial dates from Rattlesnake Mesa and the inheritance from our Lower San Pedro basin concentration depth profile provide paleo-upland erosion rates at the time of these deposits' emplacement. Paleo-erosion rates for AZ56C and AZ56G are 37 m/Myr and 47 m/Myr, respectively, and the paleo-erosion rate for AZ18 is 20 m/Myr. These rates are in agreement with other measures of post-tectonic upland erosion from nearby Safford basin (Jungers and Heimsath, 2014).

5.0 Synthesis of Landscape Reconstruction and Geochronology

Our reconstruction of the pre-incision basin surface for Aravaipa Creek basin and new age constraints for late stage basin fill above Aravaipa Creek and a Mid-Pleistocene piedmont level in the

adjacent Lower San Pedro basin allow us to suggest new insights into regional incision rates and upland erosion rates from the Pliocene to the present for this section of southeastern Arizona's Basin and Range province.

We infer that the northwest sloping aspect of Aravaipa Creek's high stand surface may have predisposed the basin to integration via spillover into the Lower San Pedro basin. For this spillover event to drive a pulse of incision that formed Aravaipa Canyon and excavated basin fill from Aravaipa Creek basin, the new base level for Aravaipa Creek must have been significantly lower than the spillover point. This requires that the Lower San Pedro had already incised well below its own high stand elevations (~1200-1350 m near Davis Mesa and Stratton Mesa), presenting Aravaipa Creek basin with a new base level several hundred meters below its integration point. We can calculate rates of incision by dividing the range of incision magnitudes determined by our landscape reconstruction (Figure 8) by the maximum age of late stage basin fill constrained by our Rattlesnake Mesa burial dates. Following this approach, maximum rates of incision approaching 150 m/Myr occurred near the downstream end of Aravaipa Canyon, while incision elsewhere in Aravaipa Creek basin averaged less than 100 m/Myr and as low as 5-10 m/Myr near the modern drainage divide with Sulphur Springs basin.

These incision rates are comparable to Pliocene and Pleistocene incision rates in nearby Safford and Lower San Pedro basins. In Safford basin, incision rates inferred from 2 Myr basin fill deposits at Frye Mesa suggest 50 m/Myr of incision near the range front of the Pinaleno Mountains. Incision rates inferred from a flight of Gila River terraces on the northeast edge of Safford basin tell a similar story of moderately slow incision. From 2.8 Myr to 1.3 Myr, the Gila incised 30 m at a rate of 20 m/Myr. Incision accelerated to 60 m/Myr from 1.3 Myr to 0.64 Myr, and then slowed again to

40 m/Myr from the Mid-Pleistocene to the present (Jungers and Heimsath, 2014). Upstream in the Duncan-Clifton basin, the Gila River apparently incised twice as rapidly from 0.64 Myr to the present at a rate of 80 m/Myr (Dethier, 2001). Since we are averaging incision rates for Aravaipa Creek over 3 Myr, they are minimum estimates, and if a shorter period of transient adjustment is considered, then inferred incision rates for Aravaipa Creek basin would be much faster.

We are also able to use our reconstruction of the volume of material eroded from Aravaipa Creek basin (~50 km^3) in conjunction with our Rattlesnake Mesa burial dates to quantify an erosion rate for the basin averaged over 3 Myr. Using a density of 2.5 g/cm^3 (cf., Larsen et al., 2014) for the eroded material and a drainage area of 1340 km^2 for Aravaipa Creek (all area above the downstream end of Aravaipa Canyon), we determine a long-term mass flux of 31 t/km^2 yr equivalent to an erosion rate of 12 m/Myr. Again Aravaipa Creek's erosion rate was likely significantly faster during its period of transient adjustment to its new base level, but we are forced to average over the time period for which we have age constraints. Likewise, our conservative approach to reconstructing the basin's paleo-surface also leads to a minimum estimate for the volume eroded from Aravaipa Creek basin. A more complete accounting for total material eroded would lead to a higher inferred erosion rate. An erosion rate of 12 m/Myr is slower than most other Pliocene/Pleistocene upland erosion rates from the region. In Safford basin most paleo-erosion rates inferred from burial dating of basin fill average ~30 m/Myr, although there was a spike in erosion rate to between 100-250 m/Myr shortly before 2 Myr. Paleo-erosion rates from two Pliocene/Pleistocene terraces of the Gila River in Safford basin are between 3-20 m/Myr, which agrees well with this inferred minimum long-term average of Aravaipa Creek (Jungers and Heimsath, 2014).

6.0 Conclusions

Aravaipa Creek basin's relatively small size, preservation of key components of its pre-incision high stand surface, and its juxtaposition with the adjacent, and still internally drained, Sulphur Springs basin make it an excellent site to quantify post-tectonic rates of landscape evolution driven primarily by drainage integration with the broader Gila River system. Maximum paleo-incision rates of 150 m/Myr or greater during the creation of Aravaipa Canyon about 3 Myr are faster than any other regional incision rates. In contrast to such rapid incision rates, the long-term average erosion rate for Aravaipa Creek basin, determined by our basin reconstruction and first order age constraint, is a modest 12 m/Myr. Aravaipa Creek appears to be fully adjusted to its current base level, its channel long profile is well graded from its junction with the Lower San Pedro River upstream to the Aravaipa/Sulphur Springs drainage divide. While Simons (1964) speculated that Aravaipa Creek will continue to capture drainage area from Sulphur Springs until ultimately Willcox Playa is integrated into the Gila River system, we do not agree with such inevitability. If Aravaipa Creek's base level remains stable, and its average slope does not change, the drainage divide between Aravaipa Creek and Sulphur Springs basin should not be driven farther to the southeast by more than 1-2 km.

This work also helps resolve the mechanism for drainage integration of Aravaipa Creek with the Lower San Pedro basin. Early explanations for the formation of Aravaipa Canyon described Aravaipa Creek's course as antecedent to uplift of a Galiuro Mountains fault block, and formation of the canyon occurred as Aravaipa Creek's incision kept pace with uplift of the Galiuro Mountains (Davis and Brooks, 1930). Simons (1964) envisaged two stages of uplift for the Galiuro Mountains during which eastward tilting initially created internal drainage in Aravaipa Creek until Aravaipa

Canyon was formed via a spillover event. During a second stage of uplift, Aravaipa Creek maintained its course in Aravaipa Canyon and continued incising as a stream antecedent to uplift. These two stages of uplift do seem appropriate for the evolution of the Galiuro Mountains with early uplift and eastern tilting associated with the breakaway fault of the Catalina detachment (Spencer and Reynolds, 1989), and the later uplift associated with some reactivation of uplift along steep normal faults associated with the Basin and Range Disturbance (Scarborough and Peirce, 1978).

However, our new burial dates for late stage fill in Aravaipa Creek basin suggest internal drainage persisted until ~3 Myr, which is considerably younger than the assertion that Aravaipa Canyon formed prior to the second stage of uplift at ~8-12 Myr. We assert that the formation of an internally drained Aravaipa Creek basin initiated with uplift of a Galiuro block 8-12 Myr, and that the basin remained internally drained until a spillover event at its northwestern edge integrated it with the broader Gila River system sometime soon after 3 Myr. Aravaipa Canyon and the deeply dissected piedmonts of Aravaipa Valley are the result of incision and erosion from 3 Myr to the present. This sequence of events supports the potential for sedimentary basin fill and spill as an important mechanism for post-tectonic landscape evolution in southeastern Arizona's Basin and Range province and the broader North American physiographic province in general. Indeed, spillover was asserted as an important process for the formation of transverse canyons such as the Gila Box upstream from Safford Basin and the Gila River's canyon through Mescal Mountains downstream of Coolidge Dam (Melton, 1965; Morrison, 1985; Douglass et al., 2009). Our results also build upon the growing understanding of the importance of basin fill and spill in the development of the lower Colorado River. House et al. (2008) report evidence for upstream-to-

downstream drainage integration from approximately modern day Lake Mead to the Gulf of California via sequential filling and spilling of brackish lakes along the modern course of the lower Colorado River. In contrast to our approach in Aravaipa Creek basin, along the lower Colorado, the elevations of spillover points are determined using the maximum elevations of lake deposits (the Bouse Formation) rather than a reconstruction of paleo-basin topography (House et al., 2008). Our work in Aravaipa Creek basin adds to a growing understanding of the importance of drainage integration and reorganization as a driver of transient erosion in the absence of active tectonics (Prince et al., 2011; Yanites et al., 2013).

References

Anderson, R. S., Repka, J. L., & Dick, G. S. (1996). Explicit treatment of inheritance in dating depositional surfaces using in situ Be-10 and Al-26.*Geology, 24*(1), 47-51.

Balco, G., & Rovey, C. W. (2008). An Isochron Method for Cosmogenic-Nuclide Dating of Buried Soils and Sediments. *American Journal of Science, 308*(10), 1083-1114.

Braucher, R., Del Castillo, P., Siame, L., Hidy, A. J., & Bourles, D. L. (2009). Determination of both exposure time and denudation rate from an in situ-produced ^{10}Be depth profile: A mathematical proof of uniqueness. Model sensitivity and applications to natural cases. *Quaternary Geochronology*, *4*(1), 56-67.

Darling, A. L., Karlstrom, K. E., Granger, D. E., Aslan, A., Kirby, E., Ouimet, W. B., et al. (2012). New incision rates along the Colorado River system based on cosmogenic burial dating of terraces: Implications for regional controls on Quaternary incision. *Geosphere, 8*(5), 1020-1041.

Davis, W. M., & Brooks, B. (1930). The Galiuro Mountains, Arizona. *American Journal of Science*, (110), 89-115.

Dethier, D. P. (2001). Pleistocene incision rates in the western United States calibrated using Lava Creek B tephra. *Geology*, *29*(9), 783-786.

Dickinson, W. (1991). *Tectonic setting of faulted Tertiary strata associated with the Catalina core complex in southern Arizona*: Geological Society of Amer.

Ditchburn R. G. and Whitehead N. E. (1994) The separation of ^{10}Be from silicates. 3d Workshop of the South Pacific Environmental Radioactivity Association, 4-7.

Douglass, J., Meek, N., Dorn, R. I., & Schmeeckle, M. W. (2009). A criteria-based methodology for determining the mechanism of transverse drainage development, with application to the southwestern United States. *Geological Society of America Bulletin*, *121*(3-4), 586-598.

Gosse, J. C., & Phillips, F. M. (2001). Terrestrial in situ cosmogenic nuclides: theory and application. *Quaternary Science Reviews, 20*(14), 1475-1560.

Granger, D. E., Kirchner, J. W., & Finkel, R. C. (1997). Quaternary downcutting rate of the New River, Virginia, measured from differential decay of cosmogenic 26Al and 10Be in cave-deposited alluvium. *Geology, 25*(2), 107-110.

Granger, D. E., & Muzikar, P. F. (2001). Dating sediment burial with in situ-produced cosmogenic nuclides: theory, techniques, and limitations. *Earth and Planetary Science Letters, 188*(1-2), 269-281.

Hidy, A. J., Gosse, J. C., Pederson, J. L., Mattern, J. P., & Finkel, R. C. (2010). A geologically constrained Monte Carlo approach to modeling exposure ages from profiles of cosmogenic nuclides: An example from Lees Ferry, Arizona. *Geochemistry, Geophysics, Geosystems*, *11*(9).

Hilley, G. E., & Strecker, M. R. (2005). Processes of oscillatory basin filling and excavation in a tectonically active orogen: Quebrada del Toro Basin, NW Argentina. *Geological Society of America Bulletin*, *117*(7-8), 887-901.

House, P.K., Pearthree, P.A., and Perkins, M.E., (2008). Stratigraphic evidence for the role of lake spillover in the inception of the lower Colorado River in southern Nevada and western Arizona, in Reheis, M.C., Hershler, R., and Miller, D.M, eds., *Late Cenozoic drainage history of the southwestern Great Basin and lower Colorado River region—geologic and biotic perspectives: Geological Society of America Special Papers*, v. 439, p. 335–353.

Kohl, C., & Nishiizumi, K. (1992). Chemical isolation of quartz for measurement of *in situ*-produced cosmogenic nuclides. *Geochimica et Cosmochimica Acta, 56*(9), 3583-3587.

Krieger, M. H. (1968). Geologic map of the Saddle Mountain quadrangle. *Pinal County, Arizona [Dudleyville 7.5 min]: US Geological Survey Geologic Quadrangle Map GQ-671*, *1*.

Melton, M. (1965). The geomorphic and paleoclimatic significance of alluvial deposits in southern Arizona. *The Journal of Geology, 73*(1), 1-38.

Meek, N. (1989). Geomorphic and hydrologic implications of the rapid incision of Afton Canyon, Mojave Desert, California. *Geology*, *17*(1), 7-10.

Meek, N., & Douglass, J. (2001). Lake overflow: An alternative hypothesis for Grand Canyon incision and development of the Colorado River. *Colorado River: Origin and evolution: Grand Canyon, Arizona, Grand Canyon Association*, 199-204.

Menges, C., & McFadden, L. (1981). Evidence for a latest Miocene to Pliocene transition from Basin-Range tectonic to post-tectonic landscape evolution in southeastern Arizona. *Arizona Geological Society Digest, 13*, 151-160.

Menges, C., & Pearthree, P. (1989). Late Cenozoic tectonism in Arizona and its impact on regional landscape evolution. *Geologic evolution of Arizona: Arizona Geological Society Digest, 17*, 649–680.

Morrison, R. (1985). Pliocene/Quaternary geology, geomorphology, and tectonics of Arizona. *Soils and Quaternary geology of the southwestern United States: Geological Society of America Special Paper, 203*, 123-146.

Prince, P. S., Spotila, J. A., & Henika, W. S. (2011). Stream capture as driver of transient landscape evolution in a tectonically quiescent setting. *Geology*,*39*(9), 823-826.

Ross, C. P. (1925). Aravaipa and Stanley Mining Districts, Arizona. *US Geol. Surv. Bull*, *763*, 1-120.

Simons, F. S. (1964). *Geology of the Klondyke quadrangle, Graham and Pinal Counties, Arizona: includes a part of the Basin and Range province and several small base-metal mining areas*. US Government Printing Office.

Scarborough, R. B., & Peirce, H. W. (1978, November). Late Cenozoic basins of Arizona. In *Land of Cochise, Southeastern Arizona, New Mexico Geological Society Twenty-Ninth Field Conference Guidebook, ed. JF Callender, JC Wilt, and RE Clemons* (pp. 253-259).

Spencer, J. E., & Reynolds, S. J. (1989). Middle Tertiary tectonics of Arizona and adjacent areas. *Geologic evolution of Arizona: Arizona Geological Society Digest*, *17*, 539-574.

Whipple, K. X., & Meade, B. J. (2006). Orogen response to changes in climatic and tectonic forcing. *Earth and Planetary Science Letters*, *243*(1), 218-228.

Yanites, B. J., Ehlers, T. A., Becker, J. K., Schnellmann, M., & Heuberger, S. (2013). High magnitude and rapid incision from river capture: Rhine River, Switzerland. *Journal of Geophysical Research: Earth Surface*, *118*(2), 1060-1084.

Table

Table 4.1 Sample locations and TCN abundances

Sample ID	Latitude	Longitude	Elevation	Depth	[^{10}Be]	±	[^{26}Al]	±
			m	cm	atoms/g_{qtz}		atoms/g_{qtz}	
AZ18A	32.52883	-110.57287	1003	0	4.96E+04	4.96E+04	n/a	n/a
AZ18B	32.52883	-110.57287	1003	100	3.08E+04	3.08E+04	n/a	n/a
AZ18C	32.52883	-110.57287	1003	150	1.69E+04	1.69E+04	n/a	n/a
AZ18D	32.52883	-110.57287	1003	200	1.19E+04	1.19E+04	n/a	n/a
AZ18E	32.52883	-110.57287	1003	300	1.16E+04	1.16E+04	n/a	n/a
AZ56C	32.72191	-110.32663	1471	n/a	7.44E+04	3.73E+03	1.29E+05	1.24E+05
AZ56G	32.72191	-110.32663	1471	n/a	5.85E+04	4.51E+03	9.72E+04	9.32E+04

Figure Captions

Figure 4.1. Overview of southeastern Arizona's Basin and Range. This region is the southeastern extent of the larger Basin and Range physiographic province of North America. The Gila River flows northwest through the Safford Basin within this region, and both the San Pedro River and Santa Cruz River flow into the Gila River northwest of the Galiuro Mountains.

Figure 4.2. Aravaipa Creek setting. Aravaipa Creek is bounded the Galiuro Mountains to the west and the Santa Teresa and Pinaleno Mountains to the north and east. To the south is a muted drainage divide with the still internally drained Sulphur Springs basin. For the purposes of this study, we divide Aravaipa Creek basin into two physiographic regions, Aravaipa Canyon downstream from the junction with Stowe Gulch and Aravaipa Valley upstream.

Figure 4.3. Simplified geology of Aravaipa Creek basin adapted from Arizona Geological Survey's state map.

Figure 4.4. Detailed summary of Aravaipa Canyon portion of Aravaipa Creek basin. Note inferred approximate integration point at 1100-1200 meters between the shoulders of Brandenburg Mountain, Flat Top Mountain and Periz Peak. Headwaters of Buzan Canyon preserve the drainage divide near the integration point. Rapid incision and drainage capture propagated up past the Hell Hole following the basin's integration with the Lower San Pedro basin.

Figure 4.5. Summary of topographic profiles used to reconstruct basin axis elevations prior to incision. Profiles extracted from a 10 m resolution DEM. Projections of Galiuro and Santa Teresa Mountain high stand piedmonts truncated at the modern basin axis. Transect 'E' shows that near the modern drainage divide, a captured portion of Sulphur Springs basin slopes up toward the paleo divide at ~1390 m as shown, but closer to 1370 m at the valley's axis.

Figure 4.6. Cross section of modern Aravaipa Creek basin and Sulphur Springs basin. Note control points derived from topographic profiles described in Figure 5. The reconstructed paleo-basin surface is a linear regression through the control points. The surface slope of the reconstructed basin surface is very comparable to the modern surface of Sulphur Springs basin, lending support to the credibility of our reconstruction.

Figure 4.7. Digital elevation model of pre-incision Aravaipa Creek basin. The paleo-basin surface slopes from ~1370 near the paleo-drainage divide 6 km northwest of the modern divide to slightly less than 1200 m near the downstream end of Aravaipa Canyon. The reconstruction is the result of fitting a plane between control points derived from the modern topography.

Figure 4.8. Map of incision magnitudes derived from subtracting the modern landscape's elevations from our reconstructed landscape. Red denotes pixels that experienced incision ranging from 1-450 m of incision. Yellow and blue pixels experienced no incision. Maximum incision of 450 m occurred near the downstream end of Aravaipa Canyon.

Figure 4.9. Erosion island plot for Rattlesnake Mesa burial dates, AZ56C and AZ56G. Best fit burial durations for both samples center at 3 Myr with significant uncertainty due to very high native Al concentrations negatively affecting AMS measurements. Paleo-erosion rates for each samples are 37 m/Myr and 47 m/Myr respectively.

Figure 4.10. Concentration depth profile for an intermediate elevation (~1000 m) piedmont surface in Lower San Pedro basin which is adjacent to Aravaipa Creek basin. Apparent exposure ages modeling best-fit denudation rate-exposure duration pairs and modeling simple exposure with no erosion are 435,000 years and 375,000 years, respectively. A paleo-upland erosion rate derived from the depth profile's inferred inheritance is approximately 20 m/Myr.

Figures

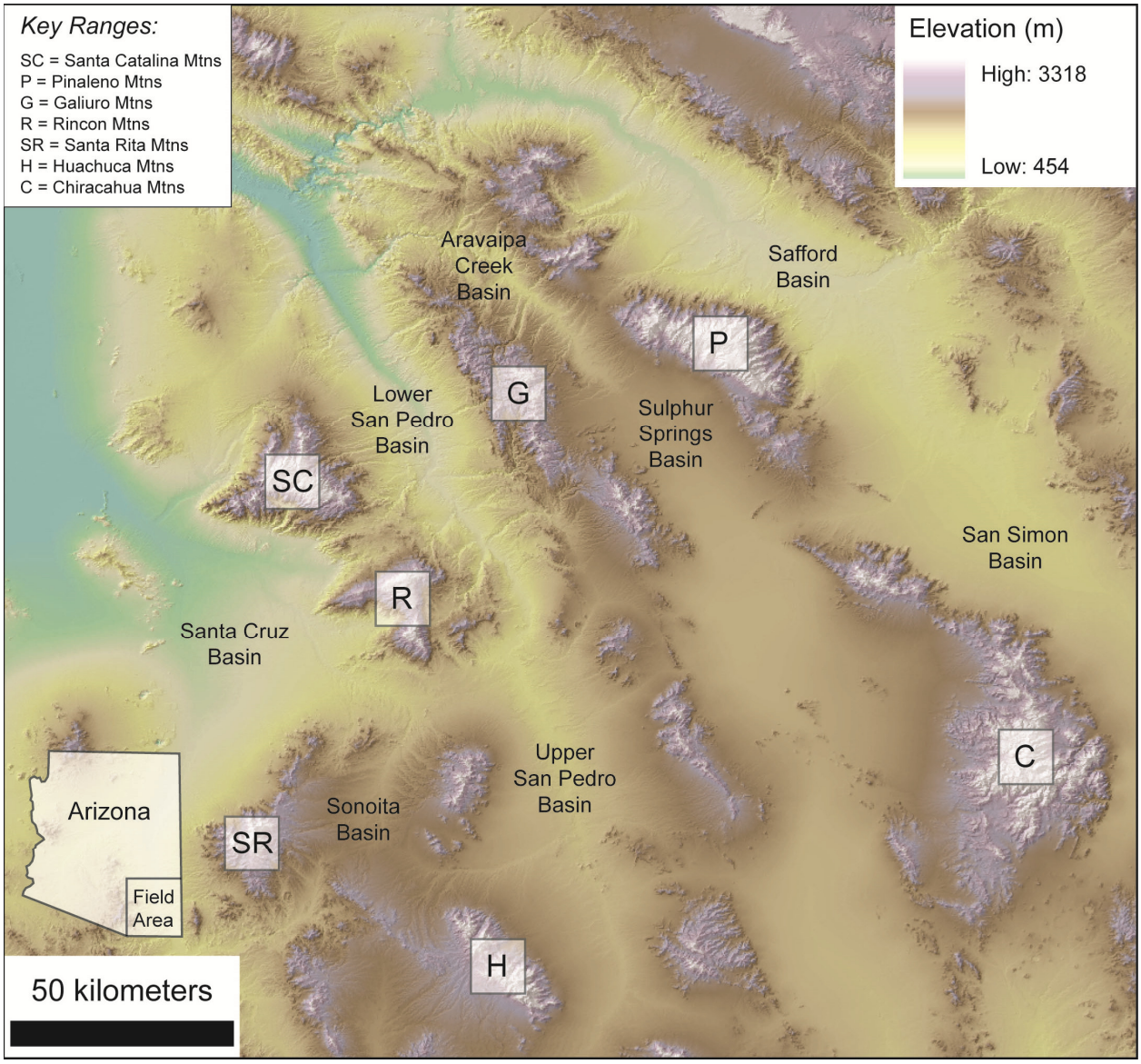

Figure 4.1.

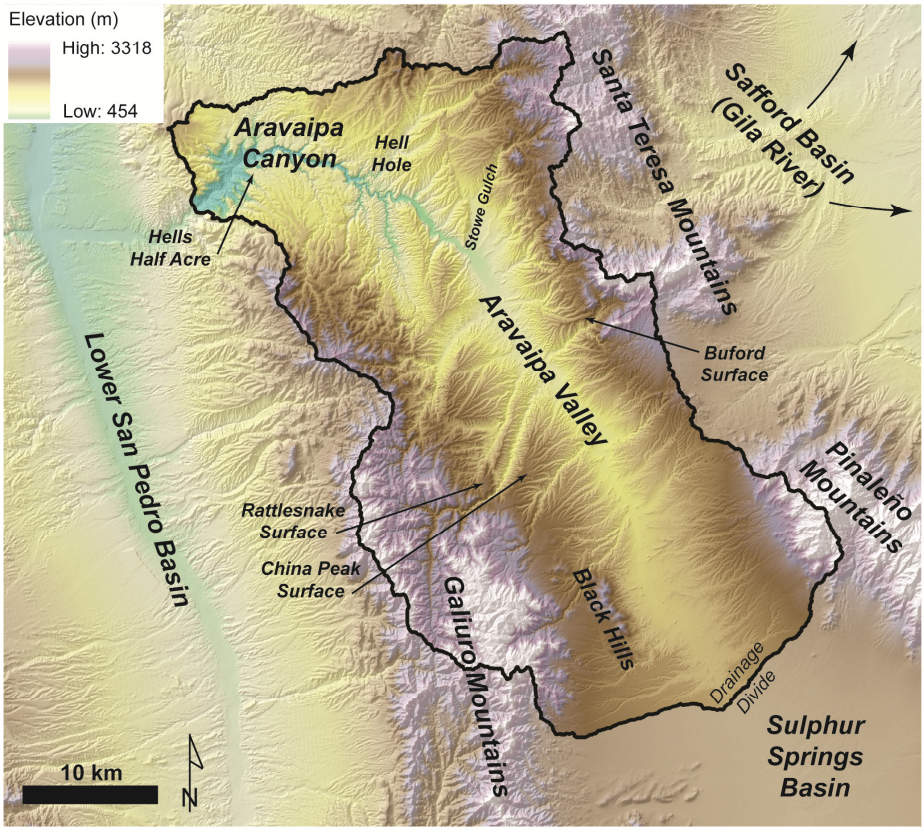
Elevation (m)
High: 3318
Low: 454
Aravaipa Canyon
Hell Hole
Stowe Gulch
Hells Half Acre
Santa Teresa Mountains
Safford Basin (Gila River)
Aravaipa Valley
Buford Surface
Lower San Pedro Basin
Pinaleño Mountains
Rattlesnake Surface
China Peak Surface
Galiuro Mountains
Black Hills
Drainage Divide
Sulphur Springs Basin
10 km
N

Figure 4.2.

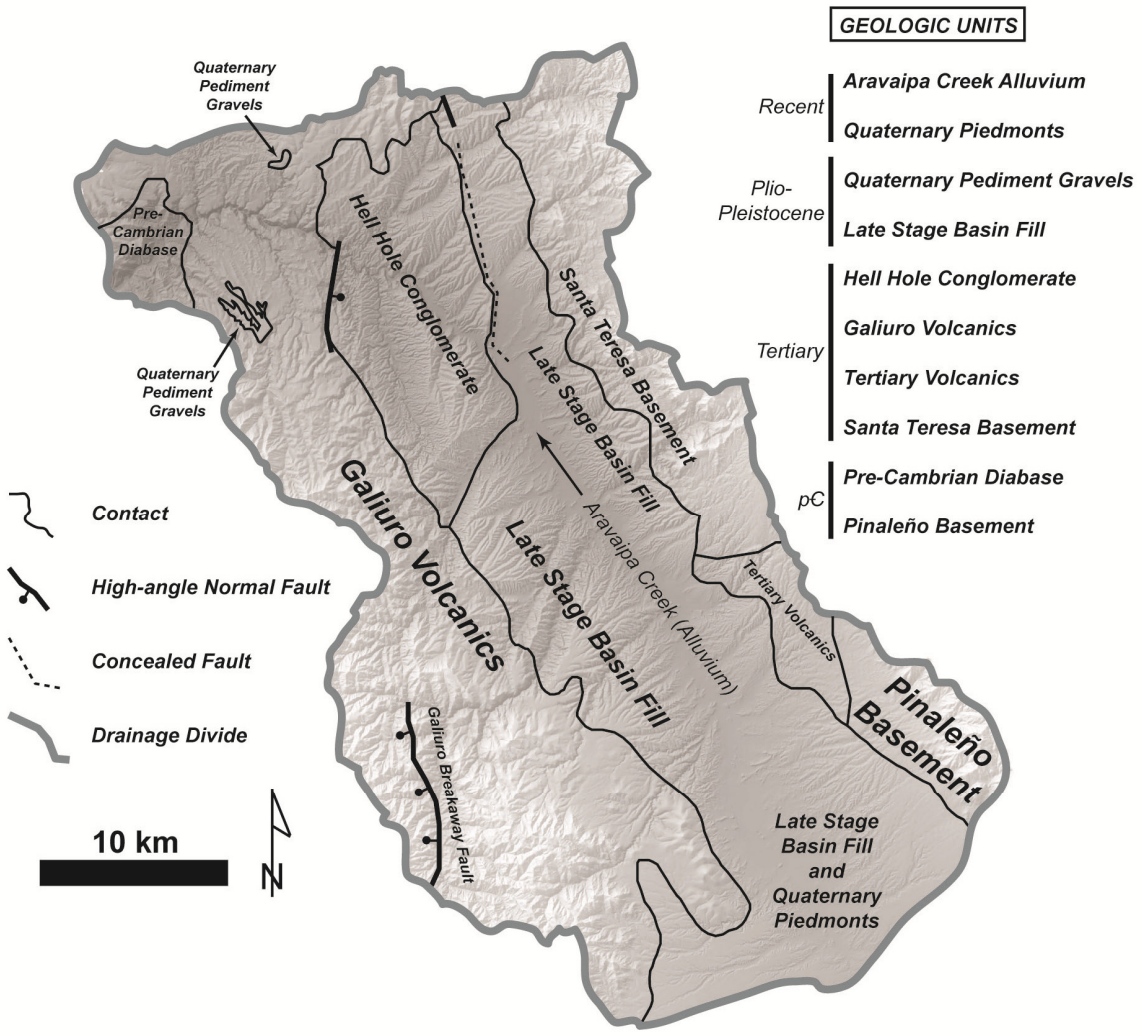
GEOLOGIC UNITS
Recent
Aravaipa Creek Alluvium
Quaternary Piedmonts
Plio-Pleistocene
Quaternary Pediment Gravels
Late Stage Basin Fill
Tertiary
Hell Hole Conglomerate
Galiuro Volcanics
Tertiary Volcanics
Santa Teresa Basement
pC
Pre-Cambrian Diabase
Pinaleño Basement
Quaternary Pediment Gravels
Pre-Cambrian Diabase
Quaternary Pediment Gravels
Hell Hole Conglomerate
Santa Teresa Basement
Late Stage Basin Fill
Aravaipa Creek (Alluvium)
Galiuro Volcanics
Late Stage Basin Fill
Tertiary Volcanics
Pinaleño Basement
Galiuro Breakaway Fault
Late Stage Basin Fill and Quaternary Piedmonts
Contact
High-angle Normal Fault
Concealed Fault
Drainage Divide
10 km
N

Figure 4.3.

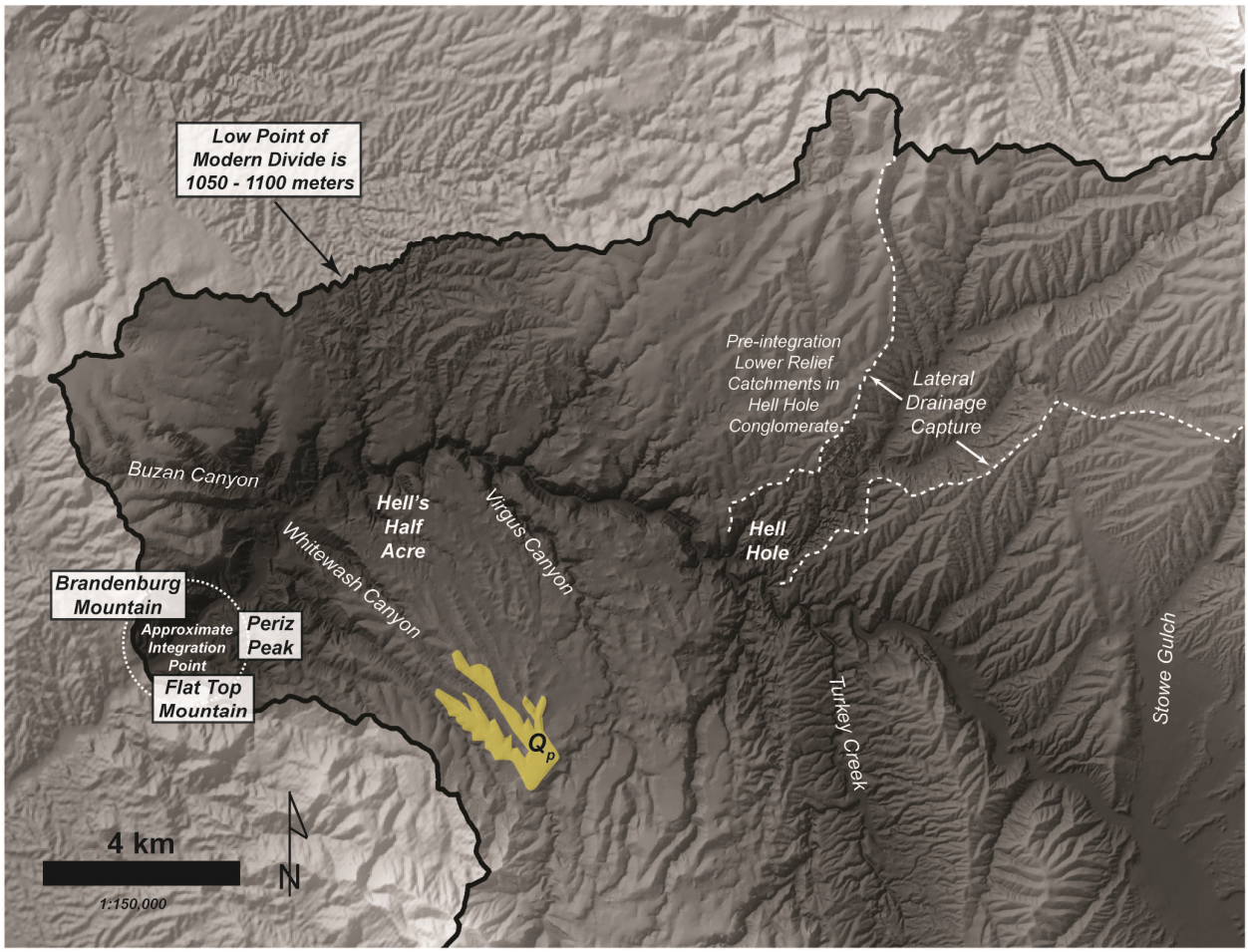
Low Point of Modern Divide is 1050 - 1100 meters
Pre-integration Lower Relief Catchments in Hell Hole Conglomerate
Lateral Drainage Capture
Buzan Canyon
Hell's Half Acre
Virgus Canyon
Whitewash Canyon
Hell Hole
Brandenburg Mountain
Approximate Integration Point
Periz Peak
Flat Top Mountain
Turkey Creek
Stowe Gulch
Q_p
4 km
1:150,000
N

Figure 4.4.

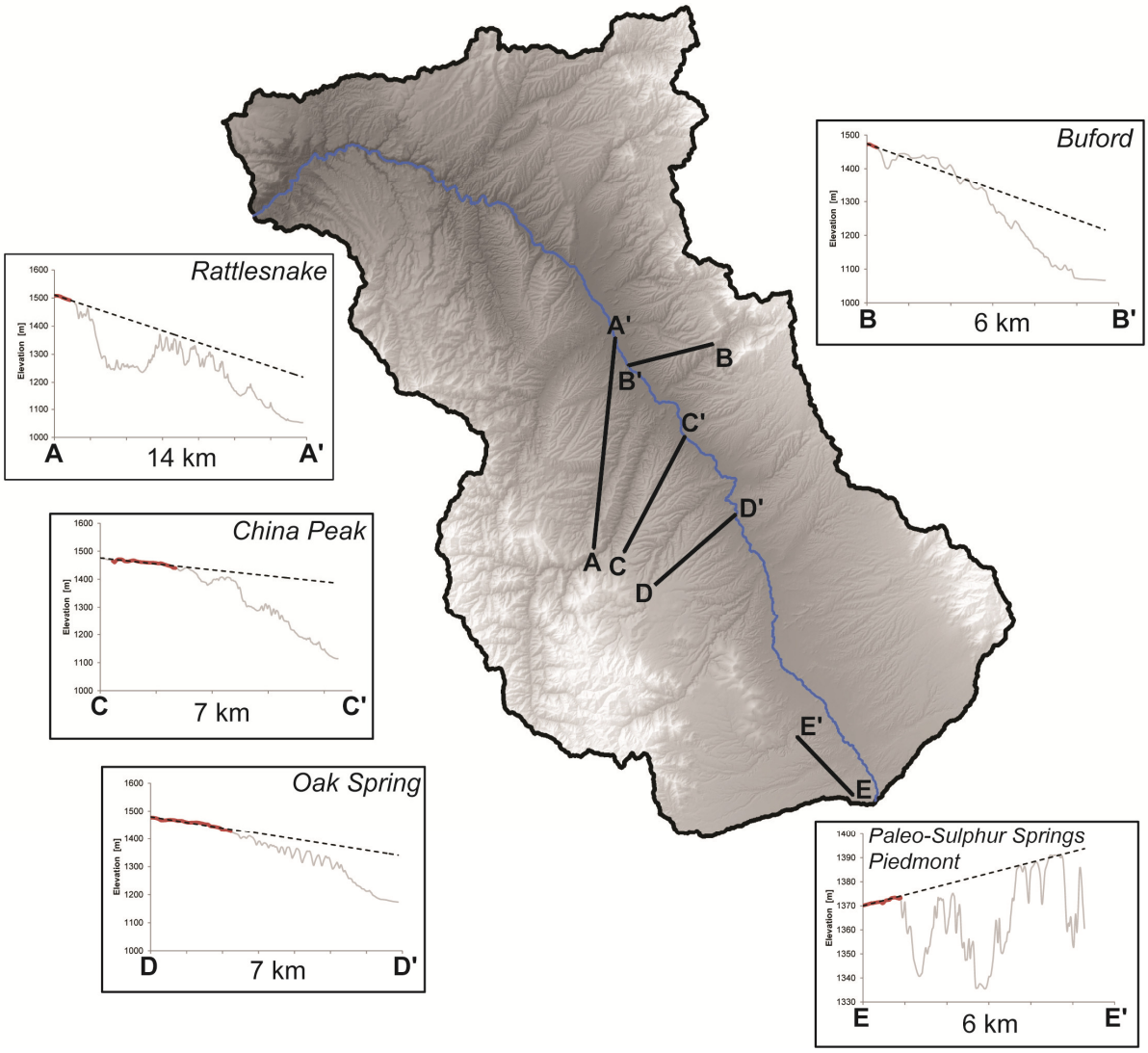
Rattlesnake
Elevation [m]
1600
1500
1400
1300
1200
1100
1000
A
14 km
A'
Buford
1500
1400
1300
1200
1100
1000
B
6 km
B'
China Peak
C
7 km
C'
Oak Spring
D
7 km
D'
Paleo-Sulphur Springs
Piedmont
1400
1390
1380
1370
1360
1350
1340
1330
E
6 km
E'
A'
B
B'
C'
D'
A
C
D
E'
E

Figure 4.5.

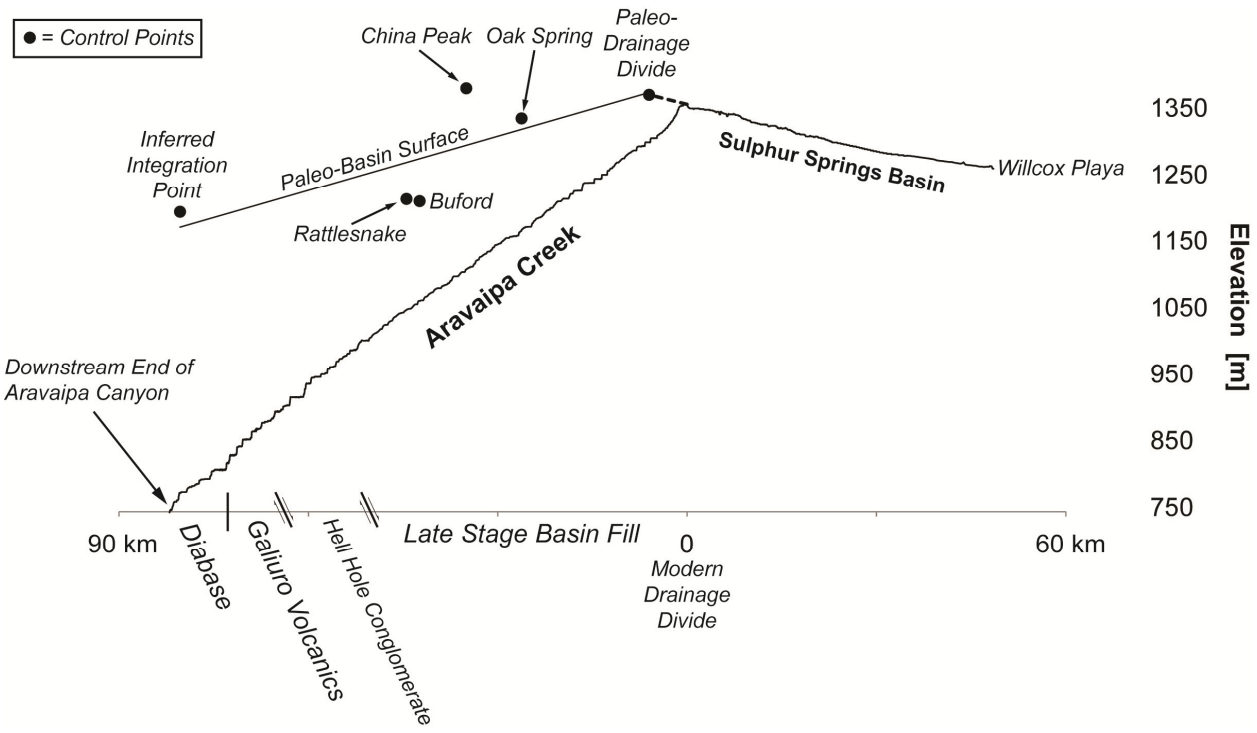
● = Control Points
China Peak
Oak Spring
Paleo-
Drainage
Divide
Inferred
Integration
Point
Paleo-Basin Surface
Buford
Rattlesnake
Sulphur Springs Basin
Willcox Playa
Aravaipa Creek
Downstream End of
Aravaipa Canyon
1350
1250
1150
1050
950
850
750
Elevation [m]
90 km
Diabase
Galiuro Volcanics
Hell Hole Conglomerate
Late Stage Basin Fill
0
Modern
Drainage
Divide
60 km

Figure 4.6.

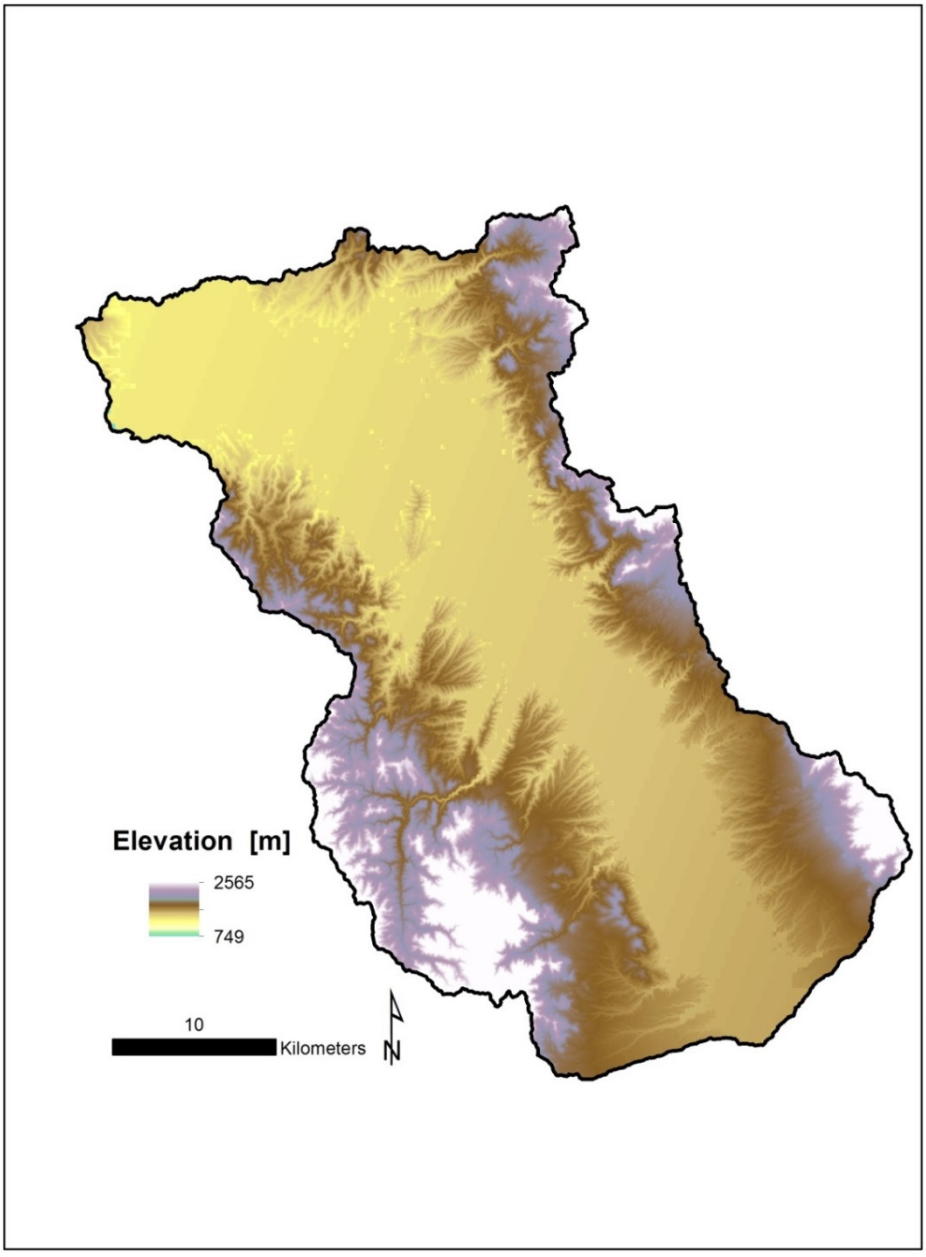

Figure 2.7.

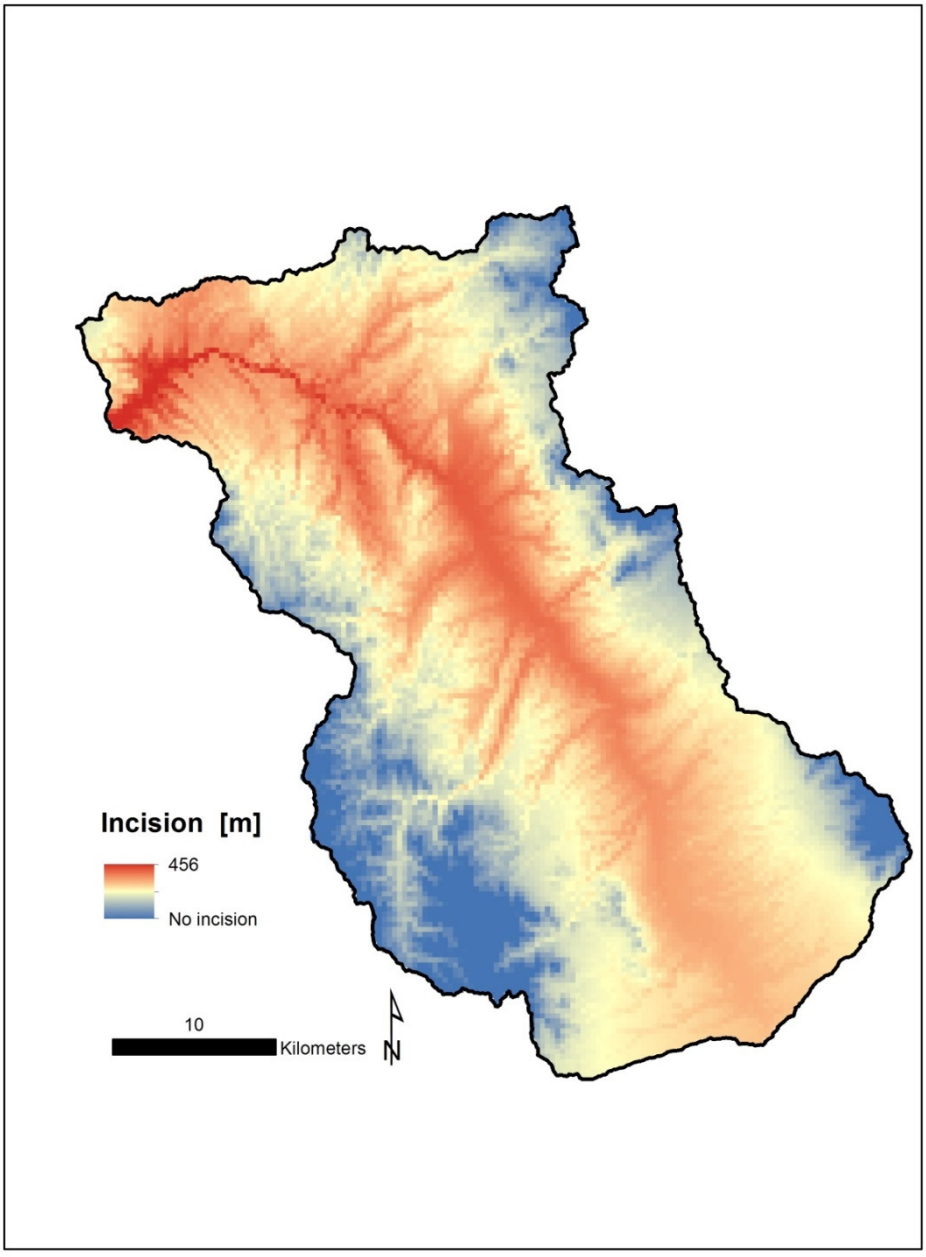

Figure 4.8.

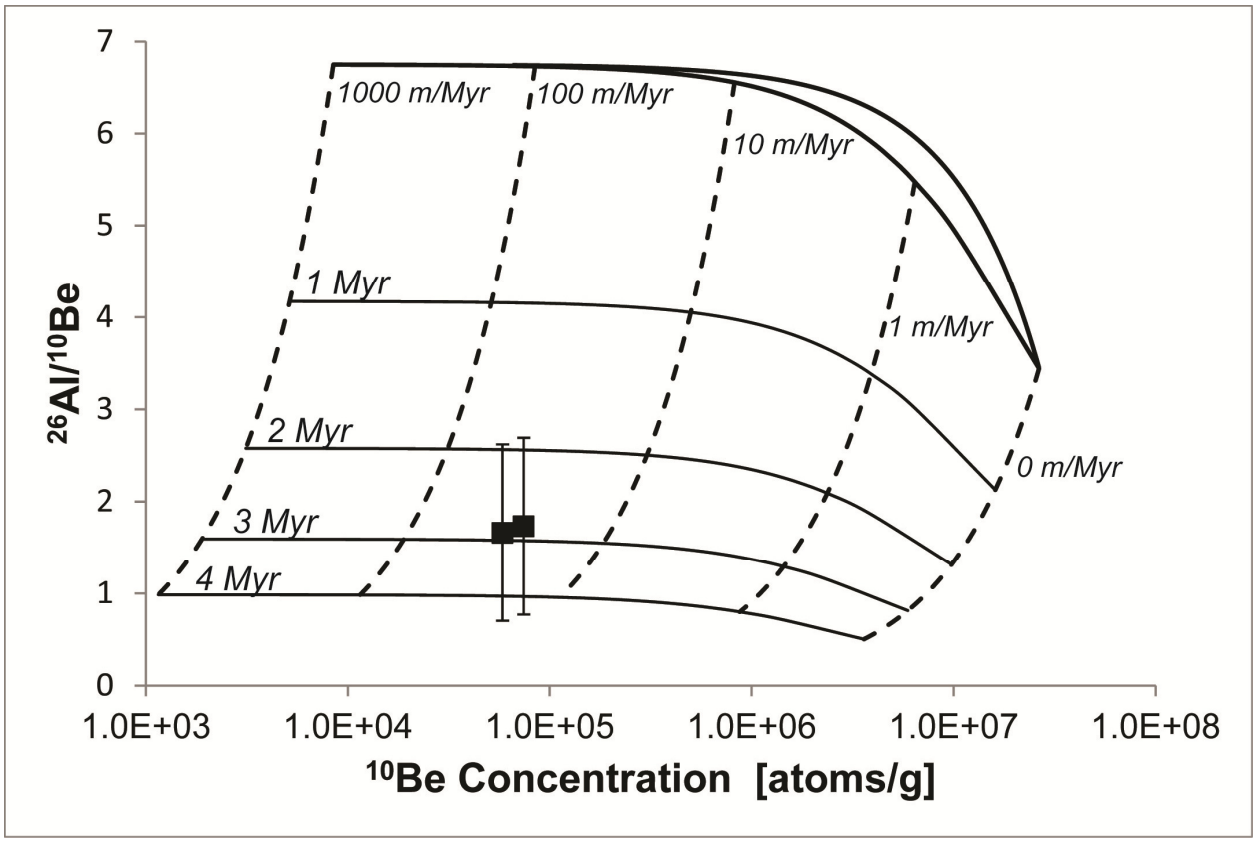
1000 m/Myr
100 m/Myr
10 m/Myr
1 m/Myr
0 m/Myr
1 Myr
2 Myr
3 Myr
4 Myr
26Al/10Be
10Be Concentration [atoms/g]
0
1
2
3
4
5
6
7
1.0E+03
1.0E+04
1.0E+05
1.0E+06
1.0E+07
1.0E+08

Figure 4.9.

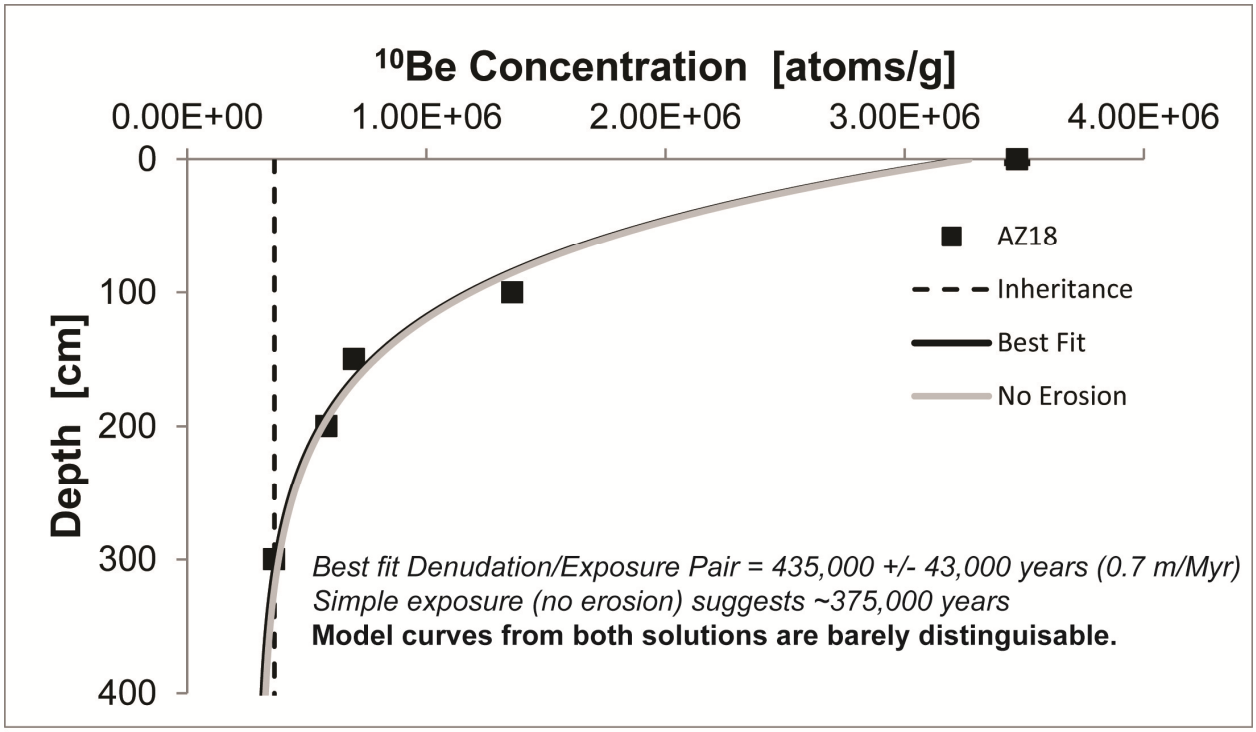
10Be Concentration [atoms/g]
0.00E+00
1.00E+06
2.00E+06
3.00E+06
4.00E+06
0
100
200
300
400
Depth [cm]
AZ18
Inheritance
Best Fit
No Erosion
Best fit Denudation/Exposure Pair = 435,000 +/- 43,000 years (0.7 m/Myr)
Simple exposure (no erosion) suggests ~375,000 years
Model curves from both solutions are barely distinguisable.

Figure 4.10.

CHAPTER 5

Post-Tectonic Landscape Evolution of a Coupled Basin and Range: Pinaleño Mountains and Safford Basin, Southeastern Arizona

Matthew C. Jungers and Arjun M. Heimsath

School of Earth and Space Exploration, Arizona State University

For submission to *Geological Society of America Bulletin*

Abstract

The Pinaleño Mountains and adjacent Safford and Sulphur Springs basins comprise a landscape defined by the extensional tectonics of the Basin and Range physiographic province, and these coupled basins and range are actively degrading under post-tectonic forces. While rates of relief generation and upland erosion during active subsidence ~12-5 Myr ago may are reflected in the geometry of the basins structure and the stratigraphy they contain, rates of post-tectonic landscape evolution from the Pliocene to the present are heretofore unknown. We combine topographic analyses of the Pinaleño Mountains with terrestrial cosmogenic nuclide (TCN) derived catchment-averaged erosion rates and burial dates of axial and piedmont deposits to quantify rates of post-tectonic landscape evolution and a chronology for the last stages of deposition and subsequent incision in Safford basin. In addition to constraining the timing of a deposit formation, TCN burial dates provide paleo-upland erosion rates at the time of deposition.

Erosion rates in the Pinaleño Mountains have been generally slow over the past 4 Myr, ranging between ~30-60 m/Myr with no strong relationship to drainage basins' modern topography. A notable acceleration of erosion rates to 100-250 m/Myra between 3.5-2 Myr correlates with an inferred period of enhanced precipitation as well as the arrival of the Gila River in Safford basin sometime shortly before 2.8 Myr. Widespread incision of Safford basin was underway by ~2 Myr as recorded by the dissection of piedmont basin high stand deposits (Frye Mesa) and two intermediate Gila River terraces on the northeast margin of Safford basin (dated to 1.8 Myr and 0.64 Myr). Gila River incision rates have ranged from 30-60 m/Myr over the past 3 Myr. Based on similarities between catchment-averaged erosion rates and topography from basins draining into the integrated Safford basin and the still internally drained Sulphur Springs basin, it appears that incision on the Gila River is not having a strong impact on upland erosion rates.

1.0 Introduction

The Basin and Range physiographic province of the North American Cordillera is a region defined by extensional tectonics (e.g. Menges and Pearthree, 1989; Dickinson, 1991; Dickinson, 2004). Rugged mountain ranges stand in stark relief adjacent to muted structural basins filled with sediment. In simplest terms, this topography resulted from uplift along normal faults that drove erosion of sediment from the uplands to be deposited into subsiding basins. These basins often remain internally drained for much of their tectonic development such that their stratigraphy could preserve a nearly full history of upland response to tectonic forcing. The deep sedimentary deposits – often 1000s of meters thick at basins' depocenters – can also host economic deposits such as copper, and are fundamentally important to the groundwater resources of the water-stressed

American Southwest. Additionally, there is active investigation into the potential for these basins to serve as reservoirs for carbon sequestration (Gootee, 2012).

While the defining period of Basin and Range development is inarguably structural in nature, it remains unclear how these basins transition to post-tectonic landscape evolution. How quickly do upland erosion rates slow in response to waning subsidence? What is the current rate at which high-relief ranges are decaying? What are the respective roles of Quaternary climate and internal sedimentary system dynamics – e.g., drainage integration between adjacent basins, and subsequent incision and lateral migration of evolving axial systems – in terms of eroding mountain ranges and degrading basin fill deposits? An understanding of these post-tectonic processes and their rates is of fundamental importance to quantifying how quickly tectonic signals may be overprinted or degraded once extensional tectonics have ceased.

Here, we apply an integrated approach of field observations, topographic analyses, and terrestrial cosmogenic nuclide (TCN) analyses to interrogate the post-tectonic landscape evolution of a paired basin and range in southeastern Arizona. TCN abundances in sediment provide both geochronologic constraints and process rates for our study. We present TCN-derived burial dates of late-stage sedimentary basin fill along the northern piedmont of the Pinaleño Mountains and burial dates for sediments deposited on a flight of terraces along the Gila River along the northeast margin of the Safford Basin (Figure 1). These dates not only constrain the timing of post-tectonic landscape evolution, but also enable quantifying regional incision rates. TCN analyses also enable quantifying paleo-erosion rates for the upland drainage basins that are the sources for the sediment. We compare these paleo-erosion rates to modern millennial scale erosion rates derived from ^{10}Be abundances in fluvial sediment collected in drainage basins along both the north and the south

margins of the Pinaleño Mountains. Drainage basins on the north side of the Pinaleño Mountains are all tributaries to the Gila River (a tributary to the Colorado River), while most of the basins on the south side drain into the still-closed Sulphur Springs Basin. This juxtaposition of base level conditions allows the possibility of distinguishing the effects of regional drainage integration on upland erosion rates.

2.0 Background

Gilbert (1875) conducted the earliest surveys of the geology and resource potential for southeastern Arizona's Basin and Range physiographic province. Indeed, for a century after his work, his broad classification of late stage basin fill as the Gila Conglomerate persisted in the literature (e.g., Heindl, 1958; Heindl, 1962). By the mid-20th century, geologists began to more fully consider the impacts of climate on the Quaternary development of the Basin and Range (Tuan, 1962; Melton, 1965), relating the transitions between glacial and interglacial periods to late-stage piedmont deposition and incision. More recently, the modern topography of the Pinaleños was considered in the context of biogeochemical dynamics set up by the climate gradient that exists from the modern basin floor to the summit of Mt. Graham (Pelletier et al., 2013).

2.1 Geology

The Pinaleño Mountains are a gneissic metamorphic core complex exhumed during early stages of regional low-angle extensional tectonics during the middle-to-late Oligocene (Spencer and Reynolds, 1989). The current physiography of Arizona's Basin and Range was driven by subsequent, high-angle normal faulting associated with the Basin and Range Disturbance which initiated at

approximately 8-12 Myr and ceased within a poorly defined window ranging from 5-2 Myr with some regional variation (Menges and Pearthree, 1989). Safford Basin, immediately to the northeast of the Pinaleño Mountains is divided into two structural sub-basins, Bear Springs Subbasin to the north and 111 Ranch Subbasin to the east, based on Bouger gravity anomalies (Wynn, 1981; Houser and Pearthree, 2002). Safford Basin is a half graben with the most subsidence occurring along a basin-bounding fault system on the north side of the Pinaleño Mountains (Thorman, 1981; Houser and Pearthree, 2002). At its deepest, the basin is filled with up to 4600 m of sedimentary basin fill (Kruger, 1991; Houser and Pearthree, 2002). The sedimentary basin fill is divided into upper and lower stratigraphic units. The purely syntectonic Midnight Canyon Conglomerate began deposition at 17 Myr and its upper bound is at approximately 10 Myr (Richter et al., 1983; Houser et al., 1985). The upper basin fill is divided into two sub-units in accordance with the subbasin that contains the sediment, the 111 Ranch Formation and the Bear Springs formation. Both formations are inferred to be Pliocene based on the biostratigraphy of deposits at 111 Ranch (Galusha et al., 1984).

The very latest stage basin fill is exposed throughout Safford Basin, but perhaps most spectacularly at Frye Mesa on the northeast side of the Pinaleño Mountains. No numerical or relative dates for this fill existed prior to our study, but the sediment was roughly correlated with the Gardner Canyon Alloformation of Sonoita Creek Basin (*sensu stricto,* Morrison, 1985), with an approximate age of 2-1 Myr (Menges and McFadden, 1981) for the final stages of basin fill deposition within Safford Basin prior to regional drainage integration of the Gila River. Regional extensional tectonics are inactive in southeastern Arizona, but there is evidence for mid-to-late Pleistocene surface rupturing earthquakes along fault systems roughly synthetic to the topographic front of the northeast Pinaleño Mountains (Pearthree, 1986). Displacement along these faults is not

more than several meters, while incision of the Gila River system within Safford Basin is over 100 m, underscoring the importance of base level fall and climate variations rather than faulting in the post-tectonic landscape evolution of this basin (Houser and Pearthree, 2002).

2.2 Climate

The Pinaleño Mountains are characterized as an ecological 'sky island', at the northern extent of the Madrean 'archipelago', due to the isolated ecosystems that developed at high elevations because of the stark contrast in temperatures and annual precipitation from the surrounding Sonoran desert (Warshall, 1995). Total relief of nearly 2500 m produces a steep gradient in mean annual temperature and precipitation as a function of increasing elevation from basin floor to the summit of the range. Mean annual temperature (MAT) ranges from 5-18°C from the highest elevations to the valley floor, respectively . Mitchell and Ober (2013) report a lapse rate for average maximum temperatures in southeastern Arizona of -7.6 °C/km of elevation gain. Importantly, this difference of greater than 10°C in average temperature occurs across a horizontal distance of only 10-15 km between the Safford Basin and the upper elevations of the Pinaleño Mountains. Mean annual precipitation (MAP) also differs dramatically between the valley floor and upper elevations, increasing from 0.25 m/yr to 1.1 m/yr. These gradients of temperature and precipitation set up a succession of ecosystems from Sonoran/Chihuahuan Desert at lowest elevations, grading into scrub and grassland, then oak and pine, then conifer, and finally spruce and fir at the highest elevations (Halvorsen et al., 2001; Mitchell and Ober, 2013). In the Pinaleños, endemic species such as the Mt. Graham squirrel inhabit only the highest elevations having potentially evolved in isolation since the last time that the regional climate was cool and wet enough to allow dispersal of populations across

basin floors between sky islands (Mitchell and Ober, 2013). The most recent period of significantly cooler and wetter climate conditions for the Pinaleños is believed to be during the Younger Dryas at ~12.7-11.5 Myr (Pigati et al., 2009).

The paleoclimate record for southeastern Arizona is best known for the late Pleistocene through the Holocene (e.g., Martin, 1963; Waters, 1989; Van Devender, 1990; Zhu et al., 1998; Allen, 2005; Holmgren et al., 2006; Pigati et al., 2009; Wagner et al., 2010; Mitchell and Ober, 2013), but some coarser resolution records do exist into the early Pliocene (Smith et al., 1993; Smith, 1994). Soil carbonates from the St. David Formation of the Upper San Pedro Basin, ~120 km to the southwest of Safford Basin and the Pinaleño Mountains, yield a paleoclimate record of precipitation from approximately 0.5-4.0 Myr (Smith et al., 1993; Smith, 1994). The precipitation record inferred from stable ^{18}O in paleosol carbonates at St. David suggests a higher total annual precipitation with a higher proportion of that moisture arriving in the winter months from ~3.5-2.0 Myr. With the transition into the Pleistocene, total precipitation decreased, as did the proportion of winter precipitation, suggesting increasing aridity and an increased importance of the North American Summer Monsoon (NASM) (Smith, 1995). Paleoclimate records for the Quaternary come from a number of proxies, including packrat middens, lake cores, lake highstands, and speleothems (Martin, 1963; Waters, 1989; Van Devender, 1990; Zhu et al., 1998; Allen, 2005; Holmgren et al., 2006; Pigati et al., 2009; Wagner et al., 2010; Mitchell and Ober, 2013). In summary, it was cooler and wetter than today during the Wisconsinan glaciation (115-110 kyr), but the coolest and wettest conditions occurred during the Last Glacial Maximum (LGM) at 24-21 kyr (Menking et al., 2004; Allen, 2005; Mitchell and Ober, 2013).

A speleothem record from the Cave of the Bells in Arizona suggests highly variable moisture availability for the southwestern United States throughout the late Pleistocene, likely a result of variable sea surface temperatures of both the Pacific Ocean and Atlantic Ocean (Wagner et al., 2010). This moisture variability is perhaps also reflected in a series of highstands from 18-10 kyr for pluvial Lake Cochise centered near modern day Willcox Playa (Waters, 1989). Willcox Playa is 65 km south of Safford Basin, and it is the modern day base level for Sulphur Springs Basin and much of the south side of the Pinaleño Mountains. The likely effect of cooler and wetter climates in the Pinaleño Mountains is a shift of the modern ecosystem boundaries to lower elevations and perhaps enhanced physical weathering due to frost-cracking at upper elevations and potentially even periglacial processes at the highest elevations (Melton, 1965). We address the geomorphic implications for these periods of enhanced cooling and moisture are now discussed in more detail.

2.3 Geomorphology

The range-scale relief of nearly 2500 m from the modern Gila River near Safford, AZ, to the summit of Mt. Graham is a product primarily of Basin and Range tectonics. However, ~500 m of relief at the lower elevations – e.g., between Frye Mesa and the modern Gila River – developed more recently by incision of the Gila River following downstream drainage integration of the Gila with the Lower San Pedro Basin. It is important to note that while incision on the north side of the Pinaleño Mountains produced 20% of the total relief, the south side of the range drains primarily to the internally drained Sulphur Springs Basin, and the total relief is accordingly 500-600 m less. Only a small fraction of the drainage basins on the west side of the range drain into Aravaipa Creek Basin, a

tributary of the San Pedro River which flows into the Gila River just 19 km downstream from the Aravaipa Creek confluence (Fig. 2).

The relief structure of the Pinaleño Mountains has the added complexity of a lower-relief patch of the landscape above elevations of ~2700 m. Upper elevations are characterized by gentler hillslopes of only 10-15°; below elevations of 2700 m, hillslopes steepen to threshold angles (~35°) where soil is present, but there are abundant rocky patches and cliffs. The upper low-relief landscape is predominantly soil-mantled, however, there is a small area of steeper terrain at high elevations within the headwaters of Grant Creek. This patch of the landscape roughly corresponds with the mapped extent of a gneiss body with a slightly different composition than the surrounding lithology. The steep hillslopes within the upper Grant Creek basin extend beyond the mapped extent of the isolated unit, so lithology alone may not explain this variation of morphology. The transition from low relief and low hillslope angles at higher elevations to the rocky, steep landscape below approximately 2700 m is reflected in the longitudinal profiles of channels draining both the north and south sides of the Pinaleño Mountains (Fig. 2). At lower elevations, just upstream of the range front, valley bottoms are often filled with debris flow deposits – e.g., Grant Creek, Jacobson Canyon, Taylor Canyon, and Tripp Creek – with many generations of debris flow lobes underscoring the importance of mass wasting in the long-term landscape evolution of the high-relief portion of the Pinaleño Mountains. We have not observed recent landslide deposits during our field work in the area, but debris flows have recently been active in the Santa Catalina Mountains, another sky island with similar lithology 90 km to the west of the Pinaleño Mountains, suggesting that debris flows remain an active process within the steeper portions of the Pinaleño Mountains (Youberg et al., 2008).

In tectonically active landscapes, abrupt transitions between low-relief and high-relief landscapes used in concert with non-equilibrium stream profiles may be evidence for a transient stage of landscape response to changes in uplift (e.g., DiBiase et al., 2010). In such a setting, with climate held relatively constant, an acceleration in uplift will force streams to steepen until a new equilibrium between uplift and erosion is achieved. During this transient readjustment, a propagating wave of incision sweeps up system, and hillslopes steepen as upland erosion rates increase in response to incision. Portions of the landscape that have not yet been affected by the propagating incision will maintain less steep channels and gentler hillslope angles that reflect a slower, relict erosion rate. It is possible that the upper elevations of the Pinaleño Mountains represent such a relict landscape, and this possibility is one of the motivating questions for our study.

In contrast, recent work focusing on the eco-pedo-geomorphology of the Pinaleño Mountains by Pelletier et al. (2013) emphasizes the potential for this transition from steep to gentle slopes as a function of elevation is driven by temperature and precipitation gradients rather than transient response to tectonics. Cooler temperatures and enhanced precipitation at higher elevations are inferred to promote the feedbacks between vegetation and soil development which in turn produces and maintains a low-relief, soil-mantled hillslope. Patchy soils and rocky slopes at lower elevations are attributed to less suitable conditions for vegetation to take hold and modify the landscape.

Relict landscapes notwithstanding, the feedbacks between climate and surface processes in the uplands of the Pinaleño Mountains are undeniably important, especially for the post-tectonic landscape evolution of the range. Some of the earliest work relating alluvial fans to paleoclimate in the American Southwest used Frye Mesa on the north side of the Pinaleño Mountains as a key

example of landscape response to glacial-interglacial cycles (Melton, 1965). Melton hypothesized that most of the mass of Frye Mesa was deposited during a cooler, wetter Illinoisan glacial period 190-130 kyr, and that the deep, red soil on the deposit's surface developed during a subsequent interglacial. He envisaged that the final lobe of very coarse, boulder-filled alluvium deposited near the fan's proximal end was the product of renewed upland erosion during the Wisconsinan glacial due to enhanced frost-wedging at high elevations under a cooler climate. Houser and Pearthree (2002) agree with Melton's correlation of the finest-grained material at the base of Frye Mesa with late Pliocene basin fill, but attribute the majority of Frye Mesa deposition to the period of waning or absent tectonics, and any variations in grain-size within the deposit to climate change at the Pliocene-Pleistocene boundary. Our study's TCN burial dates constrain the timing of late stage deposition into Safford Basin (in the form of Frye Mesa), and compare paleo-erosion rates during that time to modern, millennial-scale erosion rates.

3. Methods

3.1 Topographic Analyses

We employ a suite of digital terrain analyses to derive topographic metrics that divide the Pinaleño Mountains and Safford Basin into a series of geomorphic process domains. When paired with TCN-derived erosion rates, these topographic analyses allow us to investigate the relationship between topography and erosion rates, . Using a 10 m digital elevation model (DEM), we quantify mean basin slope and catchment-mean local relief (using a search window with a 1.5 km radius), and catchment-mean normalized channel steepness (Figure 2).

We calculated hillslope angles for each pixel in our DEM, and then calculated a mean basin slope for each catchment, defined simply as the average of all hillslope angles within a drainage basin. Low-slope valley fill in some drainage basins of interest may bias calculations of catchment mean slope. If present, fill is, therefore, excluded from such calculations.

Previous work shows that the scale used to calculate local relief is fundamentally important to quantifying topographic form (e.g. DiBiase et al., 2010). We find that local relief calculated within a window with a 3 km diameter best captures the range-scale relief structure (Figure 2). In general, local relief shows a transition to lower relief for drainage basins at the northwest and southeast tips of the range – e.g., Tripp Canyon, Marijilda Canyon, and Jacobson Canyon. Local relief calculated over smaller windows failed to capture the transition to lower relief at the range's northwest and southeast tips, and larger windows failed to define the low-relief patch of the landscape at higher elevations.

Longitudinal profiles of rivers record how well-adjusted a landscape is to external forcings such as tectonics and climate. Using normalized channel steepness index, k_{sn}, as a topographic metric enables quantifying landscape response to incision not apparent from hillslope angles when slopes are beyond threshold angles (Wobus et al., 2006; Ouimet et al., 2009; DiBiase et al., 2010). Using a reference concavity of 0.45 and minimum drainage area of 5 km^2, we extract k_{sn} values for every 500 m stream segment in the Pinaleño Mountains. Mean channel steepness for drainage basins is defined as the average of all the channel steepness values within a basin.

3.2 Terrestrial Cosmogenic Nuclides (TCNs)

Cosmogenic nuclide abundances in rock and sediment record the near surface residence time of those Earth materials. TCNs are produced during the bombardment of Earth's surface by secondary cosmic ray particles. When cosmic rays hit the Earth's atmosphere a cascade of secondary particles is produced, some of which reach the Earth's surface. Most of these particles are then quickly stopped by the mass of soil and rock within the first 1-3 meters of the surface (Gosse and Phillips, 2001). The accumulation of TCN in rock or sediment as a function of depth and duration of exposure is expressed as:

$$N(z,t) = \frac{P_0 e^{\frac{-\rho z}{\Lambda}}}{\lambda + \frac{\rho \varepsilon}{\Lambda}}\left(1 - e^{-\left(\lambda + \frac{\rho \varepsilon}{\Lambda}\right)t}\right), \qquad (1)$$

where N is TCN concentration [atoms g^{-1}], t is time [yr], ε is erosion rate[cm yr^{-1}], λ is radionuclide decay constant [yr^{-1}], z is depth below the deposit surface [cm], P_0 is TCN surface production rate [atoms g^{-1} yr^{-1}], Λ is TCN production rate attenuation length [g cm^{-2}], and ρ is rock or sediment density [g cm^{-3}]. This formulation is commonly used to determine apparent exposure ages and/or maximum surface erosion rates (e.g. Portenga and Bierman, 2011). When determining surface exposure ages for alluvial deposits or boulders an additional term must be included to account for inherited TCN abundances accumulated prior to deposition (e.g. Anderson et al., 1996):

$$N(z,t) = N_0 e^{-\lambda t} + \frac{P_0 e^{\frac{-\rho z}{\Lambda}}}{\lambda + \frac{\rho \varepsilon}{\Lambda}}\left(1 - e^{-\left(\lambda + \frac{\rho \varepsilon}{\Lambda}\right)t}\right), \qquad (2)$$

where N_0 is the inherited concentration of the cosmogenic nuclide [atoms g^{-1}] and other terms are as in Equation 1. We use Equation 2 when calculating apparent minimum exposure ages of boulders

deposited on top of Frye Mesa, and it also serves as the foundation for our calculations of both catchment-averaged erosion rates and burial dates for sedimentary basin fill. The obvious drawback of this approach is that an eroding sample will lead to a younger than actual surface age.

For an upland drainage basin that is steadily eroding – i.e., $t \gg \left(\lambda + \frac{\rho\varepsilon}{\Lambda}\right)^{-1}$ – TCN concentrations (N) in sediment eroded from the catchment are quantified as (Lal, 1991):

$$N = \frac{P_0}{\lambda + \frac{\rho\varepsilon}{\Lambda}}, \qquad (3)$$

rearranging to solve for erosion rate yields:

$$\varepsilon = \frac{\Lambda}{\rho}\left(\frac{P_0}{N} - \lambda\right) \quad (4).$$

Equation 4 is commonly used to invert TCN concentrations in detrital samples for upland erosion rates (e.g. Brown et al., 1995; Bierman and Steig, 1996; Granger et al., 1996). Balco et al. (2008, Figure 8) show, however, that in some cases (e.g., low elevation, high erosion rate sites) erosion rates will be underestimated by a few percent to several tens of percent if only Equation 4 is used. This results from not taking into account subsurface TCN production by muons (Heisinger et al., 2002a,b). We avoid this problem by determining an 'effective elevation' for each drainage basin of interest following the methods of Portenga and Bierman (2011), then calculating catchment-averaged erosion rates using the CRONUS-Earth online calculator (Balco et al., 2008; http://hess.ess.washington.edu/) which implements Heisinger et al's (2002a,b) equations for muon induced TCN production. Essentially, calculating an 'effective elevation' according to Portenga and Bierman (2011) provides an input elevation for CRONUS that will ensure a given drainage basin's TCN production rates will be scaled appropriately by the online calculator.

Cosmogenic nuclide abundances in sediment eroded from upland basins and deposited in downstream fill terraces, lakes, or sedimentary basins record both a paleo-upland erosion rate, and a burial duration since deposition (Granger et al., 1997; Granger and Muzikar, 2001). As a result, inverting measured TCN concentrations into a burial date requires the measurement of two cosmogenic nuclides to solve for those two unknowns. Importantly, at least one nuclide measured must be a radionuclide to determine burial duration and, therefore, deposition age. For this study, we use two cosmogenic radionuclides, ^{26}Al and ^{10}Be, both of which have well established production rates and half-lives. A full formulation for TCN abundances in buried sediment is determined with a combination of Equations 1, 2, and 3 (adapting the notation Balco and Rovey, 2008):

$$N_{10} = \frac{P_{10}}{\lambda_{10}+\frac{\rho\varepsilon}{\Lambda}} e^{-\lambda_{10} t_b} + \frac{P_{10} e^{\frac{-\rho z}{\Lambda}}}{\lambda_{10}+\frac{\rho\varepsilon}{\Lambda}} \left(1 - e^{-\left(\lambda_{10}+\frac{\rho\varepsilon}{\Lambda}\right) t_b}\right), \qquad (5)$$

$$N_{26} = \frac{P_{26}}{\lambda_{26}+\frac{\rho\varepsilon}{\Lambda}} e^{-\lambda_{26} t_b} + \frac{P_{26} e^{\frac{-\rho z}{\Lambda}}}{\lambda_{26}+\frac{\rho\varepsilon}{\Lambda}} \left(1 - e^{-\left(\lambda_{26}+\frac{\rho\varepsilon}{\Lambda}\right) t_b}\right), \qquad (6)$$

where *10* and *26* subscripts denote ^{10}Be and ^{26}Al, respectively, and t_b is burial duration in years. In an ideal setting, burial occurs very rapidly, and shielding from post-burial TCN production is nearly immediate. Under these conditions, the RHS of Equations 5 and 6 go to zero, and a burial date can be determined by iterating through ε and t_b pairs to find a best fit for measured TCN abundances. We refer to this approach as conventional burial dating, and it is most appropriate for sedimentary settings where transport from eroding uplands is swift, and, once deposited, sediment is fully shielded from post-burial TCN production.

Sedimentary packages with less ideal depositional histories are still datable by means of TCN burial dating, but it requires more than one sample analysis per burial date. The 'isochron approach'

(Balco and Rovey, 2008) is well suited to dating the Pliocene-Pleistocene late stage basin fill of southeastern Arizona. For the first application of this method, Balco and Rovey (2008) used TCN concentration depth profiles within buried paleosols to date a sequence of tills in the Midwestern United States. The power of their technique is that it determined a burial date by extracting an isochron from a population of sediment samples in paleosols that experienced a period of stability unique to each sediment package.

Darling et al. (2012) adapted this isochron approach to sedimentary packages along the Colorado River and its tributaries. By individually analyzing 4-7 cobbles from each fill terrace of interest, Darling et al., exploit a range of pre-burial exposure histories to evaluate whether their samples experienced significant post-burial TCN production. We adapt their methods to sedimentary basin fill in southeastern Arizona.

Each sample has a unique inheritance history depending on the erosional path followed by the sample and this history will define the spread of the isochron, in addition to preserving a range of paleo-erosion rates at the time of deposition. Since all samples for a given stratum are from the same layer, they must have experienced the same burial duration. The decay of radionuclides determines how far the slope of the isochron has decreased from the original production ratio of the two measured isotopes (Figure 4). Post-burial TCN production is likely for strata in a sedimentary basin. The magnitude of this TCN production is determined from the intercept of the isochron with the axis of the fastest produced nuclide and must be taken into account, or the burial date will be significantly underestimated. Balco and Rovey (2008) assume that TCN production during erosion is by spallation only, and upland erosion is rapid enough that radioactive decay can be ignored:

$$N_{10} = \frac{P_{10}\Lambda}{\rho\varepsilon} e^{-\lambda_{10} t_b} + N_{10,pb}\,, \qquad (7)$$

$$N_{26} = \frac{P_{26}\Lambda}{\rho\varepsilon} e^{-\lambda_{10} t_b} + N_{26,pb} \qquad (8).$$

For the sake of clarity, the second term in the RHS of Equations 5 and 6 is replaced by $N_{10,pb}$ and $N_{26,pb}$, respectively, accounting for post-burial production. Solving Equation 7 for $\frac{\Lambda}{\rho\varepsilon}$ and substituting into Equation 8 yields:

$$N_{26} = \frac{P_{26}}{P_{10}} e^{-(\lambda_{26}-\lambda_{10})t_b} N_{10} - \frac{P_{26}}{P_{10}} e^{-(\lambda_{26}-\lambda_{10})t_b} N_{10,pb} + N_{26,pb} \qquad (9).$$

Equation 9 is a linear relationship that can be fit to measured TCN abundances. We use Equation 9 to date suites of cobbles from basin fill strata or Gila River fill terraces. By dating strata at different elevations within one stratigraphic sequence, we can approximate a sediment deposition rate between our dates (change in elevation divided by change in age), and compare sedimentation rates with paleo-erosion rates. These sedimentation rates are independent of the calculated burial ages of the different layers and can be used to check our estimates of post-burial TCN production.

3.1 Isochron Burial Dates

Determining a burial date for sediment using an isochron approach is an iterative process (Balco and Rovey, 2008; Darling et al., 2012). We base our approach primarily on the methods used by Darling et al. (2012) to date fluvial fill terraces along the Colorado River and its tributaries. Our modeling approach is (adapting Balco and Rovey, 2008):

1) Fit a regression line to data in ^{10}Be-^{26}Al space. The slope of this line determines an initial estimate for the duration of sediment burial (York, 1966).

2) Use the intercept of the regression line with the axis of the TCN with the highest production rate to obtain a first estimate of post-burial TCN production

3) Using the estimates for burial age and post-depositional production, correct measured concentrations back to their values at the time of burial.

4) Determine initial $^{26}Al/^{10}Be$ ratios for samples and linearize them to a production ratio of 6.75 if necessary (corrects $^{26}Al/^{10}Be$ ratios due to very slow paleo-erosion rates).

5) Recalculate a burial date by fitting a new isochron to the corrected TCN concentrations.

6) Repeat steps 1-4 until the burial date converges on a solution.

3.2 Sample Collection and Preparation

We collected samples for detrital TCN analysis from drainage basins ranging from 2-37 km^2, with the smallest basins nested within both Ash Creek and Grant Creek. The goal of the nested samples is to isolate the erosion rate signal of the low-relief surface in the basins' headwaters. We then sieved samples of river sand to extract the 250-1000 μm fraction. For Frye Mesa and Gila River terrace burial dates (Figures 8 and 9) , sample collection depended on what approach to burial dating we planned to use. For samples where post-burial production was inferred to be minimal, we used a conventional approach to burial dating (AZ49 and AZ50sand). If post-burial production seemed significant, we used an isochron approach to burial dating (AZ29, AZ32, AZ51, and AZ52). We used roadcuts on Frye Mesa to minimize recent re-exposure of sediment to TCN production. For the Gila River terraces, we sampled within a quarry and a recently excavated gully to minimize recent re-exposure of the sediments. For the two highest elevation samples on Frye Mesa, observations in the field suggested that post-burial production was likely low, so we sampled sand which was then

sieved to the 250-1000 μm target fraction. We quantified the rest of the burial dates using the isochron approach, so we sampled 3-5 cobbles per site which we then crushed and sieved to 250-1000 μm. For the boulders atop Frye Mesa we collected several 100 g of quartz-rich material from the upper centimeter of each boulder using a hammer and chisel. We then crushed and sieved these samples to our target grain size and analyzed them for surface exposure ages.

We isolated quartz using standard methods (Kohl and Nishiizumi, 1992) via cleaning in aqua regia and subsequent etching in HF and HNO_3. We extracted ^{10}Be and ^{26}Al through column chromatography (Ditchburn and Whitehead, 1994), and measured nuclide ratios by accelerator mass spectrometry (AMS) at the Purdue Rare Isotope Measurement (PRIME) Laboratory at Purdue University. Samples analyzed for ^{10}Be analysis were spiked with either a commercial 1000 ppm Be carrier or a carrier produced at Arizona State University (ASU) containing lower levels of background ^{10}Be. We measured native Al concentrations for each sample using a Thermo iCAP6300 ICP-OES at Arizona State University's Goldwater Environmental Laboratory. Table 5.1 reports our analytical results.

4.0 Results and Discussion

4.1 Upland Erosion Rates from the Pliocene to the Present

4.1.1 Quaternary Upland Erosion Rates vs. Modern Topography

Despite their rugged appearance, the Pinaleño Mountains are not eroding as quickly as high-relief ranges in active tectonic settings (e.g., DiBiase et al., 2010). Erosion rates in the Pinaleño Mountains range from 23 ± 2 m/Myr to 59 ± 5 m/Myr. The lowest rates are from the small

catchments draining the low-relief topography of Ash Creek's headwaters. No strong correlation exists between catchment-averaged erosion rate and mean basin slope, local relief, or catchment-mean k_{sn} (Figure 2). A similar range of mean basin slopes and k_{sn} in the San Gabriel Mountains of California are characteristic of erosion rates that span three orders of magnitude with catchment averaged erosion rates ranging from 10s to 100s to 1000s of m/Myr (DiBiase et al., 2010). In the San Gabriel Mountains this range of erosion rates and the associated range of topographic metrics that characterize the landscape are a function of an uplift gradient across the range. The lowest erosion rates in the San Gabriel Mountains are contained within a low-relief portion of the range that may preserve a relict patch of the landscape that is unadjusted to faster erosion rates that exist below the bounding knickzones. Our nested samples within the headwaters of Ash Creek and Grant Creek allow for a first-order investigation regarding whether the low-relief surface above 2700 m is a similar relict landscape preserved in the Pinaleño Mountains. In Ash Creek, our samples that capture sediment shed only from the low-relief portions of the catchment are two-fold slower than the erosion rates from the outlet sample which also captures the lower-elevation, steeper portions of Ash Creek. This gradient in erosion rates lend some support to a pulse of transient erosion that steepened channels and hillslopes (and accelerated erosion) below 2700 m, but has not affected the highest elevations of the range. In contrast, there is no significant difference between erosion rates in the low-relief portions of Grant Creek versus the steeper lower sections of the catchment. The relationship between mean basin slope/local relief and erosion rate in Grant Creek offers some support to the model of Pelletier et al., (2013), which suggests that the transition to gentler, soil-mantled slopes at high elevations in the Pinaleño Mountains is a non-linear function related to temperature and precipitation gradients with increasing elevation. To fully untangle this problem of

what produced the contrasting morphologies above and below ~2700 m - a high-resolution quantification of soil production rates must be undertaken within both the low-relief and high-relief portions of the Pinaleño Mountains (e.g., Heimsath et al., 2012; Larsen et al., 2014), which is beyond the scope of this study. Transient steepening in the uplands in response to base level fall on the Gila River does not appear to be important for the morphology of the range's bedrock core since channels draining to the unintegrated Sulphur Springs Basin also display transient long profiles and catchment averaged erosion rates are comparably slow on both the north and south sides of the Pinaleño Mountains.

These modern, millennial scale erosion rates are averaged over the time period required to erode 1-2 m of material (Bierman and Steig, 1996). The slowest erosion rates are averaging over a time period of 43,000-87,000 years and the fastest rates are averaging over 17,000-34,000 years (this range is calculated by dividing the thickness of material eroded by a given erosion rate, and gives an approximation for the averaging time for our TCN-derived catchment averaged rates). This means that erosion rates in the low-relief, upper elevations of the Pinaleño Mountains are averaged across several glacial-interglacial periods, while the majority of drainage basins (those eroding at >30 m/Myr) are in equilibrium with an erosion rate developed largely since the LGM. There is not enough of a contrast between low erosion rates at high elevations and high erosion rates in the rugged lower elevations to invoke ongoing, transient landscape adjustment to rates of subsidence during the Basin and Range Disturbance (8-12 Myr; *sensu stricto* Scarborough and Peirce, 1978) to explain the relief structure of the range. It is possible that since the end of regional extensional tectonics (~3-5 Myr), the climate was not continuously wet enough to efficiently erode away the

topographic signature of tectonics. In essence, the transient landscape response to Basin and Range extension is locked in place due to inefficient erosional processes throughout the Quaternary.

4.1.2 Paleo-Erosion Rates from the Late Pliocene-Early Pleistocene

The basin fill deposits of Frye Mesa provide a unique opportunity to investigate patterns in basin-averaged erosion rate from the Pliocene to the present. TCN abundances in basin fill (once corrected for decay since burial) should reflect upland erosion rates at the time of deposition. Frye Creek is currently eroding at 30 ± 3 m/Myr, and if we assume that the deposits of Frye Mesa are largely derived from Frye Creek basin, then we can compare modern erosion rates to the paleo-erosion rates derived from our burial dating. The oldest sediment that we sampled in Frye Mesa (AZ51; 3.5 ± 0.2 Myr) records paleo-erosion rates of 39, 27, 30, and 20 m/Myr based on ^{10}Be abundances in cobbles. These rates agree with the modern erosion rate of Frye Creek suggesting long-term stability in post-tectonic upland erosion rates. This stability in erosion rates is further supported by the paleo-erosion rates for samples AZ49 and AZ50sand, 48 m/Myr and 43 m/Myr, respectively. These two samples represent the last stage of deposition before widespread dissection of Safford Basin.

However, the paleo-erosion rates recorded by the cobbles of AZ52 (1.7 ± .3 Myr) are an order of magnitude faster than nearly all the other paleo- and modern erosion rates for the coupled Frye Creek/Frye Mesa system; rates range from 98 m/Myr to 244 m/Myr for AZ52. Since all of the rates inferred from AZ52 are significantly faster than both modern rates, and rates inferred from other conventional and isochron burial dates, there must have been some change in the forcing of upland erosion rates between ~3.5 – 2 Myr. High magnitude subsidence is inferred to be absent at

this point – in fact, the period between 3.5 – 2 Myr appears to have been a time of net sediment transport from the range front rather than deposition (Figure 8) – so faster upland erosion could be linked to a wetter climate and an associated higher erosional efficiency (Bonnet and Crave, 2003). Indeed, Smith (1994) reports a wetter, less seasonal climate with higher total precipitation for southeastern Arizona from 3.5 – 2 Myr, so enhanced erosion related to a different precipitation regime is a possible explanation for the paleo-erosion rates recorded by AZ52. As mentioned above, erosion rates had returned to about ~50 m/Myr by the time AZ49 and AZ50sand were deposited in the upper strata of Frye Mesa (numerical ages indistinguishable from AZ52 within uncertainty), so this acceleration in upland erosion must have been short-lived.

Paleo-erosion rates from the Pinaleño Mountains are in agreement with other records of upland erosion rates from the Pliocene and Pleistocene across the region. In Aravaipa Creek basin to the southwest, two burial dates of 3 Myr late stage basin fill also yielded a paleo-erosion rate of ~50 m/Myr (Jungers and Heimsath, *in prep*). In the lower San Pedro basin, just east of the Santa Catalina Mountains, a ^{10}Be concentration depth profile into a Mid-Pleistocene piedmont yielded an inheritance, and thus a paleo-erosion rate, of 30 m/Myr for an upland catchment draining the Santa Catalina range (Jungers and Heimsath, *in prep*). It appears that regional post-tectonic erosion rates are uniformly slow throughout southeastern Arizona's Basin and Range province.

4.2 Timing of Late Stage Basin Fill Deposition (Frye Mesa)

Our sampling along the road leading to Frye Mesa's surface fortuitously captured a large (~30 m) cut and fill event during the deposition of late stage basin fill. A burial isochron for sample AZ52 at 1140 m yields a burial date of 1.7 ± 0.3 Myr, while a burial isochron for AZ51, initially

believed to be 30 m upsection, yields a burial date of 3.3 ± 0.2 Myr, requiring some discontinuity in the stratigraphy of Frye Mesa between the two sample sites. We interpret this discontinuity as an incision event post-3.5 Myr, and subsequent resumed deposition sometime before approximately 2 Myr (Figure 8). The two uppermost samples in Frye Mesa yield conventional burial dates of 2.0 ± 0.2 and 1.8 ± 0.2 Myr at 1275 m and 1295 m, respectively, suggesting very rapid deposition of the last 100 m of basin fill at Frye Mesa before widespread basin incision post-2 Myr.

Paleoclimate proxies for the Late Pliocene and Early Pleistocene are scarce in southeastern Arizona, but paleo-precipitation may be inferred from paleosol carbonates in the St. David Formation of the Upper San Pedro Basin (Smith, 1994). Smith infers an onset of higher total annual precipitation delivered evenly throughout the year beginning at approximately 3.5 Myr and transitioning to a monsoonal climate by 2 Myr. It is possible that increased regional precipitation drove the incision event at 3.5 Myr, and deposition was occurring farther down system until renewed deposition near the range front at ~ 2 Myr. Incision related to higher total precipitation would require significant increase in stream power and a long term shift from deposition to erosion and sediment transport near the range front between 3.5-2 Myr. An alternative explanation for a hiatus in late stage basin fill deposition near Frye Mesa from 3.5-2 Myr is the arrival of an axial Gila River during this time period (see next section for Gila River terrace chronology). An axial Gila River post-3 Myr could have eroded laterally into range front piedmonts and temporarily enhance transport of sediment down the fluvial system, rather than deposition and storage near the outlets of drainage basins along the range front. This explanation for the incision event between AZ51 and AZ52 requires no change in climate forcing, but rather an abrupt change in the axial boundary condition for Safford basin after the first arrival of the Gila River.

4.3 Arrival of the Gila River in Safford Basin and Quaternary Incision Rates

Two isochron burial dates and a Lava Creek B ash constrain the arrival of the ancestral Gila River in the Safford basin and its subsequent incision. A burial isochron for the highest elevation (1020 m) Gila terrace yields a date of 2.8 ± 0.1 Myr requiring the arrival of the Gila River pre-2.8 Myr and axial incision post-2.8 Myr. A burial isochron for the Gila River terrace upon which the Safford Municipal Airport is constructed yields a burial date of 1.5 ± 0.1 Myr, requiring that basin incision was well underway by that time.

Our burial dates of Frye Mesa sediment and Gila River gravels, in conjunction with an existing Lava Creek B ash in the lowest elevation Gila River terrace (Houser and Pearthree, 2002) allow the quantification of Pleistocene incision rates for Safford Basin. At Frye Mesa, the last stage of deposition ceased at approximately 2 Myr, and we infer that incision began soon after. The current difference between Frye Mesa's surface and modern Frye Creek is approximately 100 m, requiring an average incision rate of 50 m/Myr. Across Safford basin, at the Gila River terraces, the Gila River had incised from 1020 m to ~970 m between 2.8 and 1.3 Myr (AZ 29 to AZ32) an incision rate of 30 m/Myr and to the lowest elevation terrace at 930 m by 640 kyr, an incision rate of 61 m/Myr. Finally, the lowest elevation Gila terrace is ~30 m above the modern Gila River, suggesting an incision rate of ~50 m/Myr from the mid-Pleistocene to the present. It is compelling that these incision rates are similar to catchment-averaged erosion rates on the north side of the Pinaleño Mountains. In particular, those erosion rates could be averaging landscape response to Late Pleistocene incision on the Gila River. This interpretation is, however, complicated by similar

erosion rates in Grant Creek and Post Creek on the south side of the Pinaleño Mountains which drains to the steady base level of Sulphur Springs basin. Apparently, modern, millennial scale erosion rates of the Pinaleño Mountains are more a function of a regional forcing such as Late Pleistocene climate rather than changes in base level.

5.0 Conclusions

The Pinaleño Mountains are not currently eroding as quickly as might be predicted by the relationships between mean basin slope, local relief, or normalized channel steepness defined in other, tectonically active settings (e.g., Ouimet et al., 2009; DiBiase et al., 2010). In fact, erosion rates are on par with other decaying orogens such as the Applalachian Mountains of eastern North America (Matmon et al., 2003). Two potential explanations for this problem of a slowly eroding landscape that is still quite rugged. The first follows the reasoning of Pelletier et al. (2013), where the nonlinear transition from a steep, high-relief landscape at lower elevations to a gentler, lower-relief, soil-mantled setting above ~2700 m is purely a function of the local temperature and precipitation gradient driven by the elevation difference between Safford basin and the summit of the Pinaleño Mountains. This argument suggests that the Pinaleño Mountains may be well characterized by a uniform erosion rate, but the efficiency of that erosion is a function of vegetation biomass which is in turn a function of available energy. In this context, the transition to lower slopes and relief at high elevations is a function of more efficiently diffusive processes related to denser vegetation under cooler and wetter conditions. Our results do not strongly support or refute the argument of Pelletier et al. (2013). Erosion rates for the Pinaleño Mountains are indeed relatively uniform and low, however, our nested samples do suggest a potential two-fold difference between erosion rates

between the low and high relief portions of the range. Our nested samples are a good first step toward characterizing differences between erosion rates in these two process domains of the Pinaleño Mountains, but because the low-relief areas of the range only account for a proportionately small area of most drainage basins, catchment averaged erosion rates are not the best tool for resolving differences in erosion rates between the low-relief and high-relief portions of the Pinaleño Mountains. A second possible explanation for the disconnect between topography and measured erosion rates, is that the topography is a relict of old forcing, and that the modern erosion rates are equilibrated to the current, semi-arid climate. In this scenario, rapid subsidence centered at ~8 Myr forced a transient steepening in the drainage basins of the Pinaleño and other, similar, Mountain ranges in the southwest, and that this adjustment stalled at approximately 2700 m. As tectonics waned, the climate from ~5 Myr to the present never drove erosional processes to be high enough to overprint the tectonic signature imprinted on the range. Paleo-erosion rates from burial dates of late-stage sedimentary basin fill record maximum erosion rates of 100-250 m/Myr prior to the final stages of basin filling, but paleo-erosion rates from the latest stage fill of Frye Mesa suggest that upland erosion rates were already transitioning to 40-50 m/Myr within the last several hundred thousand years of basin fill deposition. Since the Gila River integrated with the San Pedro River downstream from Safford Basin sometime after 2 Myr, regional incision rates have been relatively steady at 40-60 m/Myr. This incision on the Gila River may play a partial role of driving upland erosion rates on the north side of the Pinaleño Mountains from the Pliocene to the present, but similar erosion rates into the internally drained Sulphur Springs basin on the south side of the range require a more regional forcing for erosion such as the modern, relatively inefficient semi-arid climate.

References

Allen, B.D., 2005. Ice age lakes in New Mexico. In: Lucas, S.G., Morgan, G.S., Zeigler, K.E. (Eds.), New Mexico's Ice Ages. New Mexico Museum of Natural History and Science Bulletin No. 28, pp. 107–114.

Anderson, L.W., (1990). Terraces and pediments of San Carlos River Valley, in Gehrels, G.E., and Spencer, J.E., eds., *Geologic excursions through the Sonoran Desert Region, Arizona and Sonora: Arizona Geological Survey Special Paper* 7, p. 24.

Anderson, R. S., Repka, J. L., & Dick, G. S. (1996). Explicit treatment of inheritance in dating depositional surfaces using in situ Be-10 and Al-26.*Geology, 24*(1), 47-51.

Balco, G., & Rovey, C. W. (2008). An Isochron Method For Cosmogenic-Nuclide Dating Of Buried Soils And Sediments. *American Journal of Science, 308*(10), 1083-1114.

Balco, G., Stone, J. O., Lifton, N. A., & Dunai, T. J. (2008). A complete and easily accessible means of calculating surface exposure ages or erosion rates from< sup> 10</sup> Be and< sup> 26</sup> Al measurements.*Quaternary Geochronology, 3*(3), 174-195.

Balco, G., & Stone, J. O. H. (2005). Measuring middle Pleistocene erosion rates with cosmic-ray-produced nuclides in buried alluvial sediment, Fisher Valley, southeastern Utah. *Earth Surface Processes and Landforms, 30*(8), 1051-1067.

Bierman, P., & Steig, E. J. (1996). Estimating rates of denudation using cosmogenic isotope abundances in sediment. *Earth Surface Processes and Landforms, 21*(2), 125-139.

Bonnet, S., & Crave, A. (2003). Landscape response to climate change: Insights from experimental modeling and implications for tectonic versus climatic uplift of topography. *Geology, 31*(2), 123-126.

Brown, E. T., Stallard, R. F., Larsen, M. C., Raisbeck, G. M., & Yiou, F. (1995). Denudation Rates Determined From The Accumulation Of In Situ-Produced Be-10 In The Luquillo Experimental Forest, Puerto-Rico. *Earth and Planetary Science Letters, 129*(1-4), 193-202.

Darling, A. L., Karlstrom, K. E., Granger, D. E., Aslan, A., Kirby, E., Ouimet, W. B., et al. (2012). New incision rates along the Colorado River system based on cosmogenic burial dating of terraces: Implications for regional controls on Quaternary incision. *Geosphere, 8*(5), 1020-1041.

DiBiase, R. A., Whipple, K. X., Heimsath, A. M., & Ouimet, W. B. (2010). Landscape form and millennial erosion rates in the San Gabriel Mountains, CA. *Earth and Planetary Science Letters, 289*(1), 134-144.

Dickinson, W. (1991). *Tectonic setting of faulted Tertiary strata associated with the Catalina core complex in southern Arizona*: Geological Society of Amer.

Dickinson, W. R. (2004). Evolution of the North American Cordillera. *Annual Review of Earth and Planetary Sciences, 32*, 13-45.

Ditchburn R. G. and Whitehead N. E. (1994) The separation of 10Be from silicates. 3d Workshop of the South Pacific Environmental Radioactivity Association, 4-7.

Galusha, Theodore, Johnson, N.M., Lindsay, E.H., Opdyke, N.D., and Tedford, R.H., 1984, Biostratigraphy and magnetostratigraphy, late Pliocene rocks, 111 Ranch, Arizona: Geological Society of America Bulletin, v. 95, p. 714-722.

Gilbert, G. (1875). Report on the geology of portions of Nevada, California, and Arizona, examined in the years 1871 and 1872, Geogr. and Geol. Expl. and Surv. west of the 100th meridian. *Vol. III*.

Gootee, B.F. (2012). Geologic Evaluation of the Safford Basin for Carbon Dioxide Sequestration Potential, *AZGS OFR-12-01*.

Gosse, J. C., & Phillips, F. M. (2001). Terrestrial in situ cosmogenic nuclides: theory and application. *Quaternary Science Reviews, 20*(14), 1475-1560.

Granger, D. E., Kirchner, J. W., & Finkel, R. (1996). Spatially averaged long-term erosion rates measured from in situ-produced cosmogenic nuclides in alluvial sediment. *Journal of Geology, 104*(3), 249-257.

Granger, D. E., Kirchner, J. W., & Finkel, R. C. (1997). Quaternary downcutting rate of the New River, Virginia, measured from differential decay of cosmogenic 26Al and 10Be in cave-deposited alluvium. *Geology, 25*(2), 107-110.

Granger, D. E., & Muzikar, P. F. (2001). Dating sediment burial with in situ-produced cosmogenic nuclides: theory, techniques, and limitations. *Earth and Planetary Science Letters, 188*(1-2), 269-281.

Halvorsen, W.L., Thomas, K., Graham, L., 2001. Arizona Gap Project Final Report. USGS Sonoran Desert Field Station. University of Arizona, Tucson.

Heimsath, A. M., DiBiase, R. A., & Whipple, K. X. (2012). Soil production limits and the transition to bedrock-dominated landscapes. *Nature Geoscience, 5*(3), 210-214.

Heindl, L. (1958). *Cenozoic alluvial deposits of the Upper Gila River area, New Mexico and Arizona: Tucson, University of Arizona.* doctoral dissertation, 249 p.

Heindl, L. A., 1962, Should the term, "Gila Conglomerate" be abandoned?: Arizona Geological Society Digest, v. 5, p. 73-88.

Heisinger, B., Lal, D., Jull, A., Kubik, P., Ivy-Ochs, S., Knie, K., et al. (2002). Production of selected cosmogenic radionuclides by muons: 2. Capture of negative muons. *Earth and Planetary Science Letters, 200*(3), 357-369.

Heisinger, B., Lal, D., Jull, A., Kubik, P., Ivy-Ochs, S., Neumaier, S., et al. (2002). Production of selected cosmogenic radionuclides by muons: 1. Fast muons. *Earth and Planetary Science Letters, 200*(3), 345-355.

Holmgren, C. A., Betancourt, J. L., & Rylander, K. A. (2006). A 36,000-yr vegetation history from the Peloncillo Mountains, southeastern Arizona, USA.*Palaeogeography, Palaeoclimatology, Palaeoecology, 240*(3), 405-422.

Houser, B.B., Richter, D.H., and Shafiqullah, M., 1985, Geologic map of the Safford quadrangle, Graham County, Arizona: U.S. Geological Survey Miscellaneous Investigation Map I-1617, Scale 1:48,000.

Houser, B.B., Pearthree, P.A., Homburg, J.A., Thrasher, L.C., eds., 2002, Friends of the Pleistocene, Rocky Mountain Cell 46th field conference, and Arizona Geological Society Fall Field Trip, 83 p.

Kohl, C., & Nishiizumi, K. (1992). Chemical isolation of quartz for measurement of *in situ*-produced cosmogenic nuclides. *Geochimica et Cosmochimica Acta, 56*(9), 3583-3587.

Kruger, J.M., 1991, Seismic crustal structure beneath the Safford basin and Pinaleño Mountains: Implications for Cenozoic extension and metamorphic core complex uplift in SE Arizona: University of Arizona, Dept. of Geosciences, Ph.D. dissertation, 158 p.

Lal, D. (1991). Cosmic-Ray Labeling Of Erosion Surfaces - Insitu Nuclide Production-Rates And Erosion Models. *Earth and Planetary Science Letters, 104*(2-4), 424-439.

Larsen, I. J., Almond, P. C., Eger, A., Stone, J. O., Montgomery, D. R., & Malcolm, B. (2014). Rapid Soil Production and Weathering in the Southern Alps, New Zealand. *Science, 343*(6171), 637-640.

Martin, P. S. (1963). Geoghronology of Pluvial Lake Cochise, Southern Arizona. II. Pollen Analysis of A 42-Meter Core. *Ecology*, 436-444.

Matmon, A., Bierman, P. R., Larsen, J., Southworth, S., Pavich, M., & Caffee, M. (2003). Temporally and spatially uniform rates of erosion in the southern Appalachian Great Smoky Mountains. *Geology*, *31*(2), 155-158.

Melton, M. (1965). The geomorphic and paleoclimatic significance of alluvial deposits in southern Arizona. *The Journal of Geology, 73*(1), 1-38.

Menges, C., & McFadden, L. (1981). Evidence for a latest Miocene to Pliocene transition from Basin-Range tectonic to post-tectonic landscape evolution in southeastern Arizona. *Arizona Geological Society Digest, 13*, 151-160.

Menges, C., & Pearthree, P. (1989). Late Cenozoic tectonism in Arizona and its impact on regional landscape evolution. *Geologic evolution of Arizona: Arizona Geological Society Digest, 17*, 649–680.

Menking, K. M., Anderson, R. Y., Shafike, N. G., Syed, K. H., & Allen, B. D. (2004). Wetter or colder during the Last Glacial Maximum? Revisiting the pluvial lake question in southwestern North America. *Quaternary Research, 62*(3), 280-288.

Mitchell, S. G., & Ober, K. A. (2013). Evolution of< i> Scaphinotus petersi</i>(Coleoptera: Carabidae) and the role of climate and geography in the Madrean sky islands of southeastern Arizona, USA. *Quaternary Research, 79*(2), 274-283.

Morrison, R. (1985). Pliocene/Quaternary geology, geomorphology, and tectonics of Arizona. *Soils and Quaternary geology of the southwestern United States: Geological Society of America Special Paper, 203*, 123-146.

Ouimet, W.B., Whipple, K.X., Granger, D.E., 2009. Beyond threshold hillslopes: channel adjustment to base-level fall in tectonically active mountain ranges. Geology 37, 579–582

Pearthree, P.A., 1986, Late Quaternary faulting and seismic hazard in southeastern Arizona and adjacent portions of New Mexico and Sonora, Mexico: Arizona Bureau of Geology and Mineral Technology Open-File Report 86-8, 22 p.

Pelletier, J. D., Barron-Gafford, G. A., Breshears, D. D., Brooks, P. D., Chorover, J., Durcik, M., et al. (2013). Coevolution of nonlinear trends in vegetation, soils, and topography with elevation and slope aspect: A case study in the sky islands of southern Arizona. *Journal of Geophysical Research: Earth Surface, 118*(2), 741-758.

Pigati, J. S., Bright, J. E., Shanahan, T. M., & Mahan, S. A. (2009). Late Pleistocene paleohydrology near the boundary of the Sonoran and Chihuahuan Deserts, southeastern Arizona, USA. *Quaternary Science Reviews, 28*(3), 286-300.

Portenga, E. W., & Bierman, P. R. (2011). Understanding Earth's eroding surface with 10 Be. *GSA Today, 21*(8), 4-10.

Richter, D.H., Houser, B.B., and Damon, P.E., 1983, Geologic map of the Guthrie quadrangle, Graham and Greenlee Counties, Arizona: U.S. Geological Survey Miscellaneous Investigations Series Map I-1455, scale 1:48,000.

Scarborough, R. B., & Peirce, H. W. (1978, November). Late Cenozoic basins of Arizona. In *Land of Cochise, Southeastern Arizona, New Mexico Geological Society Twenty-Ninth Field Conference Guidebook, ed. JF Callender, JC Wilt, and RE Clemons* (pp. 253-259).

Smith, G. A. (1994). Climatic Influences On Continental Deposition During Late-Stage Filling Of An Extensional Basin, Southeastern Arizona. *Geological Society Of America Bulletin, 106*(9), 1212-1228.

Smith, G. A., Wang, Y., Cerling, T. E., & Geissman, J. W. (1993). Comparison Of A Paleosol-Carbonate Isotope Record To Other Records Of Pliocene-Early Pleistocene Climate In The Western United-States. *Geology, 21*(8), 691-694.

Thorman, C.H., 1981, Geology of the Pinaleño Mountains, Arizona—a preliminary report, *in* Stone, Claudia and Jenney, J.P., eds.: Arizona Geological Society Digest, V. 13, p. 5-11.
Tuan, Y. (1962). Structure, climate, and basin land forms in Arizona and New Mexico. *Annals of the Association of American Geographers, 52*(1), 51-68.

Van Devender, T.R., 1990. Late Quaternary vegetation and climate of the Chihuahuan Desert, United States and Mexico. In: Betancourt, J.L., Van Devender, T.R., Martin, P.S. (Eds.), Packrat Middens: the Last 40,000 Years of Biotic Change. University of Arizona Press, Tucson, pp. 104–133.

Wagner, J. D. M., Cole, J. E., Beck, J. W., Patchett, P. J., Henderson, G. M., & Barnett, H. R. (2010). Moisture variability in the southwestern United States linked to abrupt glacial climate change. *Nature Geoscience, 3*(2), 110-113.

Warshall, P. (1995). The Madrean sky island archipelago: a planetary overview. *Biodiversity and management of the Madrean Archipelago: the sky islands of southwestern United States and northwestern Mexico*, 6-18.

Waters, M. R. (1989). Late Quaternary lacustrine history and paleoclimatic significance of pluvial Lake Cochise, southeastern Arizona. *Quaternary Research, 32*(1), 1-11.

Wobus, C., Whipple, K.X., Kirby, E., Snyder, N., Johnson, J., Spyropolou, K., Crosby, B., Sheehan, D., 2006. Tectonics from topography: procedures, promise, and pitfalls. Geol. Soc. Am. Spec. Pap. 398, 55–74.

Wynn, J.C., 1981, Complete Bouguer gravity anomaly map of the Silver City 1ox2o quadrangle, New Mexico-Arizona: Miscellaneous Investigations Series Map I-1310-A, scale 1:250,000.

York, D. (1966). Least-squares fitting of a straight line. *Canadian Journal of Physics, 44*(5), 1079-1086.

Youberg, A., M.L. Cline, J.P. Cook, P.A. Pearthree, and R.H Webb, (2008). Geologic mapping of the debris flow deposits in the Santa Catalina Mountains, Pima County, Arizona. *AZGS Report OFR-08-06*.

Zhu, C., Waddell, R. K., Star, I., & Ostrander, M. (1998). Responses of ground water in the Black Mesa basin, northeastern Arizona, to paleoclimatic changes during the late Pleistocene and Holocene. *Geology*, *26*(2), 127-130.

Table

Table 5.1 Sample locations and TCN abundances

Sample ID	Latitude	Longitude	Elevation	[^{10}Be]	±	[^{26}Al]	±
			m	atoms/g_{qtz}		atoms/g_{qtz}	
AZ35	32.69940	-109.78759	2204	2.51E+05	7.64E+03	n/a	n/a
AZ37	32.72307	-109.90204	2599	6.56E+05	1.87E+04	n/a	n/a
AZ38	32.71482	-109.90458	2693	8.61E+05	1.57E+04	n/a	n/a
AZ39	32.68398	-109.76542	2204	2.69E+05	6.25E+03	n/a	n/a
AZ40	32.79155	-109.85514	2297	3.09E+05	6.28E+03	n/a	n/a
AZ41	32.78917	-109.99151	1843	3.72E+05	6.99E+03	n/a	n/a
AZ43	32.83993	-110.05198	1843	3.89E+05	1.70E+04	n/a	n/a
AZ44	32.74870	-109.83780	1657	1.53E+06	3.06E+04	n/a	n/a
AZ46	32.74870	-109.83780	1657	9.30E+05	1.86E+04	n/a	n/a
AZ47	32.74870	-109.83780	1657	1.34E+06	2.98E+04	n/a	n/a
AZ53	32.67220	-109.91560	2515	5.70E+05	1.38E+04	n/a	n/a
AZ54	32.66898	-109.91380	2515	5.80E+05	8.65E+03	n/a	n/a
AZ55	32.64935	-109.92539	2515	6.74E+05	1.13E+04	n/a	n/a
AZ29A	32.87442	-109.61732	1006	3.59E+05	6.77E+03	9.93E+05	1.47E+05
AZ29B	32.87442	-109.61732	1006	1.75E+05	3.50E+03	7.25E+05	1.85E+05
AZ29C	32.87442	-109.61732	1006	1.56E+05	3.11E+03	6.70E+05	7.81E+04
AZ32C	32.84193	-109.63189	946	1.46E+05	2.91E+03	7.13E+05	7.17E+04
AZ32E	32.84193	-109.63189	946	8.82E+05	1.76E+04	3.13E+06	2.44E+05
AZ32F	32.84193	-109.63189	946	3.02E+05	6.04E+03	1.11E+06	1.65E+05
AZ49	32.77400	-109.82906	1295	1.00E+05	2.00E+03	2.80E+05	6.95E+04
AZ50sand	32.77382	-109.83117	1275	1.00E+05	2.01E+03	2.40E+05	3.30E+04
AZ51A	32.77933	-109.83090	1179	6.65E+04	1.33E+03	1.79E+05	2.86E+04
AZ51B	32.77933	-109.83090	1179	9.03E+04	1.81E+03	2.24E+05	9.44E+04
AZ51C	32.77933	-109.83090	1179	8.15E+04	1.63E+03	1.91E+05	5.29E+04
AZ51D	32.77933	-109.83090	1179	1.16E+05	2.33E+03	2.41E+05	2.57E+04
AZ52A	32.77833	-109.82896	1150	5.12E+04	1.02E+03	1.64E+05	2.85E+04
AZ52B	32.77833	-109.82896	1150	2.07E+04	4.15E+02	6.86E+04	1.93E+04
AZ52C	32.77833	-109.82896	1150	4.32E+04	8.64E+02	1.07E+05	6.03E+04
AZ52D	32.77833	-109.82896	1150	4.13E+04	8.26E+02	1.35E+05	2.61E+04
AZ52E	32.77833	-109.82896	1150	3.08E+04	6.16E+02	1.21E+05	4.35E+04

Figure Captions

Figure 5.1.Overview of southeastern Arizona's Basin and Range. This region is the southeastern extent of the larger Basin and Range physiographic province of North America. The Gila River flows northwest through the Safford Basin within this region, and both the San Pedro River and Santa Cruz River flow into the Gila River northwest of the Galiuro Mountains.

Figure 5.2. The Pinaleño Mountains and Safford Basin. (A) Drainage basins sampled for detrital TCN analyses are highlighted by arrows as are Frye Mesa and Gila River terraces sampled for TCN burial dates. Catchments on the north side of the Pinaleño Mountains drain to the Gila River which in turn is integrated with the lorado River. The majority of catchments on the south side of the range - including Post Creek and Grant Creek – drain to Willcox Playa within the internally drained Sulphur Springs Basin. Base map is 10 m DEM draped over shaded relief. (B) Steep hillslope angles (red) dominate the range below an elevation of ~2700 while the upper elevations have gentler slopes (green). (C) Local relief calculated in a moving window with 1.5 km radius captures the low relief patch of the Pinaleño Mountains at high elevations. Local relief is highest on the north and south flanks of the range, and there is subtle decrease in local relief at the northwest and southeast tips of the range. (D) Normalized channel steepness index draped on top of a DEM and shaded relief, with drainage basins of interest outlined in black. The highest channel steepness values track well with areas of high local relief.

Figure 5.3. Schematic for the accumulation of terrestrial cosmogenic nuclides (TCN) in alluvial sediment from source to sample. TCN production begins within sediment or bedrock at a depth

equivalent to the attenuation length for TCN production, Λ, divided by the bulk density of the bedrock or sediment, ϱ – inception of TCN production is t_0. The TCN production rate increases exponentially during sediment exhumation until a maximum production rate is achieved at the Earth's surface – i.e., Λ/ ϱ is zero. TCN continues to accumulate as sediment is transported down the hillslope, t_{hs}, through the drainage network, t_{dn}, past the range front, t_{rf}, and across alluvial fans or piedmonts, t_{af}. After sediment is deposited on the piedmont surface, TCN concentration increases along surface exposure curves. If sediment is rapidly buried, TCN production ceases and decay of radio-TCN commences. By measuring the ratio of a radio-TCN like ^{10}Be and a stable TCN like ^{21}Ne we can determine how long sediment has been buried based on a decay trajectory from some original TCN ratio defined by the ratio of TCN production rates and exposure/erosion history at the Earth's surface.

Figure 5.4. Summary of isochron approach to terrestrial cosmogenic nuclide (TCN) burial dating. Samples for a given stratum should ideally be individual quartz-rich cobbles in order to maximize differences in initial nuclide concentrations **(a)**. The slope of a TCN ratio for unburied samples will be equal to the ratio of the production rate for the paired nuclides. When sediment is shielded from TCN production, one or both nuclides begin to decay according to their individual exponential decay constants – at least one TCN must be a radionuclide when determining a burial duration. The ratio of TCN changes as decay continues and production is fully or significantly shielded. As a result, the slope of the isochron decreases, and this new slope allows the calculation of a burial duration **(b)**. If sediment is not fully shielded from TCN production, then some nuclides will accumulate

during burial. This post-burial production will increase the intercept of the isochron with the axis belonging to the nuclide with the higher production rate **(c).**

Figure 5.5. Summary of ^{10}Be-derived catchment averaged erosion rates and basin statistics for the catchments sampled. Clipped slope maps for each basin helps visualize the distribution of slopes within each basin, and what percentage of the low-relief, low-slope upper elevations each basin contains in its headwaters. Note nested samples for Ash Creek and Grant Creek.

Figure 5.6. Summary of relationships between topographic metrics and catchment averaged erosion rates. (A) Mean basin slope, (B) Local relief, and (C) Catchment-mean normalized channel steepness. No strong relationship exists between any of these topographic metrics and catchment averaged erosion rate. Erosion rates between 20-30 m/Myr dominate, and even the fastest rates only reach 59 m/Myr. These rates are much slower than erosion rates in mountain ranges defined by similar steep hillslopes and channels as those of the Pinaleño Mountains.

Figure 5.7. Burial isochron plots for AZ29, AZ32, AZ51, and AZ52. AZ29 and AZ 32 required correction for post-burial production and were linearized before their final fit. AZ51 required correction for post-burial production. AZ52 required no correction for post-burial production.

Figure 5.8. Setting of Frye Mesa. (A) Photograph of Frye Mesa and the north side of the Pinaleño Mountains taken at ground level just several meters above the modern elevation of the Gila River (March 2010). (B) Aerial photograph of Frye Mesa and the Pinaleño Mountains from ~11,300 m en

route between PHX and IAH, June 2014. Note the look angle for (C). (C) Oblique perspective of Frye Mesa from Google Earth showing burial dates and inferred erosion surface that developed after the deposition of AZ51 sediment. Post ~2 Myr rapid deposition of basin fill once again buried AZ51 as recorded by the sediment of AZ52, AZ49, and AZ50sand. Incision of Frye Mesa occurred soon after 2 Myr.

Figure 5.9. Summary of Gila River terraces and sites for numerical dates, northeast margin of Saford basin. The highest and intermediate elevation terraces were dated using an isochron approach to TCN burial dating, while the lowest elevation terrace is constrained by an interbedded Lava Creek B ash (Houser et al., 2002).

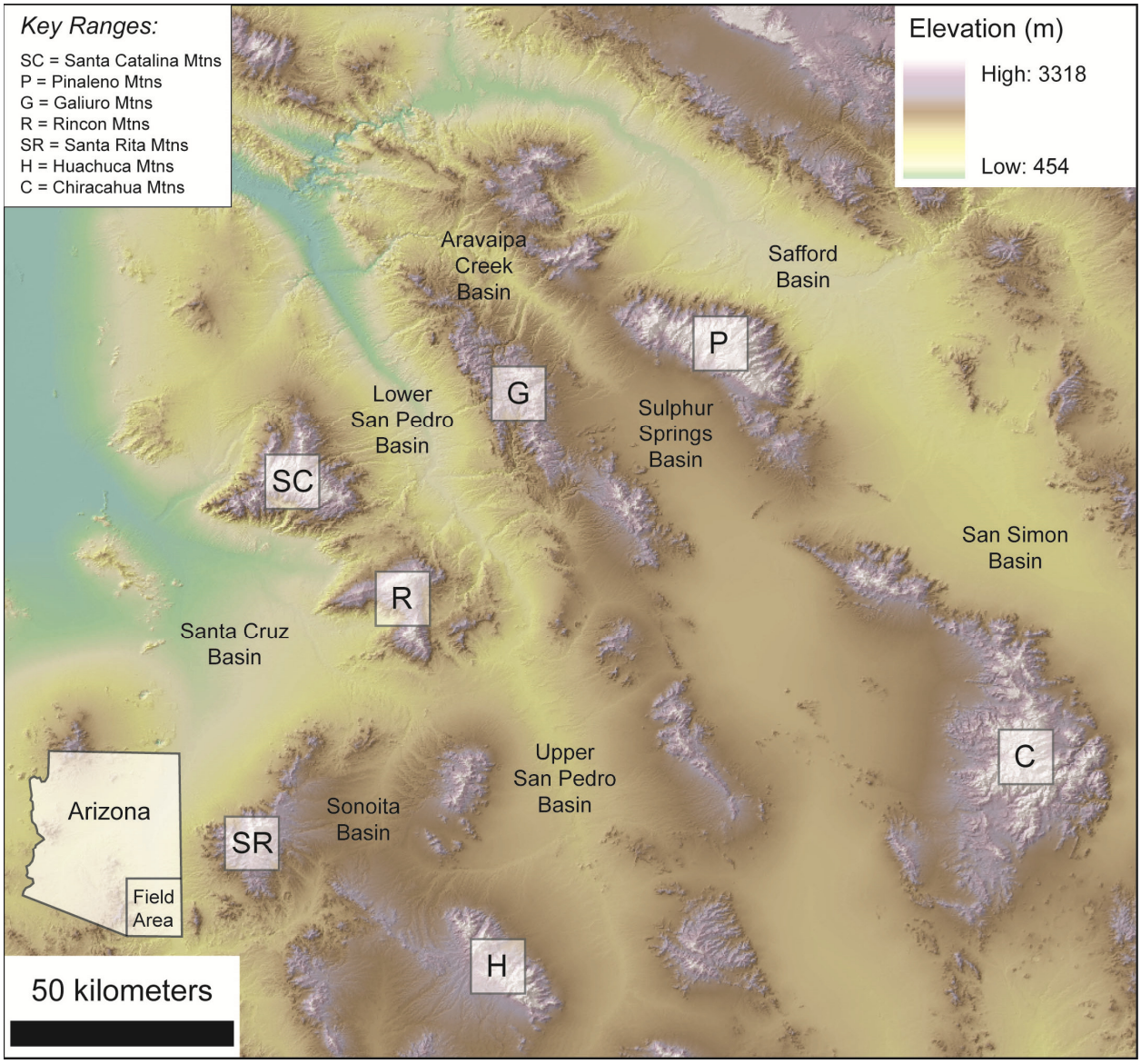
Key Ranges:
SC = Santa Catalina Mtns
P = Pinaleno Mtns
G = Galiuro Mtns
R = Rincon Mtns
SR = Santa Rita Mtns
H = Huachuca Mtns
C = Chiracahua Mtns
Elevation (m)
High: 3318
Low: 454
Aravaipa Creek Basin
Safford Basin
P
G
Lower San Pedro Basin
Sulphur Springs Basin
SC
San Simon Basin
R
Santa Cruz Basin
Upper San Pedro Basin
C
Arizona
Sonoita Basin
SR
Field Area
H
50 kilometers

Figure 5.1.

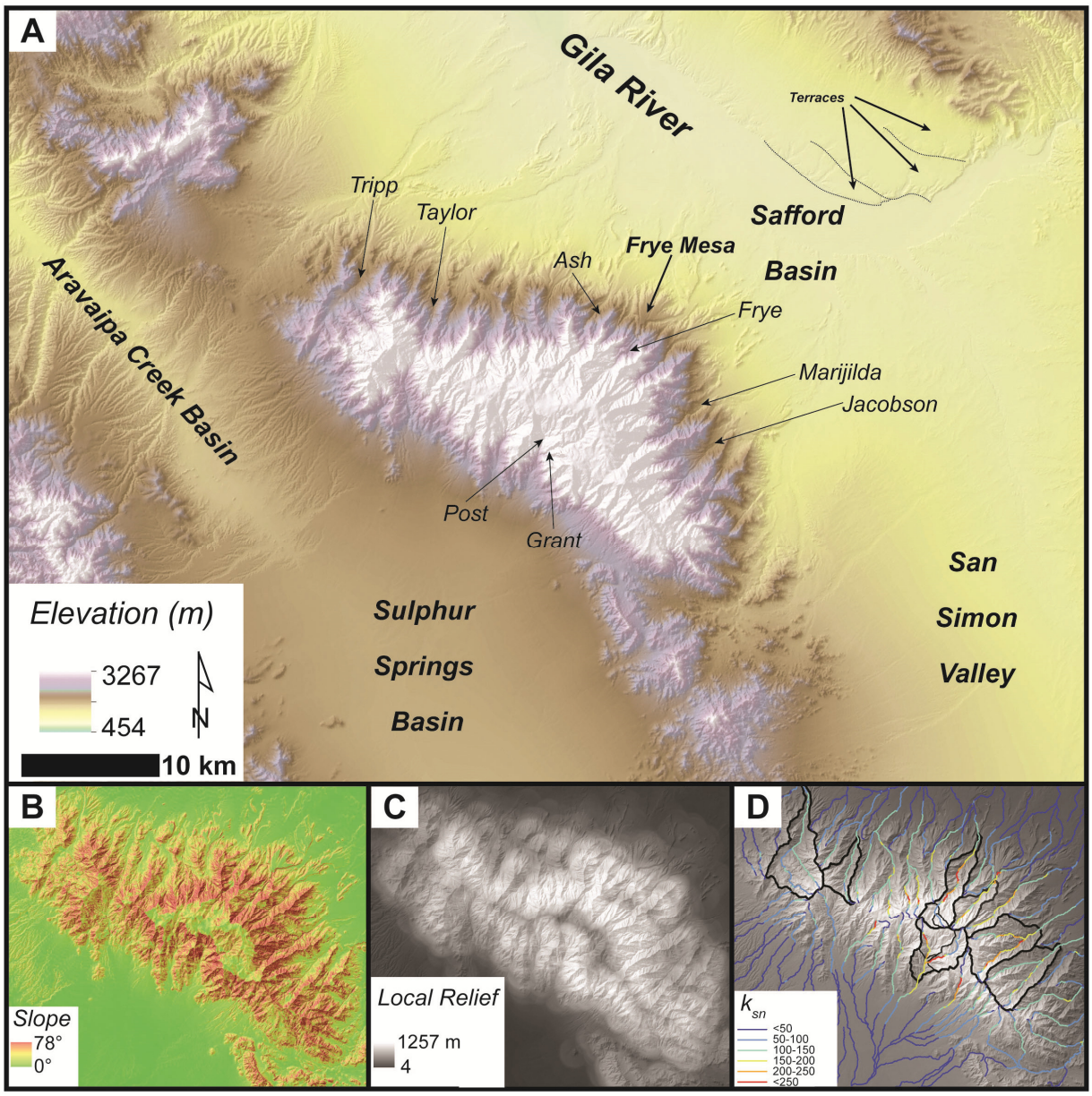
A
Gila River
Terraces
Tripp
Taylor
Safford
Basin
Frye Mesa
Ash
Frye
Aravaipa Creek Basin
Marijilda
Jacobson
Post
Grant
San
Simon
Valley
Sulphur
Springs
Basin
Elevation (m)
3267
454
N
10 km
B
Slope
78°
0°
C
Local Relief
1257 m
4
D
k_{sn}
<50
50-100
100-150
150-200
200-250
<250

Figure 5.2.

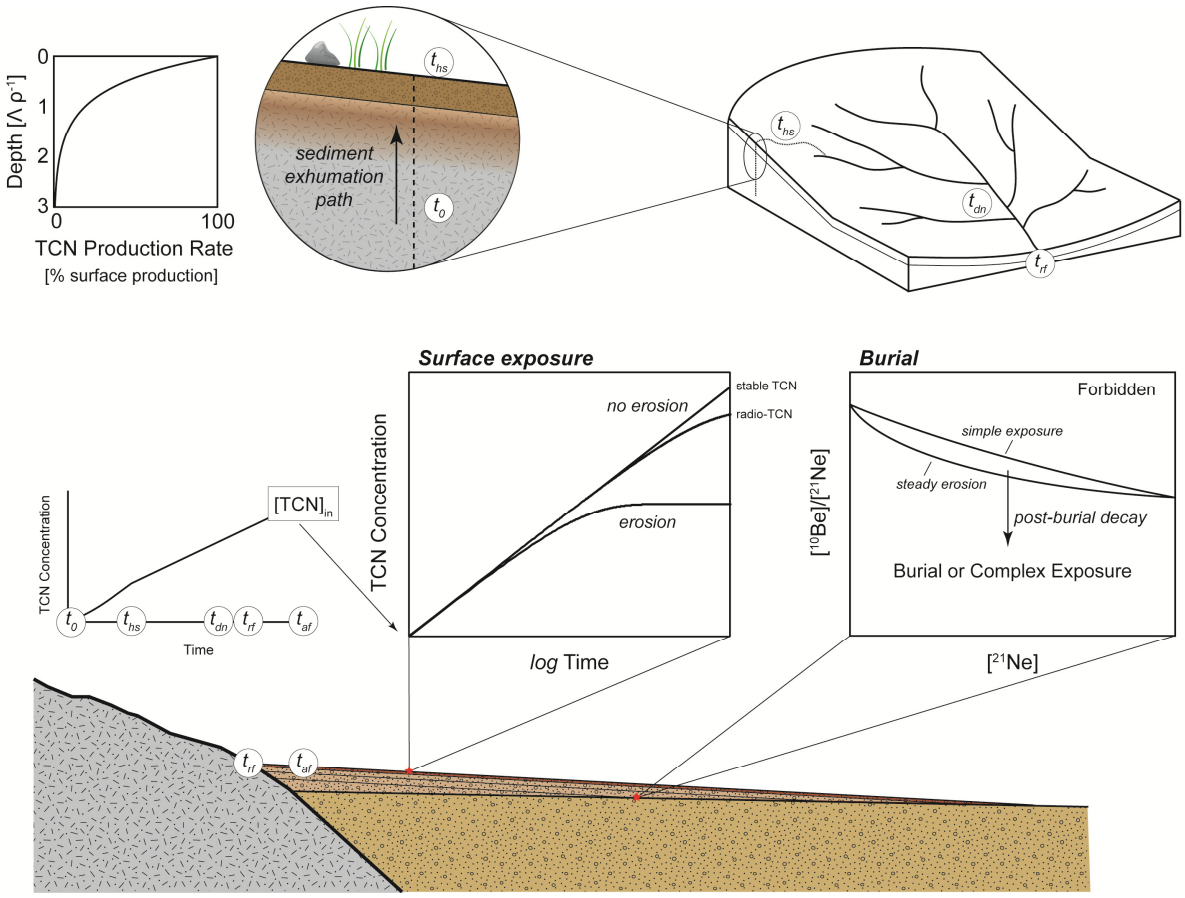
Depth [Λ ρ-1]
0
1
2
3
0
100
TCN Production Rate
[% surface production]
sediment
exhumation
path
Surface exposure
TCN Concentration
stable TCN
radio-TCN
no erosion
erosion
log Time
Burial
Forbidden
simple exposure
steady erosion
post-burial decay
Burial or Complex Exposure
[10Be]/[21Ne]
[21Ne]
[TCN]in
TCN Concentration
Time

Figure 5.3.

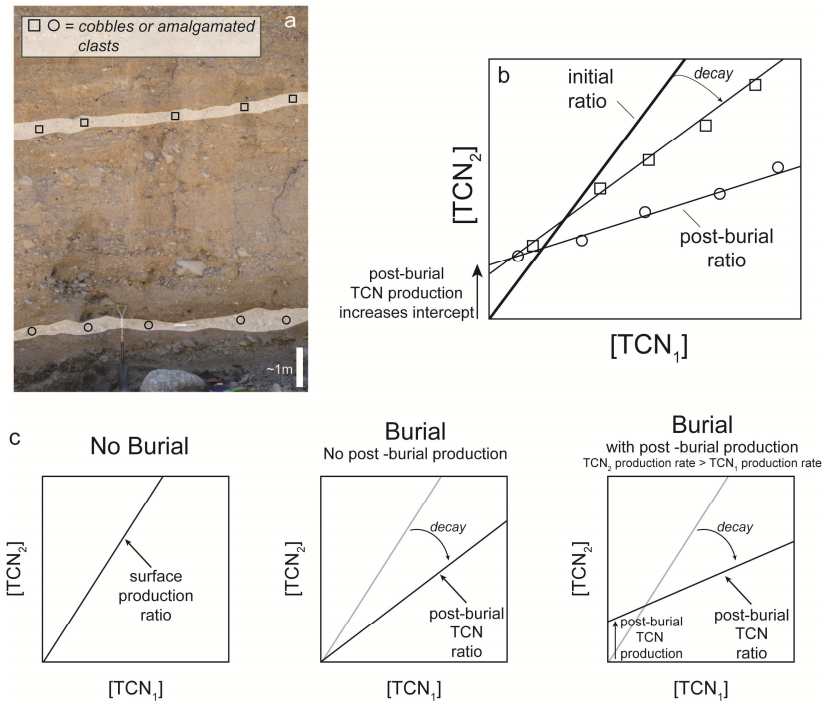
□ ○ = cobbles or amalgamated clasts
a
~1m
b
initial ratio
decay
post-burial ratio
post-burial TCN production increases intercept
[TCN2]
[TCN1]
c
No Burial
surface production ratio
Burial
No post -burial production
decay
post-burial TCN ratio
Burial
with post -burial production
TCN2 production rate > TCN1 production rate
decay
post-burial TCN production
post-burial TCN ratio

Figure 5.4.

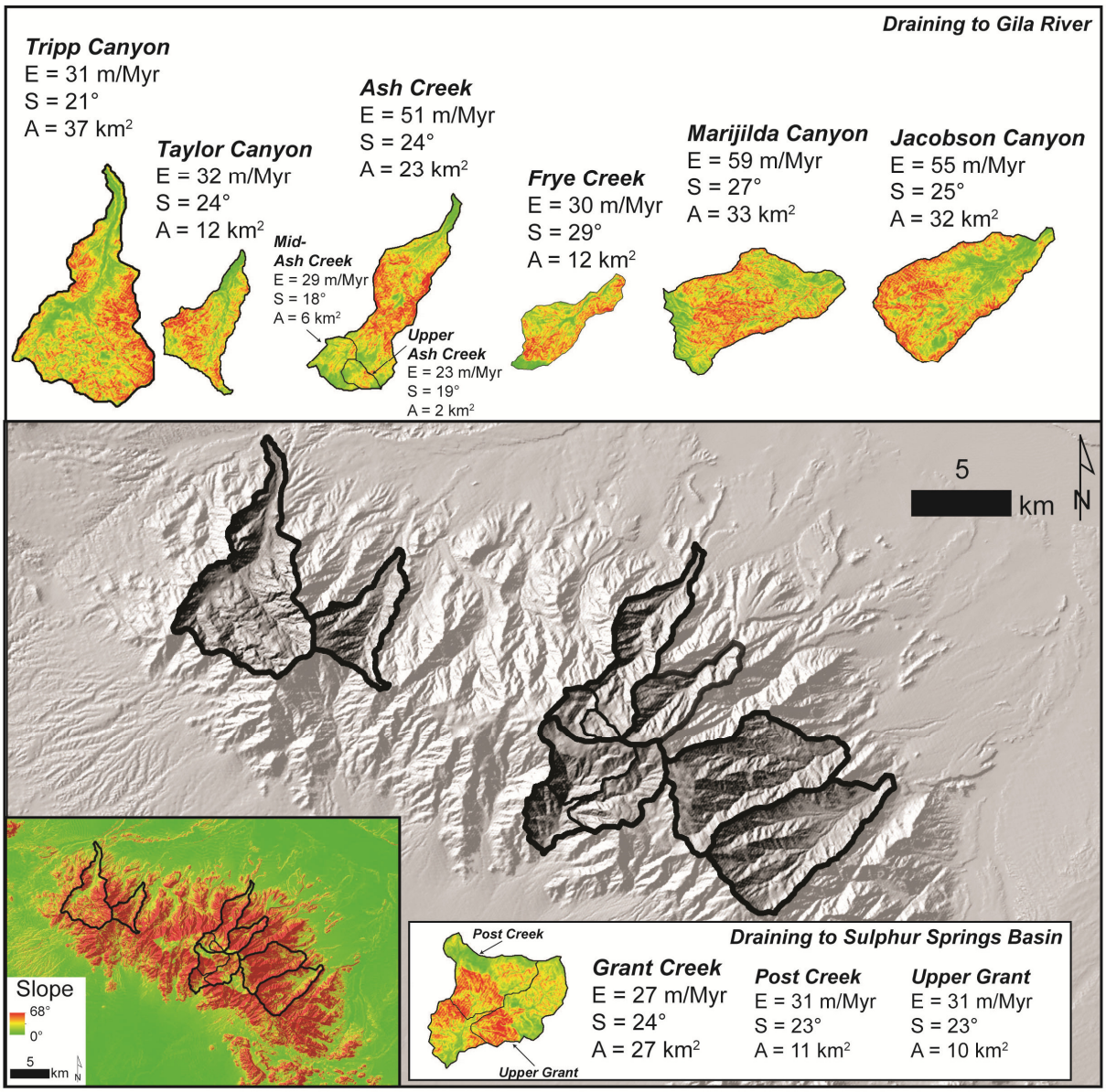
Draining to Gila River
Tripp Canyon
E = 31 m/Myr
S = 21°
A = 37 km²
Taylor Canyon
E = 32 m/Myr
S = 24°
A = 12 km²
Ash Creek
E = 51 m/Myr
S = 24°
A = 23 km²
Mid-
Ash Creek
E = 29 m/Myr
S = 18°
A = 6 km²
Upper
Ash Creek
E = 23 m/Myr
S = 19°
A = 2 km²
Frye Creek
E = 30 m/Myr
S = 29°
A = 12 km²
Marijilda Canyon
E = 59 m/Myr
S = 27°
A = 33 km²
Jacobson Canyon
E = 55 m/Myr
S = 25°
A = 32 km²
5
km
N
Slope
68°
0°
5
km
N
Post Creek
Upper Grant
Draining to Sulphur Springs Basin
Grant Creek
E = 27 m/Myr
S = 24°
A = 27 km²
Post Creek
E = 31 m/Myr
S = 23°
A = 11 km²
Upper Grant
E = 31 m/Myr
S = 23°
A = 10 km²

Figure 5.5.

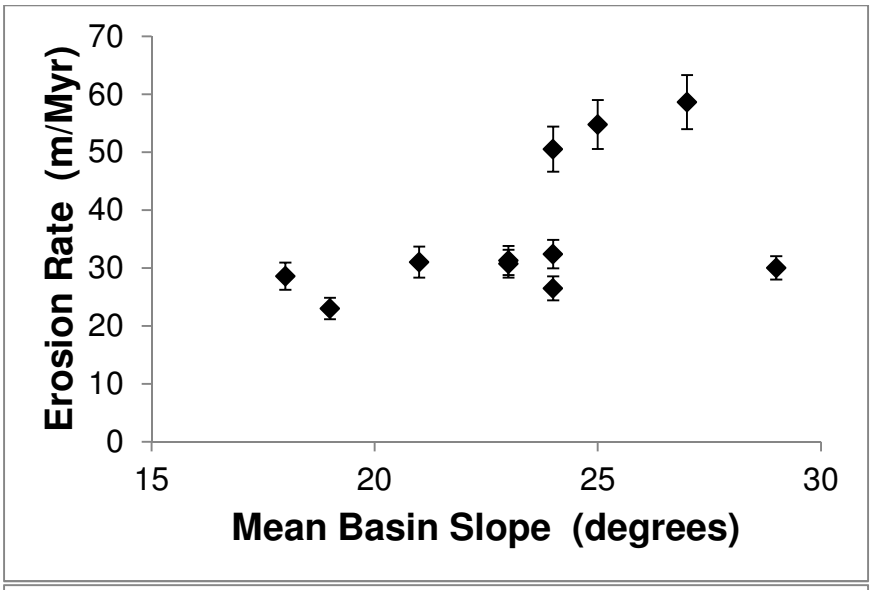
Erosion Rate (m/Myr)
70
60
50
40
30
20
10
0
15
20
25
30
Mean Basin Slope (degrees)

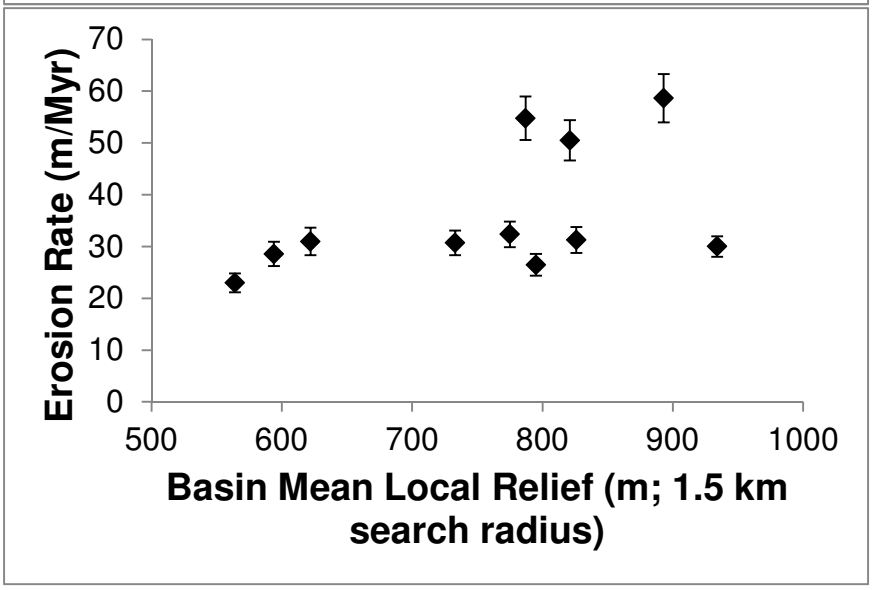
Erosion Rate (m/Myr)
70
60
50
40
30
20
10
0
500
600
700
800
900
1000
Basin Mean Local Relief (m; 1.5 km search radius)

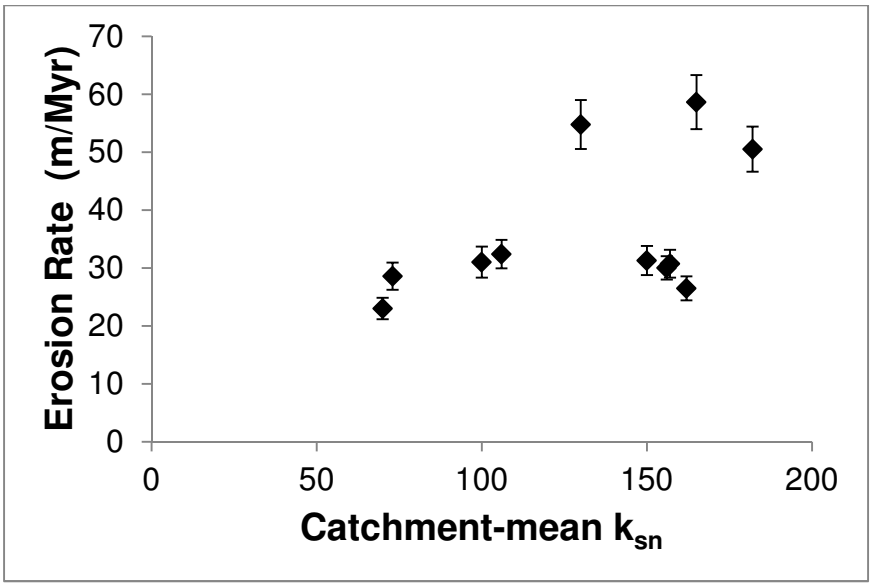
Erosion Rate (m/Myr)
70
60
50
40
30
20
10
0
0
50
100
150
200
Catchment-mean k_{sn}

Figure 5.6.

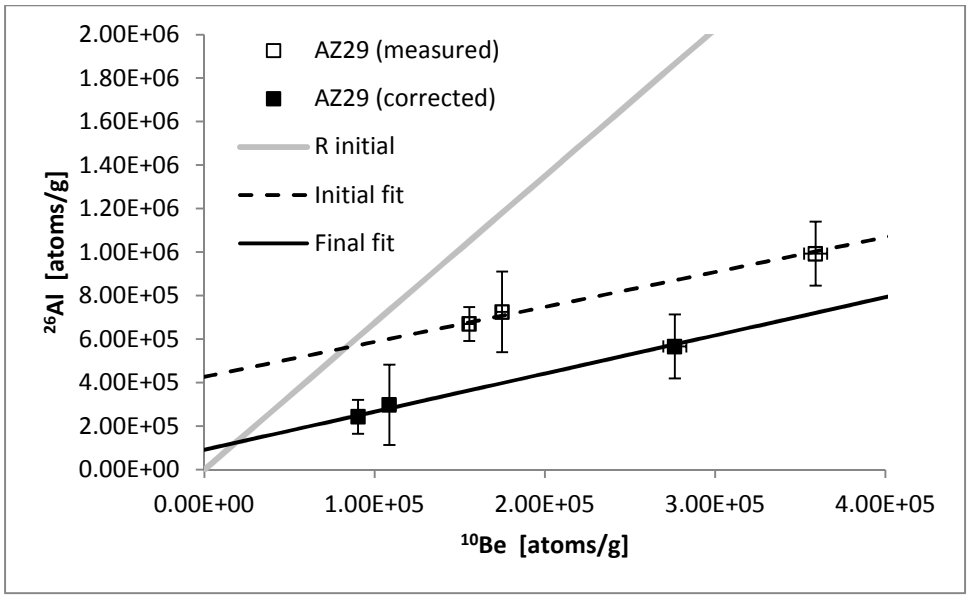
AZ29 (measured)
AZ29 (corrected)
R initial
Initial fit
Final fit
26Al [atoms/g]
10Be [atoms/g]
2.00E+06
1.80E+06
1.60E+06
1.40E+06
1.20E+06
1.00E+06
8.00E+05
6.00E+05
4.00E+05
2.00E+05
0.00E+00
0.00E+00
1.00E+05
2.00E+05
3.00E+05
4.00E+05

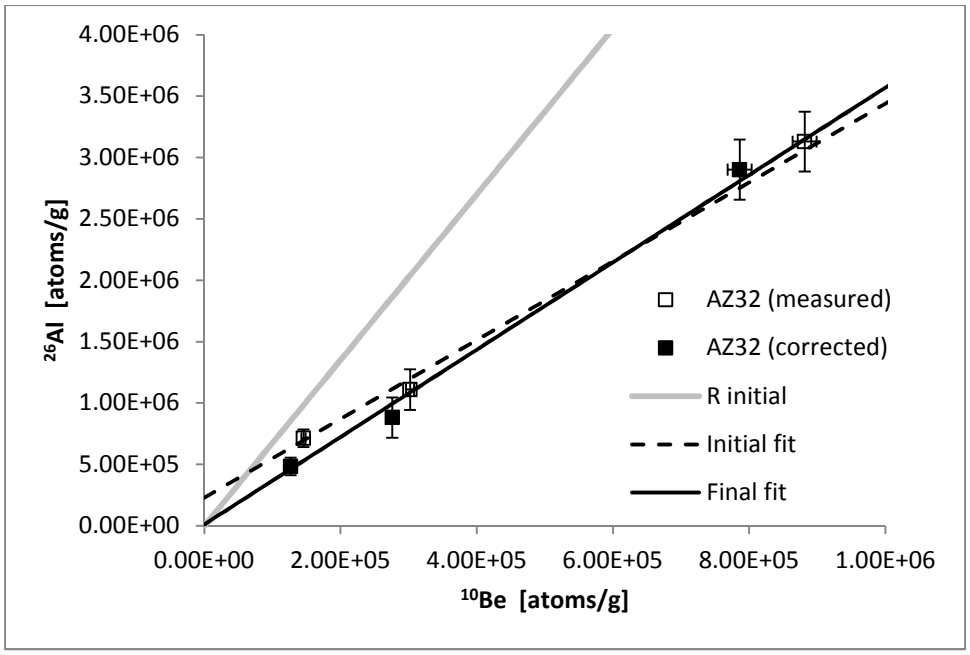
AZ32 (measured)
AZ32 (corrected)
R initial
Initial fit
Final fit
26Al [atoms/g]
10Be [atoms/g]
4.00E+06
3.50E+06
3.00E+06
2.50E+06
2.00E+06
1.50E+06
1.00E+06
5.00E+05
0.00E+00
0.00E+00
2.00E+05
4.00E+05
6.00E+05
8.00E+05
1.00E+06

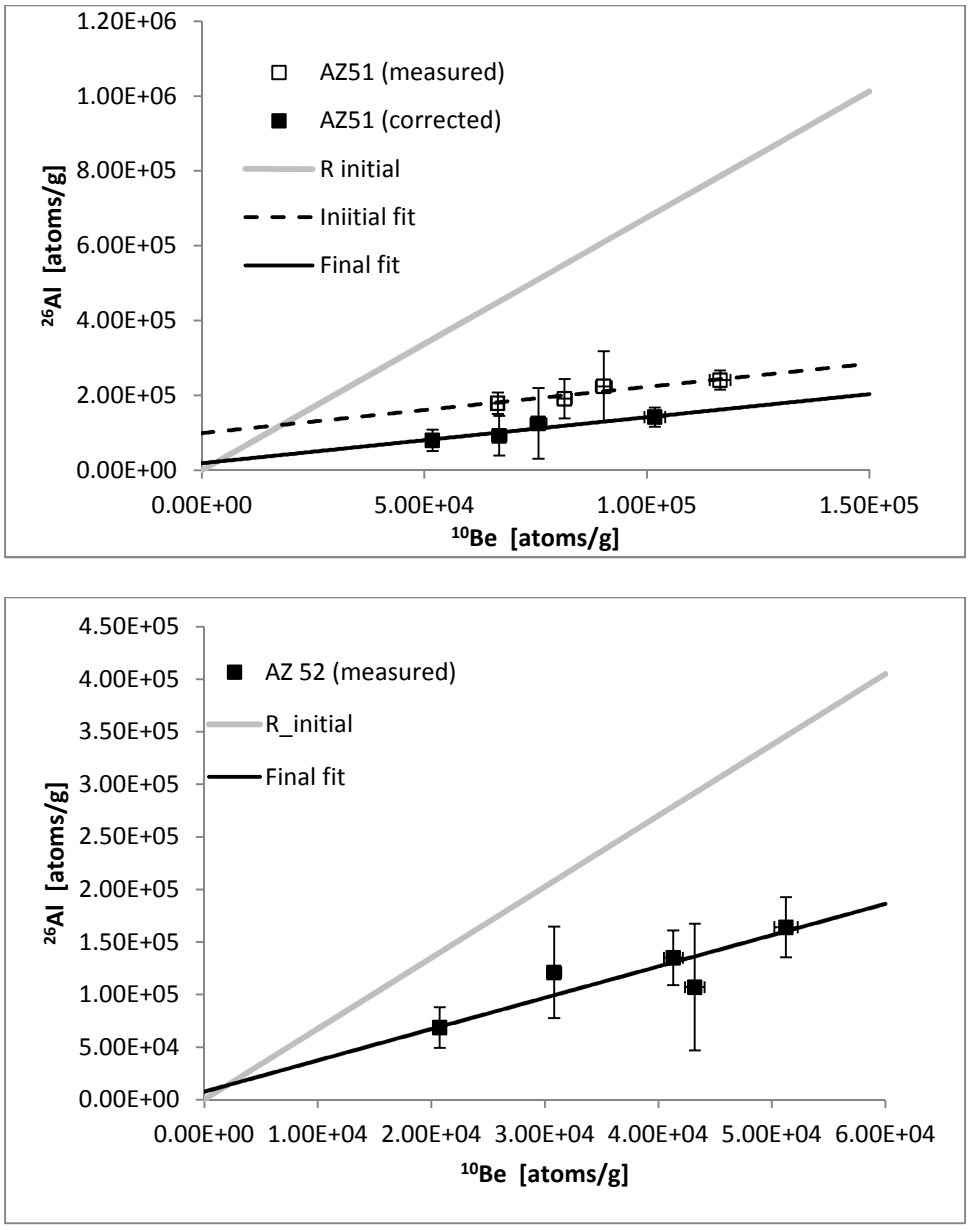
1.20E+06
1.00E+06
8.00E+05
6.00E+05
4.00E+05
2.00E+05
0.00E+00
0.00E+00
5.00E+04
1.00E+05
1.50E+05
^{26}Al [atoms/g]
^{10}Be [atoms/g]
AZ51 (measured)
AZ51 (corrected)
R initial
Iniitial fit
Final fit
4.50E+05
4.00E+05
3.50E+05
3.00E+05
2.50E+05
2.00E+05
1.50E+05
1.00E+05
5.00E+04
0.00E+00
0.00E+00
1.00E+04
2.00E+04
3.00E+04
4.00E+04
5.00E+04
6.00E+04
^{26}Al [atoms/g]
^{10}Be [atoms/g]
AZ 52 (measured)
R_initial
Final fit

Figure 5.7.

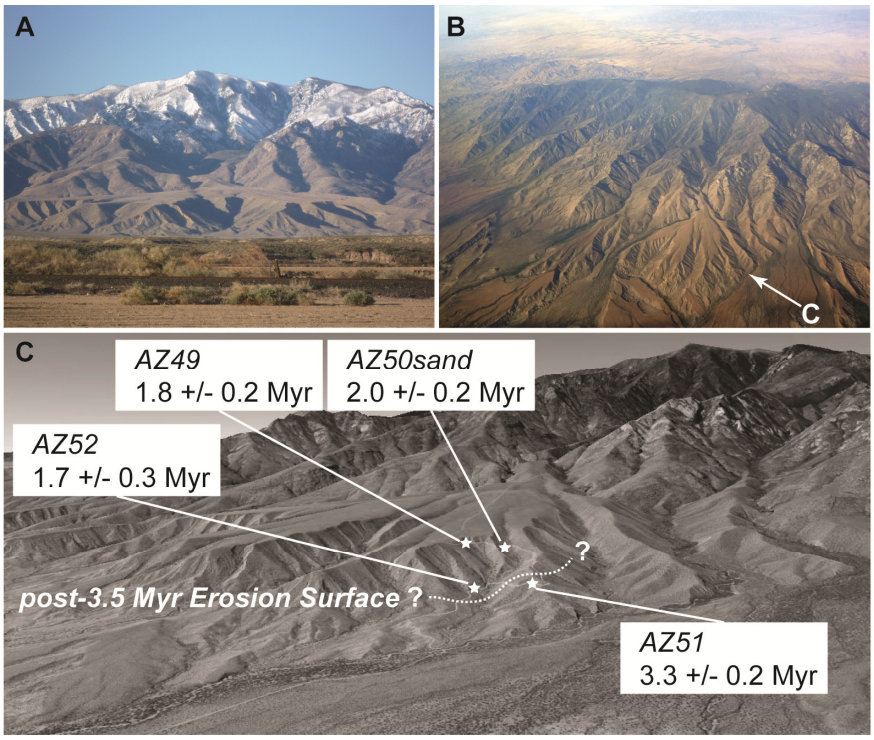
A
B
C
C
AZ49
1.8 +/- 0.2 Myr
AZ50sand
2.0 +/- 0.2 Myr
AZ52
1.7 +/- 0.3 Myr
post-3.5 Myr Erosion Surface ?
?
AZ51
3.3 +/- 0.2 Myr

Figure 5.8.

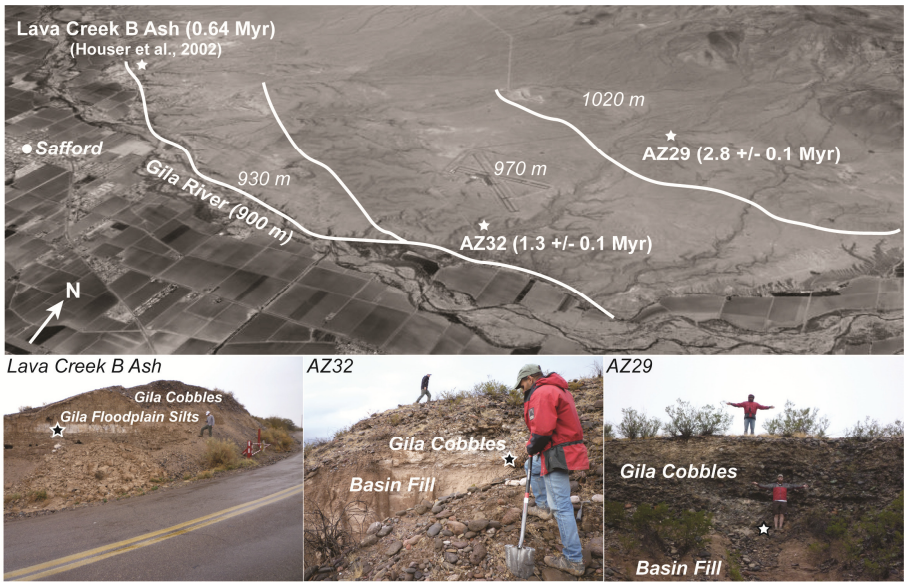
Lava Creek B Ash (0.64 Myr)
(Houser et al., 2002)
1020 m
Safford
AZ29 (2.8 +/- 0.1 Myr)
930 m
970 m
Gila River (900 m)
AZ32 (1.3 +/- 0.1 Myr)
N
Lava Creek B Ash
Gila Cobbles
Gila Floodplain Silts
AZ32
Gila Cobbles
Basin Fill
AZ29
Gila Cobbles
Basin Fill

Figure 5.9.

CHAPTER 6

Synthesis

The research reported in this dissertation helps clarify when southeastern Arizona's Basin and Range began its transition from a tectonically active to tectonically quiescent, and how that transition is reflected in rates of upland erosion. Additionally, we push forward the state of the art for integrated analyses of Late Cenozoic landscape evolution using a myriad of TCN techniques. An isochron approach to $^{26}Al/^{10}Be$ burial dating has not been applied to sedimentary basin fill before this work, and the benefit of extracting multiple paleo-erosion rates from each date was underscored by our results. Our techniques are applicable to actively subsiding coupled basins and ranges and could provide much needed insight into the evolution of such tectonic settings. Our work with multiple TCN in the Atacama Desert of northern Chile helped inform our approach to work in Arizona – i.e, a move to burial dating instead of surface exposure dating – and more importantly it provided new insight regarding fluvial processes in a hyperarid environment. The incredibly slow rates of landscape evolution in the Atacama Desert warrant considerable caution when trying to apply 'standard' TCN techniques, as shown by our broader suite of paired $^{21}Ne/^{10}Be$ analyses from northern Chile that revealed multiple generations of exposure to TCN production in sediment.

Rates of Post-Tectonic Landscape Evolution in Southeastern Arizona

Upland erosion rates in southeastern Arizona's Basin and Range have been remarkably stable over the last ~4 Myr of tectonic quiescence. Chapter 5 reports TCN-derived millennial scale erosion rates for upland drainage basins of the Pinaleno Mountains ranging from ~30-50 m/Myr. In a

comparison of the modern topography of the Pinaleno Mountains to that of an actively uplifting orogeny, predictions of erosion rates one to two orders of magnitude would be reasonable. In the absence of active subsidence in the basin adjacent to the range, upland erosion rates have slowed dramatically. Paleo-erosion rates from TCN burial dates support a long-term stability of erosion rates post-tectonics. The majority of paleo-erosion rates range from 20-50 m/Myr, approximately the same range as modern rates. However, there was a spike in erosion rates just prior to ~2 Myr that could be attributed to a wetter climate from ~3.5-2 Myr.

Post-tectonic erosion rates reported for Aravaipa Creek basin in Chapter 3 are similarly slow. Paleo-erosion rates from two conventional TCN burial dates are ~40-50 m/Myr, and a long term erosion rate derived from our landscape reconstruction and the dates of the latest stage basin fill is ~12 m/Myr. In Aravaipa Creek basin, rapid incision of at least 150 m/Myr is inferred for the formation of Aravaipa Canyon, but this rapid rate reflects a period of transient readjustment to drainage integration.

Pace and Pattern of Drainage Integration for the Modern Gila River System

Our new dates for late stage basin fill in both Safford basin and Aravaipa Creek basin support earlier estimates for the ages of basin high stand remnants (Menges and McFadden, 1981; Morrison, 1985). Aravaipa Creek basin integrated with the Lower San Pedro basin sometime soon after ~3 Myr. The Gila River had arrived in Safford basin – presumably after integrating from the Duncan-Clifton basin upstream – before 3 Myr based on a 2.8 Myr isochron burial date for the highest elevation Gila River terrace in Safford basin. The Gila River incised 50 m by 1.3 Myr, and in doing so it initiated dissection of late stage basin fill such as Frye Mesa by 2 Myr (supported by our

burial dates at Frye Mesa). It is reasonable to infer that incision on the Gila River between 2.8 and 1.3 Myr was related to integration of the Gila River across the Mescal Mountains into the Lower San Pedro basin. The exact timing of this integration event is difficult to ascertain since we have no dates from the San Carlos basin, between Safford basin and the Mescal Mountains, but tributaries to the Gila River in the San Carlos basin did not incise until after the emplacement of Peridot Mesa at 3.6 Myr (Anderson, 1990; Connell et al., 2005), which supports our model. We have no dates for the basin high stands in the Lower San Pedro basin, but our inference that rapid incision of Aravaipa Canyon was driven by a significant elevation difference between Aravaipa Creek basin's spillover point and the Lower San Pedro basin requires that the Lower San Pedro basin had incised below its high stand sometime before 3 Myr.

Rates of regional incision throughout the Gila River system have been moderate throughout the Quaternary. The Gila River incised at 60 m/Myr between 1.3 and 0.64 Myr, and at 47 m/Myr from 0.64 m/Myr to the present. Based on our one surface exposure date for a Pleistocene piedmont in the Lower San Pedro basin, range front systems for that basin have been incising at ~50 m/Myr from 400 kyr to the present. These rates are all in agreement with previous estimates of regional incision rates from the Mid-Pleistocene to the present (Dethier, 2001). It would be easy to assert that these slow and steady incision rates are the driving force behind equally slow and steady modern erosion rates in ranges such as the Santa Catalina and Pinaleno Mountains, but our results from the south side of the Pinaleno Mountains beg caution. Grant Creek on the south side of the Pinaleno Mountains drains to Sulphur Springs basin which is still internally drained and has not experienced any base level fall associated with incision on the Gila River. Nonetheless, upland erosion rates for Grant Creek are ~30 m/Myr, equal to the low end of rates for drainage basins on

the north side of the range that drain to the Gila River in Safford basin. Thus, it must be some combination of Quaternary climate and long-term incision that is setting the pace for post-tectonic landscape evolution in southeastern Arizona.

A Renewed Need for Multiple TCN Studies?

As new research continues to embrace TCN for quantifying rates of surface processes and constraining the chronology of Late Tertiary and Quaternary alluvial deposits, the utility of measuring multiple TCN, common in early studies, to evaluate whether the underlying assumptions of the technique are being met. We use multiple nuclides in Chapters 2-5 for multiple purposes: evaluating sediment sources, determining whether sediment has undergone more than one episode of exposure-burial-reworking, conventional and isochron burial dates, and determining paleo-erosion rates in concert with those burial dates. In Arizona, paleo-erosion rates derived from $^{26}Al/^{10}Be$ ratios supported modern millennial rates that at first blush were strikingly slow and uniform. In Chile, measuring multiple TCN prevented us from reporting dramatically wrong exposure ages that could have propagated into others' interpretations of the relationship between climate and tectonics of the Andes. Future studies of landscape evolution in the Atacama Desert would be well-served by establishing a baseline for TCN systematics in their region of interest. This requires a significant investment upfront in terms of TCN analyses on expensive mass spectrometers, but it could prevent the wasting of money in the long run.

Future Research Directions

Pliocene Paleoclimate of Southeastern Arizona

Very little is known about the Pliocene climate of southeastern Arizona despite its importance for the Late Cenozoic landscape evolution of the region. Promising work using stable carbon and oxygen isotopes in paleosols of the St. David formation of the Upper San Pedro bain to infer paleo-ecology and paleoclimate could be adapted to similar deposits throughout the region (Smith et al., 1993; Smith, 1994). In particular, we have identified pedogenic carbonates in the basin depocenter facies of late stage basin fill in Sonoita Creek basin that could yield a paleoclimate record from ~5-3 Myr. Such a study would be of methodological significance, too, since Sonoita Creek basin is adjacent to the Upper San Pedro basin so the results would be very closely relatable to the aforementioned work of Smith et al. (1993) and Smith (1994).

More Constraints for Quaternary Incision in Southeastern Arizona

Our surface exposure date for an intermediate piedmont in the Lower San Pedro basin is a first step toward constraining the mid-Pleistocene to present evolution of the Gila River system. A more thorough campaign that dates similar suites of piedmont surfaces across several basins would provide a higher resolution look at how uniform regional incision has been through the Quaternary. Much of the hard work of carefully mapping these units has already been done by the Arizona Geological Survey (AZGS), and collaboration with the geologists at the AZGS would be natural and recommended for this work. Since most of these piedmonts are likely ~500 kyr or younger, surface exposure dating via TCN concentration depth profiles would be required instead of TCN burial dating (too young for $^{26}Al/^{10}Be$ burial dating).

Systematic Analysis of Source-to-Sink TCN Abundances for the Rio Loa, Northern Chile

A comprehensive study of TCN accumulation from source-to-sink for the Rio Loa, adapting the approach of Kober et al. (2007) and Kober et al.(2009), would be of great value for future studies of landscape evolution in northern Chile. Binnie et al. (2013) report downstream decreases in TCN abundance for large systems draining from the Andes to the Pacific Ocean in northern Chile, and I believe that at least some of their data are from the Rio Loa. Their results support the potential for significant, long term sediment storage in the Rio Loa system and thus complex exposure histories in terms of TCN production. Systematic sampling of fill terraces along the course of the Rio Loa and analysis for multiple TCN could provide insight into the duration of sediment storage throughout the system. Such a study may also help resolve how much sediment, if any, is being delivered to the Rio Loa from the very slowly eroding uplands of the Central Depression (in contrast to sediment from the Andes).

References

Anderson, L. W. (1990). Terraces and pediments of San Carlos River Valley.*Geologic Excursions Through the Sonoran Desert Region, Arizona and Sonora, Arizona Geological Survey Special Paper*, *7*, 24.

Binnie, S. A., Liermann, A., Dunai, T.J., Dewald, A., Heinze, S. (2013). Constraints on sediment transfer from the Andes to the coast of northern Chile. *Geophysical Research Abstracts, Vol. 15, EGU2013-5952.*

Connell, S. D., Hawley, J. W., & Love, D. W. (2005). Late Cenozoic drainage development in the southeastern Basin and Range of New Mexico, southeasternmost Arizona, and western Texas. *New Mexico's ice ages*, *28*, 125-150.

Dethier, D. P. (2001). Pleistocene incision rates in the western United States calibrated using Lava Creek B tephra. *Geology*, *29*(9), 783-786.

Kober, F., Ivy-Ochs, S., Schlunegger, F., Baur, H., Kubik, P. W., & Wieler, R. (2007). Denudation rates and a topography-driven rainfall threshold in northern Chile: Multiple cosmogenic nuclide data and sediment yield budgets.*Geomorphology*, *83*(1), 97-120.

Kober, F., Ivy-Ochs, S., Zeilinger, G., Schlunegger, F., Kubik, P. W., Baur, H., & Wieler, R. (2009). Complex multiple cosmogenic nuclide concentration and histories in the arid Rio Lluta catchment, northern Chile. *Earth Surface Processes and Landforms*, *34*(3), 398-412.

Menges, C. M., & McFadden, L. D. (1981). Evidence for a latest Miocene to Pliocene transition from Basin-Range tectonic to post-tectonic landscape evolution in southeastern Arizona: Arizona Geological Society Digest 13. *Soc. Digest*, *13*, 151-160.

Morrison, R. B. (1985). Pliocene/Quaternary geology, geomorphology, and tectonics of Arizona. *Geological Society of America Special Papers*, *203*, 123-146.

Smith, G. A., Wang, Y., Cerling, T. E., & Geissman, J. W. (1993). Comparison of a paleosol-carbonate isotope record to other records of Pliocene-early Pleistocene climate in the western United States. *Geology*, *21*(8), 691-694.

Smith, G. A. (1994). Climatic influences on continental deposition during late-stage filling of an extensional basin, southeastern Arizona. *Geological Society of America Bulletin*, *106*(9), 1212-1228.

7.0 Comprehensive References

Allen, B.D., 2005. Ice age lakes in New Mexico. In: Lucas, S.G., Morgan, G.S., Zeigler, K.E. (Eds.), New Mexico's Ice Ages. New Mexico Museum of Natural History and Science Bulletin No. 28, pp. 107–114.

Alpers, Charles N., and George H. Brimhall. "Middle Miocene climatic change in the Atacama Desert, northern Chile: Evidence from supergene mineralization at La Escondida." *Geological Society of America Bulletin* 100.10 (1988): 1640-1656.

Ammann, C., Jenny, B., Kammer, K., Messerli, B., 2001. Late Quaternary Glacier response to humidity changes in the arid Andes of Chile (18-29 degrees S). Palaeogeography Palaeoclimatology Palaeoecology 172, 313-326.

Amundson, R., Dietrich, W., Bellugi, D., Ewing, S., Nishiizumi, K., Chong, G., Owen, J., Finkel, R., Heimsath, A., Stewart, B., 2012. Geomorphologic evidence for the late Pliocene onset of hyperaridity in the Atacama Desert. Geological Society of America Bulletin 124, 1048-1070.

Anderson, L.W., (1990). Terraces and pediments of San Carlos River Valley, in Gehrels, G.E., and Spencer, J.E., eds., *Geologic excursions through the Sonoran Desert Region, Arizona and Sonora: Arizona Geological Survey Special Paper* 7, p. 24.

Anderson, R.S., Repka, J.L., Dick, G.S., 1996. Explicit treatment of inheritance in dating depositional surfaces using in situ Be-10 and Al-26. Geology 24, 47-51.

Balco, G., & Rovey, C. W. (2008). An Isochron Method for Cosmogenic-Nuclide Dating of Buried Soils and Sediments. *American Journal of Science, 308*(10), 1083-1114.

Balco, G., Shuster, D.L., 2009. Production rate of cosmogenic Ne-21 in quartz estimated from Be-10, Al-26, and Ne-21 concentrations in slowly eroding Antarctic bedrock surfaces. Earth and Planetary Science Letters 281, 48-58.

Balco, G., Stone, J. O., Lifton, N. A., & Dunai, T. J. (2008). A complete and easily accessible means of calculating surface exposure ages or erosion rates from< sup> 10</sup> Be and< sup> 26</sup> Al measurements.*Quaternary Geochronology, 3*(3), 174-195.

Balco, G., & Stone, J. O. H. (2005). Measuring middle Pleistocene erosion rates with cosmic-ray-produced nuclides in buried alluvial sediment, Fisher Valley, southeastern Utah. *Earth Surface Processes and Landforms, 30*(8), 1051-1067.

Bard, E., Rickaby, R.E.M., 2009. Migration of the subtropical front as a modulator of glacial climate. Nature 460, 380-U393.

Bierman, P. R., & Caffee, M. (2001). Slow rates of rock surface erosion and sediment production across the Namib Desert and escarpment, southern Africa.*American Journal of Science*, *301*(4-5), 326-358.

Bierman, P., & Steig, E. J. (1996). Estimating rates of denudation using cosmogenic isotope abundances in sediment. *Earth Surface Processes and Landforms, 21*(2), 125-139.

Bonnet, S., & Crave, A. (2003). Landscape response to climate change: Insights from experimental modeling and implications for tectonic versus climatic uplift of topography. *Geology, 31*(2), 123-126.

Braucher, R., Del Castillo, P., Siame, L., Hidy, A. J., & Bourles, D. L. (2009). Determination of both exposure time and denudation rate from an in situ-produced ^{10}Be depth profile: A mathematical proof of uniqueness. Model sensitivity and applications to natural cases. *Quaternary Geochronology*, *4*(1), 56-67.

Brown, E. T., Stallard, R. F., Larsen, M. C., Raisbeck, G. M., & Yiou, F. (1995). Denudation Rates Determined From The Accumulation Of In Situ-Produced Be-10 In The Luquillo Experimental Forest, Puerto-Rico. *Earth and Planetary Science Letters, 129*(1-4), 193-202.

Bull, W.B., 2009. Geomorphic Responses to Climatic Change. The Blackburn Press, New Jersey.

Carrizo, D., Gonzalez, G., Dunai, T., 2008. Neogene constriction in the northern Chilean Coastal Cordillera: Neotectonics and surface dating using cosmogenic Ne-21. Revista Geologica De Chile 35, 1-38.

Clapp, E.M., Bierman, P.R., Nichols, K.K., Pavich, M., Caffee, M., 2001. Rates of sediment supply to arroyos from upland erosion determined using in situ produced cosmogenic Be-10 and Al-26. Quaternary Research 55, 235-245.

Darling, A. L., Karlstrom, K. E., Granger, D. E., Aslan, A., Kirby, E., Ouimet, W. B., et al. (2012). New incision rates along the Colorado River system based on cosmogenic burial dating of terraces: Implications for regional controls on Quaternary incision. *Geosphere, 8*(5), 1020-1041.

Davis, W. M., & Brooks, B. (1930). The Galiuro Mountains, Arizona. *American Journal of Science*, (110), 89-115.

Dethier, D. P. (2001). Pleistocene incision rates in the western United States calibrated using Lava Creek B tephra. *Geology*, *29*(9), 783-786.

DiBiase, R. A., Whipple, K. X., Heimsath, A. M., & Ouimet, W. B. (2010). Landscape form and millennial erosion rates in the San Gabriel Mountains, CA.*Earth and Planetary Science Letters*, *289*(1), 134-144.

Dickinson, W. (1991). *Tectonic setting of faulted Tertiary strata associated with the Catalina core complex in southern Arizona*: Geological Society of Amer.

Dickinson, W. R. (2004). Evolution of the North American Cordillera. *Annual Review of Earth and Planetary Sciences, 32*, 13-45.

Ditchburn R. G. and Whitehead N. E. (1994) The separation of ^{10}Be from silicates. 3d Workshop of the South Pacific Environmental Radioactivity Association, 4-7.

Douglass, J., Meek, N., Dorn, R. I., & Schmeeckle, M. W. (2009). A criteria-based methodology for determining the mechanism of transverse drainage development, with application to the southwestern United States. *Geological Society of America Bulletin*, *121*(3-4), 586-598.

Dunai, T.J., Lopez, G.A.G., Juez-Larre, J., 2005. Oligocene-Miocene age of aridity in the Atacama Desert revealed by exposure dating of erosion-sensitive landforms. Geology 33, 321-324.

Evenstar, L.A., Hartley, A.J., Stuart, F.M., Mather, A.E., Rice, C.M., Chong, G., 2009. Multiphase development of the Atacama Planation Surface recorded by cosmogenic He-3 exposure ages: Implications for uplift and Cenozoic climate change in western South America. Geology 37, 27-30.

Ewing, S.A., Michalski, G., Thiemens, M., Quinn, R.C., Macalady, J.L., Kohl, S., Wankel, S.D., Kendall, C., McKay, C.P., Amundson, R., 2007. Rainfall limit of the N cycle on Earth. Global Biogeochemical Cycles 21.

Ewing, S.A., Yang, W., DePaolo, D.J., Michalski, G., Kendall, C., Stewart, B.W., Thiemens, M., Amundson, R., 2008. Non-biological fractionation of stable Ca isotopes in soils of the Atacama Desert, Chile. Geochimica Et Cosmochimica Acta 72, 1096-1110.

Galusha, Theodore, Johnson, N.M., Lindsay, E.H., Opdyke, N.D., and Tedford, R.H., 1984, Biostratigraphy and magnetostratigraphy, late Pliocene rocks, 111 Ranch, Arizona: Geological Society of America Bulletin, v. 95, p. 714-722.

Gilbert, G. (1875). Report on the geology of portions of Nevada, California, and Arizona, examined in the years 1871 and 1872, Geogr. and Geol. Expl. and Surv. west of the 100th meridian. *Vol. III*.

Gonzalez, G., Dunai, T., Carrizo, D., Allmendinger, R., 2006. Young displacements on the Atacama Fault System, northern Chile from field observations and cosmogenic Ne-21 concentrations. Tectonics 25.

Gootee, B.F. (2012). Geologic Evaluation of the Safford Basin for Carbon Dioxide Sequestration Potential, *AZGS OFR-12-01*.

Gosse, J. C., & Phillips, F. M. (2001). Terrestrial in situ cosmogenic nuclides: theory and application. *Quaternary Science Reviews*, *20*(14), 1475-1560.

Granger, D. E., Kirchner, J. W., & Finkel, R. (1996). Spatially averaged long-term erosion rates measured from in situ-produced cosmogenic nuclides in alluvial sediment. *Journal of Geology, 104*(3), 249-257.

Granger, D. E., Kirchner, J. W., & Finkel, R. C. (1997). Quaternary downcutting rate of the New River, Virginia, measured from differential decay of cosmogenic 26Al and 10Be in cave-deposited alluvium. *Geology, 25*(2), 107-110.

Granger, D. E., & Muzikar, P. F. (2001). Dating sediment burial with in situ-produced cosmogenic nuclides: theory, techniques, and limitations. *Earth and Planetary Science Letters, 188*(1-2), 269-281.

Granger, D., Riebe, C., 2007. Cosmogenic nuclides in weathering and erosion. Treatise on Geochemistry: Oxford, Pergamon, 1-42.

Halvorsen, W.L., Thomas, K., Graham, L., 2001. Arizona Gap Project Final Report. USGS Sonoran Desert Field Station. University of Arizona, Tucson.

Hartley, A. J., & Chong, G. (2002). Late Pliocene age for the Atacama Desert: Implications for the desertification of western South America. *Geology*, *30*(1), 43-46.

Heimsath, A. M., DiBiase, R. A., & Whipple, K. X. (2012). Soil production limits and the transition to bedrock-dominated landscapes. *Nature Geoscience*, *5*(3), 210-214.

Heindl, L. (1958). *Cenozoic alluvial deposits of the Upper Gila River area, New Mexico and Arizona: Tucson, University of Arizona.* doctoral dissertation, 249 p.

Heindl, L. A., 1962, Should the term, "Gila Conglomerate" be abandoned?: Arizona Geological Society Digest, v. 5, p. 73-88.

Heisinger, B., Lal, D., Jull, A., Kubik, P., Ivy-Ochs, S., Knie, K., et al. (2002). Production of selected cosmogenic radionuclides by muons: 2. Capture of negative muons. *Earth and Planetary Science Letters, 200*(3), 357-369.

Heisinger, B., Lal, D., Jull, A., Kubik, P., Ivy-Ochs, S., Neumaier, S., et al. (2002). Production of selected cosmogenic radionuclides by muons: 1. Fast muons. *Earth and Planetary Science Letters, 200*(3), 345-355.

Herzog, G. F., Vogt, S., Albrecht, A., Xue, S., Fink, D., Klein, J., ... & Schultz, L. (1997). Complex exposure histories for meteorites with "short" exposure ages. *Meteoritics & Planetary Science*, *32*(3), 413-422.

Heusser, L., Heusser, C., Mix, A., McManus, J., 2006. Chilean and Southeast Pacific paleoclimate variations during the last glacial cycle: directly correlated pollen and delta 18O records from ODP Site 1234. Quaternary Science Reviews 25, 3404-3415.

Hidy, A. J., Gosse, J. C., Pederson, J. L., Mattern, J. P., & Finkel, R. C. (2010). A geologically constrained Monte Carlo approach to modeling exposure ages from profiles of cosmogenic nuclides: An example from Lees Ferry, Arizona. *Geochemistry, Geophysics, Geosystems*, *11*(9).

Hilley, G. E., & Strecker, M. R. (2005). Processes of oscillatory basin filling and excavation in a tectonically active orogen: Quebrada del Toro Basin, NW Argentina. *Geological Society of America Bulletin*, *117*(7-8), 887-901.

Holmgren, C. A., Betancourt, J. L., & Rylander, K. A. (2006). A 36,000-yr vegetation history from the Peloncillo Mountains, southeastern Arizona, USA.*Palaeogeography, Palaeoclimatology, Palaeoecology, 240*(3), 405-422.

Hoke, G. D., Isacks, B. L., Jordan, T. E., Blanco, N., Tomlinson, A. J., & Ramezani, J. (2007). Geomorphic evidence for post-10 Ma uplift of the western flank of the central Andes 18 30'–22 S. *Tectonics*, *26*(5).

House, P.K., Pearthree, P.A., and Perkins, M.E., (2008). Stratigraphic evidence for the role of lake spillover in the inception of the lower Colorado River in southern Nevada and western Arizona, in Reheis, M.C., Hershler, R., and Miller, D.M, eds., *Late Cenozoic drainage history of the southwestern Great Basin and lower Colorado River region—geologic and biotic perspectives: Geological Society of America Special Papers*, v. 439, p. 335–353.

Houser, B.B., Richter, D.H., and Shafiqullah, M., 1985, Geologic map of the Safford quadrangle, Graham County, Arizona: U.S. Geological Survey Miscellaneous Investigation Map I-1617, Scale 1:48,000.

Houser, B.B., Pearthree, P.A., Homburg, J.A., Thrasher, L.C., eds., 2002, Friends of the Pleistocene, Rocky Mountain Cell 46th field conference, and Arizona Geological Society Fall Field Trip, 83 p.

Houston, J., 2006. Variability of precipitation in the Atacama desert: Its causes and hydrological impact. International Journal of Climatology 26, 2181-2198.

Jungers, M.C., Bierman, P.R., Matmon, A., Nichols, K., Larsen, J., Finkel, R., 2009. Tracing hillslope sediment production and transport with in situ and meteoric Be-10. Journal of Geophysical Research-Earth Surface 114.

Kober, F., Ivy-Ochs, S., Schlunegger, F., Baur, H., Kubik, P. W., & Wieler, R. (2007). Denudation rates and a topography-driven rainfall threshold in northern Chile: Multiple cosmogenic nuclide data and sediment yield budgets.*Geomorphology*, *83*(1), 97-120.

Kober, F., Ivy-Ochs, S., Zeilinger, G., Schlunegger, F., Kubik, P.W., Baur, H., Wieler, R., 2009. Complex multiple cosmogenic nuclide concentration and histories in the arid Rio Lluta catchment, northern Chile. Earth Surface Processes and Landforms 34, 398-412.

Kohl, C., & Nishiizumi, K. (1992). Chemical isolation of quartz for measurement of *in situ*-produced cosmogenic nuclides. *Geochimica et Cosmochimica Acta, 56*(9), 3583-3587.

Krieger, M. H. (1968). Geologic map of the Saddle Mountain quadrangle. *Pinal County, Arizona [Dudleyville 7.5 min]: US Geological Survey Geologic Quadrangle Map GQ-671*, *1*.

Kruger, J.M., 1991, Seismic crustal structure beneath the Safford basin and Pinaleño Mountains: Implications for Cenozoic extension and metamorphic core complex uplift in SE Arizona: University of Arizona, Dept. of Geosciences, Ph.D. dissertation, 158 p.

Lal, D., Arnold, J., 1985. Tracing quartz through the environment. Journal of Earth System Science 94, 1-5.

Lal, D. (1991). Cosmic ray labeling of erosion surfaces:< i> in situ</i> nuclide production rates and erosion models. *Earth and Planetary Science Letters*,*104*(2), 424-439.

Lamb, S., & Davis, P. (2003). Cenozoic climate change as a possible cause for the rise of the Andes. *Nature*, *425*(6960), 792-797.

Lamy, F., Hebbeln, D., Wefer, G., 1998. Late quaternary precessional cycles of terrigenous sediment input off the Norte Chico, Chile (27.5 degrees S) and palaeoclimatic implications. Palaeogeography Palaeoclimatology Palaeoecology 141, 233-251.

Lamy, F., Klump, J., Hebbeln, D., Wefer, G., 2000. Late Quaternary rapid climate change in northern Chile. Terra Nova 12, 8-13.

Larsen, I. J., Almond, P. C., Eger, A., Stone, J. O., Montgomery, D. R., & Malcolm, B. (2014). Rapid soil production and weathering in the Southern Alps, New Zealand. *Science*, *343*(6171), 637-640.

Latorre, C., Betancourt, J.L., Arroyo, M.T.K., 2006. Late Quaternary vegetation and climate history of a perennial river canyon in the Rio Salado basin (22 degrees S) of Northern Chile. Quaternary Research 65, 450-466.

Maldonado, A., Betancourt, J.L., Latorre, C., Villagran, C., 2005. Pollen analyses from a 50 000-yr rodent midden series in the southern Atacama Desert (25 degrees 30 ' S). Journal of Quaternary Science 20, 493-507.

Martin, P. S. (1963). Geoghronology of Pluvial Lake Cochise, Southern Arizona. II. Pollen Analysis of A 42-Meter Core. *Ecology*, 436-444.

Matmon, A., Bierman, P. R., Larsen, J., Southworth, S., Pavich, M., & Caffee, M. (2003). Temporally and spatially uniform rates of erosion in the southern Appalachian Great Smoky Mountains. *Geology*, *31*(2), 155-158.

Melton, M. (1965). The geomorphic and paleoclimatic significance of alluvial deposits in southern Arizona. *The Journal of Geology, 73*(1), 1-38.

Meek, N. (1989). Geomorphic and hydrologic implications of the rapid incision of Afton Canyon, Mojave Desert, California. *Geology*, *17*(1), 7-10.

Meek, N., & Douglass, J. (2001). Lake overflow: An alternative hypothesis for Grand Canyon incision and development of the Colorado River. *Colorado River: Origin and evolution: Grand Canyon, Arizona, Grand Canyon Association*, 199-204.

Menges, C. M., & McFadden, L. D. (1981). Evidence for a latest Miocene to Pliocene transition from Basin-Range tectonic to post-tectonic landscape evolution in southeastern Arizona: Arizona Geological Society Digest 13. *Soc. Digest*, *13*, 151-160.

Menges, C. M., & Pearthree, P. A. (1989). Late Cenozoic tectonism in Arizona and its impact on regional landscape evolution. *Geologic evolution of Arizona: Arizona Geological Society Digest*, *17*, 649-680.

Menking, K. M., Anderson, R. Y., Shafike, N. G., Syed, K. H., & Allen, B. D. (2004). Wetter or colder during the Last Glacial Maximum? Revisiting the pluvial lake question in southwestern North America. *Quaternary Research, 62*(3), 280-288.

Mitchell, S. G., & Ober, K. A. (2013). Evolution of< i> Scaphinotus petersi</i>(Coleoptera: Carabidae) and the role of climate and geography in the Madrean sky islands of southeastern Arizona, USA. *Quaternary Research, 79*(2), 274-283.

Molnar, P., & England, P. (1990). Late Cenozoic uplift of mountain ranges and global climate change: chicken or egg?. *Nature*, *346*(6279), 29-34.

Morrison, R. B. (1985). Pliocene/Quaternary geology, geomorphology, and tectonics of Arizona. *Geological Society of America Special Papers*, *203*, 123-146.

Mortimer, C. (1973). The Cenozoic history of the southern Atacama desert, Chile. *Journal of the Geological Society*, *129*(5), 505-526.

Mortimer, C. (1980). Drainage evolution in the Atacama Desert of northernmost Chile. *Andean Geology*, (11).

Navarro-Gonzalez, R., Rainey, F.A., Molina, P., Bagaley, D.R., Hollen, B.J., de la Rosa, J., Small, A.M., Quinn, R.C., Grunthaner, F.J., Caceres, L., Gomez-Silva, B., McKay, C.P., 2003. Mars-like soils in the Atacama Desert, Chile, and the dry limit of microbial life. Science 302, 1018-1021.

Nichols, K.K., Bierman, P.R., Hooke, R.L., Clapp, E.M., Caffee, M., 2002. Quantifying sediment transport on desert piedmonts using Be-10 and Al-26. Geomorphology 45, 105-125.

Niedermann, S. (2002). Cosmic-ray-produced noble gases in terrestrial rocks: dating tools for surface processes. *Reviews in Mineralogy and Geochemistry*,*47*(1), 731-784.

Nishiizumi, K., Caffee, M.W., Finkel, R.C., Brimhall, G., Mote, T., 2005. Remnants of a fossil alluvial fan landscape of Miocene age in the Atacama Desert of northern Chile using cosmogenic nuclide exposure age dating. Earth and Planetary Science Letters 237, 499-507.

Owen, J.J., Amundson, R., Dietrich, W.E., Nishiizumi, K., Sutter, B., Chong, G., 2011. The sensitivity of hillslope bedrock erosion to precipitation. Earth Surface Processes and Landforms 36, 117-135.

Ouimet, W.B., Whipple, K.X., Granger, D.E., 2009. Beyond threshold hillslopes: channel adjustment to base-level fall in tectonically active mountain ranges. Geology 37, 579–582

Pearthree, P.A., 1986, Late Quaternary faulting and seismic hazard in southeastern Arizona and adjacent portions of New Mexico and Sonora, Mexico: Arizona Bureau of Geology and Mineral Technology Open-File Report 86-8, 22 p.

Pelletier, J. D., Barron-Gafford, G. A., Breshears, D. D., Brooks, P. D., Chorover, J., Durcik, M., et al. (2013). Coevolution of nonlinear trends in vegetation, soils, and topography with elevation and slope aspect: A case study in the sky islands of southern Arizona. *Journal of Geophysical Research: Earth Surface, 118*(2), 741-758.

Perg, L.A., Anderson, R.S., Finkel, R.C., 2001. Use of a new Be-10 and Al-26 inventory method to date marine terraces, Santa Cruz, California, USA. Geology 29, 879-882.

Phillips, W.M., McDonald, E.V., Reneau, S.L., Poths, J., 1998. Dating soils and alluvium with cosmogenic Ne-21 depth profiles: case studies from the Pajarito Plateau, New Mexico, USA. Earth and Planetary Science Letters 160, 209-223.

Pigati, J. S., Bright, J. E., Shanahan, T. M., & Mahan, S. A. (2009). Late Pleistocene paleohydrology near the boundary of the Sonoran and Chihuahuan Deserts, southeastern Arizona, USA. *Quaternary Science Reviews, 28*(3), 286-300.

Placzek, C.J., Matmon, A., Granger, D.E., Quade, J., Niedermann, S., 2010. Evidence for active landscape evolution in the hyperarid Atacama from multiple terrestrial cosmogenic nuclides. Earth and Planetary Science Letters 295, 12-20.

Portenga, E. W., & Bierman, P. R. (2011). Understanding Earth's eroding surface with 10 Be. *GSA Today, 21*(8), 4-10.

Prince, P. S., Spotila, J. A., & Henika, W. S. (2011). Stream capture as driver of transient landscape evolution in a tectonically quiescent setting. *Geology*,*39*(9), 823-826.

Putkonen, J., Balco, G., Morgan, D., 2008. Slow regolith degradation without creep determined by cosmogenic nuclide measurements in Arena Valley, Antarctica. Quaternary Research 69.

Quade, J., Rech, J.A., Betancourt, J.L., Latorre, C., Quade, B., Rylander, K.A., Fisher, T., 2008. Paleowetlands and regional climate change in the central Atacama Desert, northern Chile. Quaternary Research 69, 343-360.

Rech, J.A., Currie, B.S., Michalski, G., Cowan, A.M., 2006. Neogene climate change and uplift in the Atacama Desert, Chile. Geology 34, 761-764.

Richter, D.H., Houser, B.B., and Damon, P.E., 1983, Geologic map of the Guthrie quadrangle, Graham and Greenlee Counties, Arizona: U.S. Geological Survey Miscellaneous Investigations Series Map I-1455, scale 1:48,000.

Riihimaki, C. A., Anderson, R. S., Safran, E. B., Dethier, D. P., Finkel, R. C., & Bierman, P. R. (2006). Longevity and progressive abandonment of the Rocky Flats surface, Front Range, Colorado. *Geomorphology*, *78*(3), 265-278.

Rodríguez, M. P., Carretier, S., Charrier, R., Saillard, M., Regard, V., Hérail, G., ... & Audin, L. (2013). Geochronology of pediments and marine terraces in north-central Chile and their implications for Quaternary uplift in the Western Andes. *Geomorphology*, *180*, 33-46.

Ross, C. P. (1925). Aravaipa and Stanley Mining Districts, Arizona. *US Geol. Surv. Bull*, *763*, 1-120.

Rundel, P.W., Dillon, M.O., Palma, B., Mooney, H.A., Gulmon, S.L., Ehleringer, J.R., 1991. The Phytogeography and Ecology of the Coastal Atacama and Peruvian Deserts. Aliso 13, 1-50.

Scarborough, R. B., & Peirce, H. W. (1978, November). Late Cenozoic basins of Arizona. In *Land of Cochise, Southeastern Arizona, New Mexico Geological Society Twenty-Ninth Field Conference Guidebook, ed. JF Callender, JC Wilt, and RE Clemons* (pp. 253-259).

Simons, F. S. (1964). *Geology of the Klondyke quadrangle, Graham and Pinal Counties, Arizona: includes a part of the Basin and Range province and several small base-metal mining areas*. US Government Printing Office.

Smith, G. A. (1994). Climatic influences on continental deposition during late-stage filling of an extensional basin, southeastern Arizona. *Geological Society of America Bulletin*, *106*(9), 1212-1228.

Smith, G. A., Wang, Y., Cerling, T. E., & Geissman, J. W. (1993). Comparison Of A Paleosol-Carbonate Isotope Record To Other Records Of Pliocene-Early Pleistocene Climate In The Western United-States. *Geology, 21*(8), 691-694.

Spencer, J. E., & Reynolds, S. J. (1989). Middle Tertiary tectonics of Arizona and adjacent areas. *Geologic evolution of Arizona: Arizona Geological Society Digest*, *17*, 539-574.

Stuut, J.B.W., Lamy, F., 2004. Climate variability at the southern boundaries of the Namib (Southwestern Africa) and Atacama (northern Chile) coastal deserts during the last 120,000 yr. Quaternary Research 62, 301-309.

Stuut, J.B.W., Lamy, F., 2004. Climate variability at the southern boundaries of the Namib (Southwestern Africa) and Atacama (northern Chile) coastal deserts during the last 120,000 yr. Quaternary Research 62, 301-309.

Thorman, C.H., 1981, Geology of the Pinaleño Mountains, Arizona—a preliminary report, *in* Stone, Claudia and Jenney, J.P., eds.: Arizona Geological Society Digest, V. 13, p. 5-11.
Tuan, Y. (1962). Structure, climate, and basin land forms in Arizona and New Mexico. *Annals of the Association of American Geographers, 52*(1), 51-68.

Van Devender, T.R., 1990. Late Quaternary vegetation and climate of the Chihuahuan Desert, United States and Mexico. In: Betancourt, J.L., Van Devender, T.R., Martin, P.S. (Eds.), Packrat Middens: the Last 40,000 Years of Biotic Change. University of Arizona Press, Tucson, pp. 104–133.

Wagner, J. D. M., Cole, J. E., Beck, J. W., Patchett, P. J., Henderson, G. M., & Barnett, H. R. (2010). Moisture variability in the southwestern United States linked to abrupt glacial climate change. *Nature Geoscience, 3*(2), 110-113.

Wara, M.W., Ravelo, A.C., Delaney, M.L., 2005. Permanent El Nino-like conditions during the Pliocene warm period. Science 309, 758-761.

Warshall, P. (1995). The Madrean sky island archipelago: a planetary overview. *Biodiversity and management of the Madrean Archipelago: the sky islands of southwestern United States and northwestern Mexico*, 6-18.

Waters, M. R. (1989). Late Quaternary lacustrine history and paleoclimatic significance of pluvial Lake Cochise, southeastern Arizona. *Quaternary Research, 32*(1), 1-11.

Whipple, K. X., & Meade, B. J. (2006). Orogen response to changes in climatic and tectonic forcing. *Earth and Planetary Science Letters*, *243*(1), 218-228.

Wobus, C., Whipple, K.X., Kirby, E., Snyder, N., Johnson, J., Spyropolou, K., Crosby, B., Sheehan, D., 2006. Tectonics from topography: procedures, promise, and pitfalls. Geol. Soc. Am. Spec. Pap. 398, 55–74.

Wynn, J.C., 1981, Complete Bouguer gravity anomaly map of the Silver City 1ox2o quadrangle, New Mexico-Arizona: Miscellaneous Investigations Series Map I-1310-A, scale 1:250,000.

Yanites, B. J., Ehlers, T. A., Becker, J. K., Schnellmann, M., & Heuberger, S. (2013). High magnitude and rapid incision from river capture: Rhine River, Switzerland. *Journal of Geophysical Research: Earth Surface*, *118*(2), 1060-1084.

York, D. (1966). Least-squares fitting of a straight line. *Canadian Journal of Physics, 44*(5), 1079-1086.

Youberg, A., M.L. Cline, J.P. Cook, P.A. Pearthree, and R.H Webb, (2008). Geologic mapping of the debris flow deposits in the Santa Catalina Mountains, Pima County, Arizona. *AZGS Report OFR-08-06*.

Zhou, J.Y., Lau, K.M., 1998. Does a monsoon climate exist over South America? Journal of Climate 11, 1020-1040.

Zhu, C., Waddell, R. K., Star, I., & Ostrander, M. (1998). Responses of ground water in the Black Mesa basin, northeastern Arizona, to paleoclimatic changes during the late Pleistocene and Holocene. *Geology*, *26*(2), 127-130.